



EX LIBRIS
UNIVERSITATIS
ALBERTENSIS

The Bruce Peel
Special Collections
Library

University of Alberta

Library Release Form

Name of Author: **Marianne Christina McKenzie**

Title of Thesis: **Carbonates of the Upper Devonian Leduc Formation, Southwestern Peace River Arch, Alberta: Indications for Tectonically-Induced Fluid Flow**

Degree: **Master of Science**

Year this Degree Granted: **1999**

Permission is hereby granted to the University of Alberta Library to reproduce single copies of this thesis and to lend or sell such copies for private, scholarly, or scientific research purposes only.

The author reserves all other publication and other rights in association with the copyright in the thesis, and except as herein before provided, neither the thesis nor any substantial portion thereof may be printed or otherwise reproduced in any material form whatever without the author's prior written permission.

University of Alberta

**Carbonates of the Upper Devonian Leduc Formation, Southwestern Peace River
Arch, Alberta: Indications for Tectonically Induced Fluid Flow**

by

Marianne Christina McKenzie




A thesis submitted to the Faculty of Graduate Studies and Research in partial fulfillment
of the requirements for the degree of Master of Science

Department of Earth and Atmospheric Sciences

Edmonton, Alberta

Fall, 1999



Digitized by the Internet Archive
in 2025 with funding from
University of Alberta Library

<https://archive.org/details/0162010842662>

University of Alberta

Faculty of Graduate Studies and Research

The undersigned certify that they have read, and recommend to the Faculty of Graduate Studies and Research for acceptance, a thesis entitled ***Carbonates of the Upper Devonian Leduc Formation, Southwestern Peace River Arch, Alberta: Indications for Tectonically-Induced Fluid Flow*** submitted by ***Marianne Christina McKenzie*** in partial fulfillment of the requirements for the degree of Master of Science.

ACKNOWLEDGEMENTS

This study was funded in part by Amoco Canada, Chevron Canada Resources, Crestar Energy, Husky Oil Operations Ltd., Numac Energy, Petro-Canada, and by a National Sciences and Engineering Research Council grant awarded to Dr. H.G. Machel. The author would like to thank Dr. H.G. Machel and Dr. P.A. Cavell for their critical reviews, guidance, and support. Thanks to Dr. R.A. Creaser, Dr. K. Muehlenbachs, and Rob Hardy for laboratory support, and to the Petroleum Research Group at the University of Alberta for their encouragement and some fun along the way! Special thanks to Cathy Skilliter for helping me with many little snags during the writing of this thesis and for being there to listen. The author would also like to thank her family and Scott Doehler for their constant love, support, and encouragement.

ABSTRACT

Carbonates of the Upper Devonian Leduc Formation in the Peace River Arch area of Western Canada have undergone a complex tectonic and diagenetic history. twenty-one diagenetic phases have been identified. The principal diagenetic products include matrix-replacive dolomite, rhombohedral and saddle dolomite cements, milky and limpid calcite cements, three generations of anhydrite, and fluorite.

Carbon, oxygen, and strontium isotope data from the diagenetic cements suggest that several fluid events have affected these Devonian carbonate strata. $^{87}\text{Sr}/^{86}\text{Sr}$ ratios for late-stage cements indicate that there was an injection of ^{87}Sr during intermediate and deep burial of the Leduc. Potential sources of ^{87}Sr in the Peace River Arch area include the clastic Granite Wash Formation, the Precambrian basement rocks, and the metasedimentary rocks of the Miette Group in the adjacent Rocky Mountains. Migration of the ^{87}Sr -rich fluids may have occurred via basement faults, lateral flow through the Devonian aquifer system, or by a combined route.

Timing of the injection of ^{87}Sr -rich fluids coincided with the Laramide Orogeny in the Late Cretaceous. It is feasible that some of the ^{87}Sr was injected into the Devonian carbonates at the edge of the disturbed belt via the tectonic-expulsion of fluids. However, the complexity of the Peace River Arch tectonic history suggests that additional hydrodynamic processes may have played a role during the diagenetic evolution of the Leduc Formation.

TABLE OF CONTENTS

	Page
Chapter 1: Introduction	1
1.1 General Introduction	1
1.2 Previous and Ongoing Work	2
1.3 Objectives of Study	5
1.4 Study Area, Sampling Technique, and Methods	5
1.5 Regional Geologic Setting	6
Chapter 2: The Leduc Formation	14
2.1 Peace River Arch Leduc Depositional Environments	14
2.1.1 Stratigraphy	14
2.1.2 Structure	16
2.1.3 Facies Distribution	18
2.1.4 Facies Types	24
2.2 Post-Depositional Tectonic Development	31
2.3 Source Rocks, Hydrogeology, and Possible Migration Pathways	34
Chapter 3: Petrography of Diagenetic Fabrics in the Leduc Formation	39
3.1 Petrography of Diagenetic Phases	41
3.1.1 Limestones	41
3.1.2 Matrix-replacement dolomites	41
3.1.3 Dolomite cements	45
3.1.4 Calcite cements	48
3.1.5 Anhydrite cement phases	52
3.1.6 Fluorite	55
3.1.7 Other diagenetic cements	55
3.2 Other Diagenetic Features	58
3.2.1 Stylolites	58
3.2.2 Fractures	58

3.3 Summary	61
Chapter 4: Geochemistry	63
4.1 Introduction	63
4.2 Methodology	66
4.3 Stable Isotopes	68
4.4 Strontium Isotopes	73
4.5 Fluid Inclusion Microthermometry	80
Chapter 5: Discussion	90
5.1 Diagenetic Fluids and Burial History	90
5.1.1 Fluid event #1: matrix dolomitization	90
5.1.2 Fluid event #2: hydrocarbon migration	94
5.1.3 Fluid event #3: TSR and initial injection of ^{87}Sr -enriched brines	94
5.1.4 Fluid event #4: main injection of ^{87}Sr -enriched brines	96
5.1.5 Fluid event #5: relaxation of ^{87}Sr -enriched brine injection and re-equilibration	97
5.2 Sources and Migration Pathways of Strontium Bearing Fluids	98
5.3 Implications for Tectonically-Expelled “Squeegee” Flow in the Peace River Arch Area	103
5.3.1 Migration pathways of tectonically-expelled fluids	105
5.3.2 Fluid flux and the lateral extent of fluid movement	108
5.4 Comparison with Dix’s (1993) Study	109
Chapter 6: Summary	111
REFERENCES	113
APPENDIX A – GEOCHEMICAL DATABASE	123
APPENDIX B – GEOCHEMICAL METHODS	129

LIST OF TABLES

	Page
1.1 Summary of cores examined	9
A-1 Summary of geochemical data	123

LIST OF FIGURES

	Page
1.1 Distribution map of Woodbend Group carbonate complexes	3
1.2 Map of the study area, Peace River Arch, Alberta	7
1.3 Stratigraphic column	8
1.4 Tectonic domains, NW Alberta and NE British Columbia	11
1.5 Schematic cross-section through the Peace River Arch	13
2.1 Woodbend & Winterburn Group transgressive-regressive cycles	15
2.2 Isopach map of the Leduc Formation	17
2.3 Structural contour map of the Leduc Formation	19
2.4 Isopach map of the Granite Wash and underlying basement structure	20
2.5 Stratigraphic cross-section of the Leduc Formation	23
2.6 Core photographs of intertidal to shallow subtidal facies	25
2.7 Core photographs of lagoonal facies	26
2.8 Core photographs of fore-reef facies	28
2.9 Core photographs of slope to basinal facies	29
2.10 Core photographs of syndepositional breccias	30
2.11 Location map of major structural features in the study area	32
2.12 Sketch of the Dawson Creek Graben Complex	33
2.13 Stratigraphic relationships between source rocks, reservoirs and hydrocarbons in the study area	35
2.14 Hydrostratigraphy in the Peace River Arch study area	36
3.1 Paragenetic sequence	40
3.2 Photomicrographs of M1 and M2 dolomite	42
3.3 Photomicrographs of M3, M4, and M5 dolomite	44
3.4 Photomicrographs of rhombohedral dolomite cement	46
3.5 Photomicrographs of saddle dolomite cement	47
3.6 Core photo and photomicrographs of milky calcite cement	49
3.7 Photomicrographs of limpid calcite cement	51
3.8 Core photo and photomicrographs of anhydrite cements	53
3.9 Photo of blocky fluorite cement	56

3.10	Photo of native sulphur infilling a vug	57
3.11	Core photo and photomicrographs of fracture types	59
4.1	Interpreted $^{87}\text{Sr}/^{86}\text{Sr}$ seawater curve	67
4.2	Stable isotope plot of $\delta^{18}\text{O}$ versus $\delta^{13}\text{C}$	69
4.3	Plot of $\delta^{13}\text{C}$ versus $^{87}\text{Sr}/^{86}\text{Sr}$	74
4.4	Plot of $\delta^{18}\text{O}$ versus $^{87}\text{Sr}/^{86}\text{Sr}$	76
4.5	Cumulative weight fraction Sr versus $^{87}\text{Sr}/^{86}\text{Sr}$ to define MASIRBAS	78
4.5	Plot of $^{87}\text{Sr}/^{86}\text{Sr}$ for fluorite and anhydrite cements	83
4.6	Fluid inclusion homogenization temperature histograms	84
4.7	Fluid inclusion eutectic temperature histograms	86
4.8	Fluid inclusion final melting temperature histograms	88
4.9	Fluid inclusion freezing point depression curves	89
5.1	Paragenetic sequence and burial history of the Leduc	91
5.2	Plan view map of tectonically-induced fluid flow pathways	102
5.3	Cross-section of inferred tectonically-induced fluid flow through the Rocky Mountains and the deep foreland basin	106
5.4	Cross-section illustrating Mid-Cretaceous to Devonian paleo-hydrostratigraphic flow systems in the southwestern WCSB	107

CHAPTER 1

INTRODUCTION

1.1 General Introduction

Hydrocarbon exploration in the Western Canada Sedimentary Basin (WCSB) has made a significant contribution to the Albertan and Canadian economies since the discovery of oil at Turner Valley in 1914. Of the billions of barrels of oil and trillions of cubic feet of gas that have been discovered, Devonian reservoirs account for approximately 2/3 of the conventional oil and 1/3 of the gas in Alberta (Creaney and Allen, 1989). The discovery of oil in the Imperial Leduc No. 1 well in the spring of 1947 escalated petroleum exploration via the pursuit of Devonian reefs in the subsurface of Alberta (Barfoot and Rodgers, 1984). Since then, the Frasnian aged, dolomitic Leduc Formation has been one of the main targets for exploration and exploitation of hydrocarbon reserves.

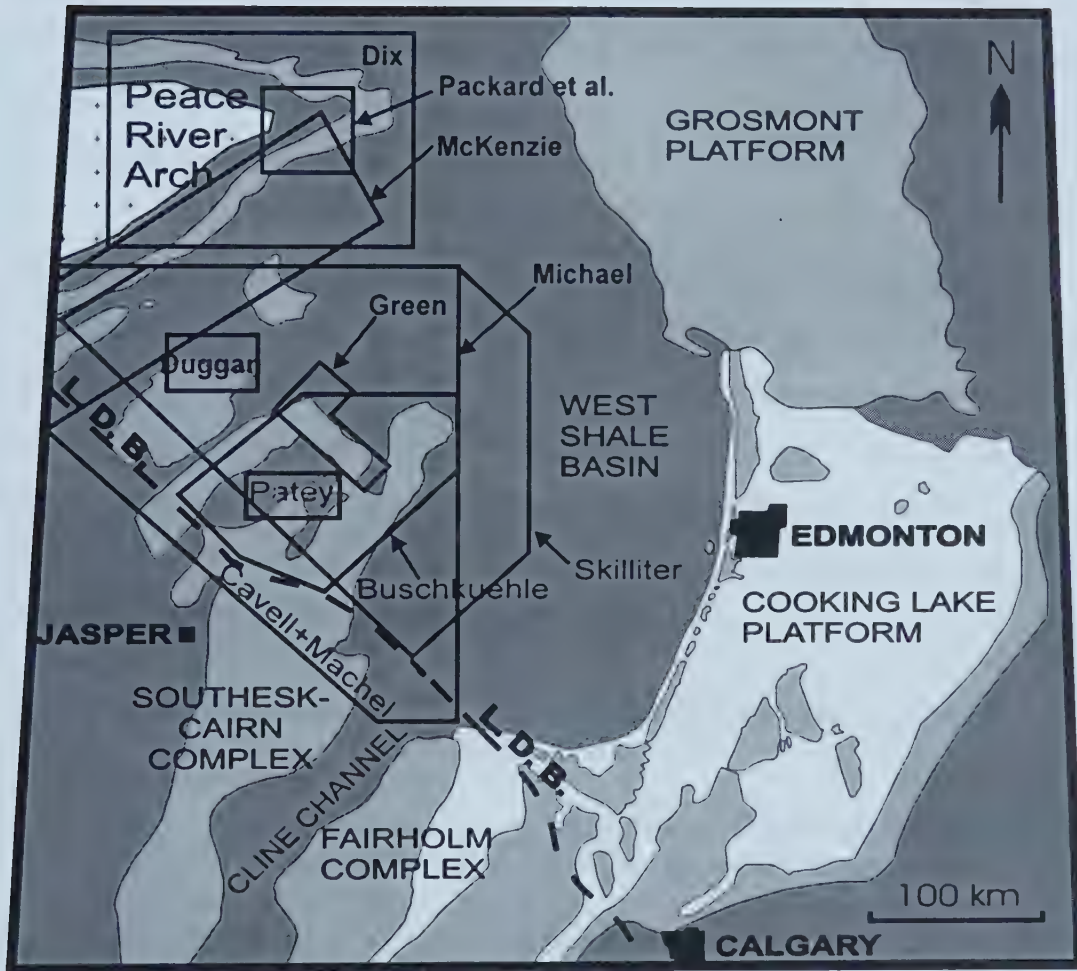
The popularity of Devonian hydrocarbon plays, coupled with their great depths (3-6 km) near the western edge of the basin, has made it imperative to investigate reservoir quality and diagenetic processes that affected the timing of hydrocarbon migration and entrapment. Within and near to the disturbed belt in Alberta, reservoir dynamics and migration pathways are comparatively more complex than elsewhere in the WCSB due to tectonic modification of the strata during the Laramide Orogeny. Among the processes that affected porosity and permeability development in Devonian reservoirs, it has been postulated that fluids originating from the Rocky Mountains have migrated into and along regional Devonian aquifer systems, thereby diagenetically modifying the carbonate rocks that they passed through (Machel *et al.*, 1996). Furthermore, it has been argued that the tectonic expulsion of fluids from thrust sheets during orogenesis is probable, and models have been proposed to account for the movement of fluids along aquifers and into foreland basins (Oliver, 1986; Bradbury and Woodwell, 1987). Therefore, a study to document the effects of tectonically expelled fluids into Devonian strata and the foreland basin potentially has significant economic implications for successful exploration within these units in the WCSB.

1.2 Previous and Ongoing Work

Recent studies near to and within the disturbed belt in Alberta (Figure 1.1) have developed a stratigraphic, lithologic, and geochemical database. Diagenetic cements in Devonian carbonate complexes and reefal buildups have been analyzed for both stable (C and O) and radiogenic (Sr) isotopes, and in all cases were found to contain anomalously high $^{87}\text{Sr}/^{86}\text{Sr}$ values. In the Obed area, calcite and dolomite cements have $^{87}\text{Sr}/^{86}\text{Sr}$ values ranging from 0.7086 - 0.7252 (Patey, 1995). Some carbonates have since been identified as having been diagenetically modified during deep burial and recrystallization at great depths (5-7 km) by hot brines that were tectonically expelled from the Rocky Mountains by overthrusting during the Laramide orogeny (Machel *et al.*, 1996). As well, Duggan's (1997) study of the Swan Hills Simonette field and Green's (1999) study of the Wabamun and Leduc formations at Pine Creek Field, and the Swan Hills Formation at Kaybob South field revealed that late-stage carbonate cements in these reservoirs also contained highly radiogenic $^{87}\text{Sr}/^{86}\text{Sr}$. In both Duggan's and Green's study areas it was revealed that basement faulting likely provided conduits that channelled hot fluids upward into Devonian strata from the Precambrian basement. Ongoing studies in the Southesk-Cairn complex (Buschkuehle, in prep.) also indicate the presence of late-diagenetic calcite cements with similar geochemical signatures. Furthermore, a study on the isotopic compositions of Upper Devonian shales (Cavell and Machel, 1997) has determined the maximum strontium isotope ratio that could be released from basinal shales under normal diagenetic conditions in the WCSB, constraining the isotopic source for highly radiogenic strontium. Ongoing stratigraphic and geochemical studies of the Devonian shales in the western part of the WCSB (Skilliter *et al.*, 1998; Skilliter, in prep.) further constrain the fluid migration pathways in Devonian strata.

The only other areas reported to contain rocks with similar $^{87}\text{Sr}/^{86}\text{Sr}$ values are 1) the Proterozoic slates of the Miette Group in the Rocky Mountains to the southwest of the Obed field (Koffyberg, 1994); 2) fracture-filling calcite cements in the Wabamun in the Peace River Arch (PRA) (Packard *et al.*, 1990); and 3) calcite samples from the Leduc Formation in the northern and southeast parts of the PRA (Dix, 1993). Isotopic evidence suggests that Leduc dolomitization occurred during shallow and intermediate burial depths by similar

Figure 1.1 - Simplified distribution map of Devonian platform and reef carbonates of the Late Devonian Woodbend Group in the Alberta part of the Western Canada Sedimentary Basin (WCSB). White & light grey fills indicate undifferentiated Cooking Lake and/or Leduc Formations (in subsurface, east of the limit of the disturbed belt and their outcrop equivalents west of the limit of the disturbed belt [L.D.B.], palinspastically restored); dark grey fill denotes the West Shale Basin, off-reef equivalents, and areas of basinal shale deposition. The Grosmont Platform/Shelf in the northeast of the basin consists of Woodbend and overlying Winterburn Group carbonates. East of the limit of the disturbed belt, the regional structural dip is to the SW, with present subsurface depths ranging from zero to 300 m for the Grosmont platform, increasing to more than 4 km close to the limit of the disturbed belt. Boxes and names denote individual study areas. Modified from Machel and Cavell, 1999.



fluids and processes that have occurred in Devonian aged carbonates throughout the Alberta Basin (e.g. Mountjoy and Amthor, 1994). However, several of the $^{87}\text{Sr}/^{86}\text{Sr}$ ratios in Leduc Peace River Arch dolomite cements are found to be higher than that of Late Devonian seawater present at the time of dolomitization (Dix, 1993). This observation has been attributed to the mixing of the dolomitizing fluids prior to water-rock interaction. Furthermore, late stage fracture-filling dolomite cements, associated with deep burial diagenesis in this area, are found to have increasingly negative $\delta^{18}\text{O}$ values, which are attributed to hot, circulating basement-derived fluids. These fracture-filling cements can also be traced along sub-vertical fractures from the Precambrian basement through to the overlying Wabamun Formation (Packard *et al.*, 1990; Dix, 1993).

1.3 Objectives of Study

Initial observations suggest that some of the Leduc carbonates in the southwestern Peace River Arch area may have been affected during diagenesis by tectonically-expelled fluids such as those associated with diagenetic processes in the Obed area. This study will attempt to confirm the initial hypothesis that fluids expelled from the Rockies did flow into the foreland basin, and did have an effect on Devonian Leduc carbonates in the Peace River Arch area. The main objectives of this study are to:

- 1) characterize the geochemical nature of the diagenetic fluids in the Leduc Formation in the southwestern Peace River Arch area,
- 2) provide isotopic evidence for the emplacement and recrystallization of carbonate cements by tectonically-expelled fluids from the Rocky Mountains, and
- 3) define the extent of influence of the tectonically-expelled fluids into the foreland basin in the Peace River Arch area.

In addition, this paper will compare the results and observations made in the study area to other areas previously and currently being examined south of the Peace River Arch.

1.4 Study Area, Sampling Technique, and Methods

The study area is located in the southwest part of the Peace River Arch including

Townships 65 - 80 north, and Ranges 22 - 27 west of the 5th, and 1- 12 west of the 6th Meridians (Figure 1.2). The stratigraphic unit of interest is the Late Devonian Leduc Formation, which lies at a depth of approximately 2700 and 4300 metres in the subsurface. The underlying Woodbend Group and overlying Ireton, Nisku, and Wabamun Formations were also examined, in part, to provide a regional perception of the Peace River Arch stratigraphy (Figure 1.3).

A total of 23 cores were examined (refer to Figure 1.2 for locations). A summary of the core data is presented in Table 1.1. Within the Peace River Arch study area, core control is limited and, where subsurface data are available, the Leduc Formation is frequently cored only within the uppermost interval. This has made a thorough stratigraphic study of the area challenging. However, this does not hinder the geochemical analysis of diagenetic cements within the Late Devonian aquifer system. A total of 80 thin sections were cut, and longitudinally stained with alizarin red. After the careful examination of the core and thin sections, 52 samples were selected for isotopic analyses (Appendix A). Samples were chosen from across the study area, both along strike and perpendicular to the disturbed belt, and at varying stratigraphic levels. Minerals analyzed include matrix limestone and dolomite, and different phases of diagenetic dolomite, calcite, anhydrite, and fluorite. Geochemical techniques used in this study include stable ($\delta^{13}\text{C}$, $\delta^{18}\text{O}$) and radiogenic ($^{87}\text{Sr}/^{86}\text{Sr}$) isotope analyses, X-ray diffraction (XRD), and fluid inclusion microthermometry. The details of these procedures are summarized in Appendix B.

1.5 Regional Geologic Setting

The Peace River Arch (PRA) in northwestern Alberta and northeastern British Columbia represents a Late Palaeozoic uplift of Precambrian basement rocks overlain by younger carbonate and clastic rocks. The arch was first discovered in 1949 when the Imperial Spirit River No.1 well encountered the Precambrian basement at an atypically high elevation and unconformably overlain by Devonian strata (deMille, 1958).

Since then many studies have attempted to unravel the geologic history of the Devonian and Carboniferous carbonate and clastic sediments in this area. The unique tectonic setting of the arch has influenced the location of hydrocarbon accumulation in

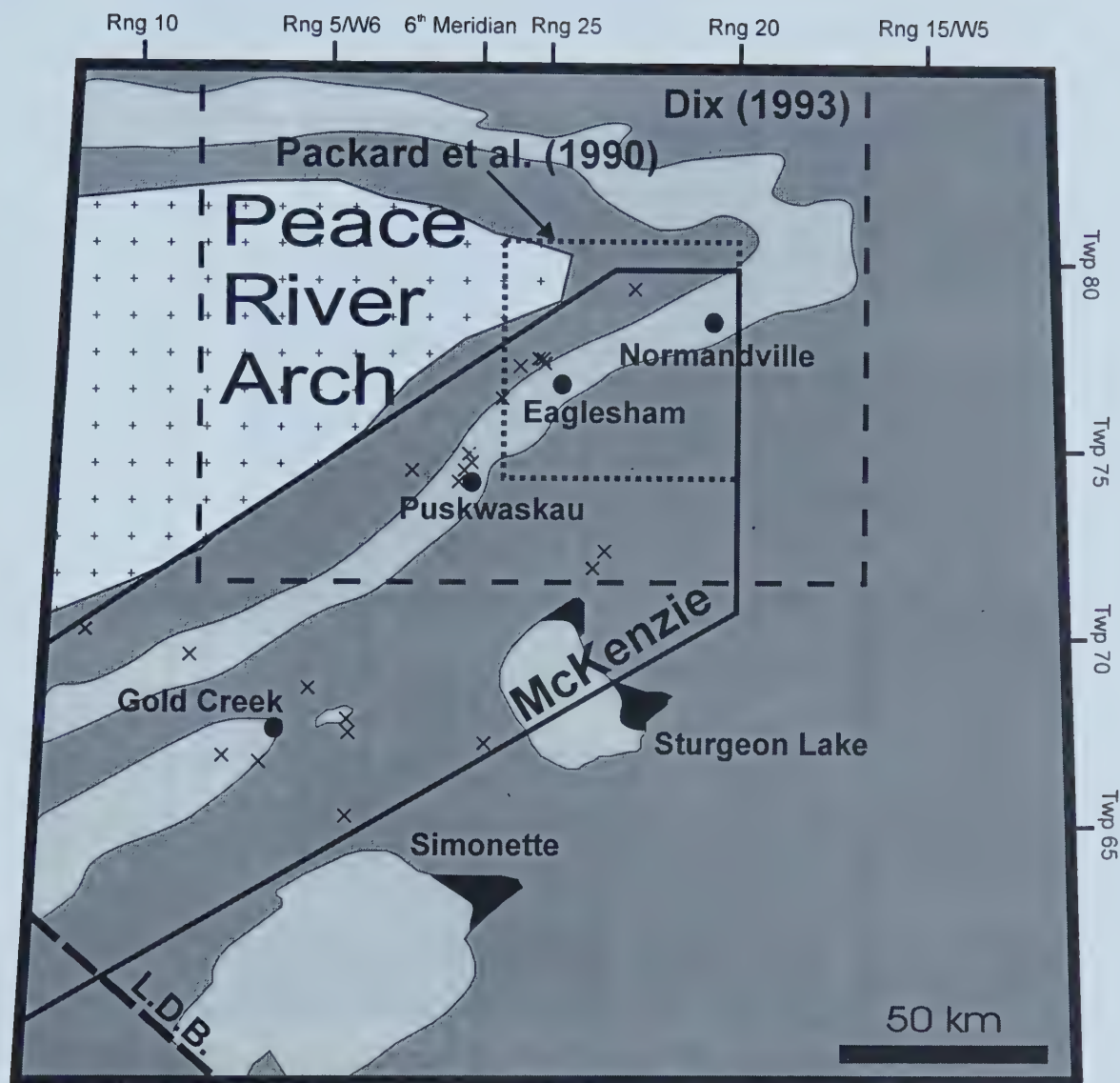


Figure 1.2 - Study area in the southwest Peace River Arch (PRA) as labelled and outlined with the solid line. Devonian aged Leduc carbonates comprise the fringing reef and surrounding buildups are shown in light grey fill. The PRA granite landmass is indicated with the patterned fill, and the surrounding off-reef carbonates and basinal facies are shown in dark grey fill. Dix's (1993) and Packard *et al.*'s (1990) study areas are outlined by the dashed line boxes. Normandville, Eaglesham, Puskwaskau, Gold Creek, Simonette, and Sturgeon Lake Fields are labelled and their locations are indicated by the black fill. The limit of the disturbed belt (L.D.B.) is shown in the southwest corner of the study area. Wells with core examined in this study are indicated with an "X". Wells located off of the main reefal units are cored in the intertidal, lagoon, or slope facies.

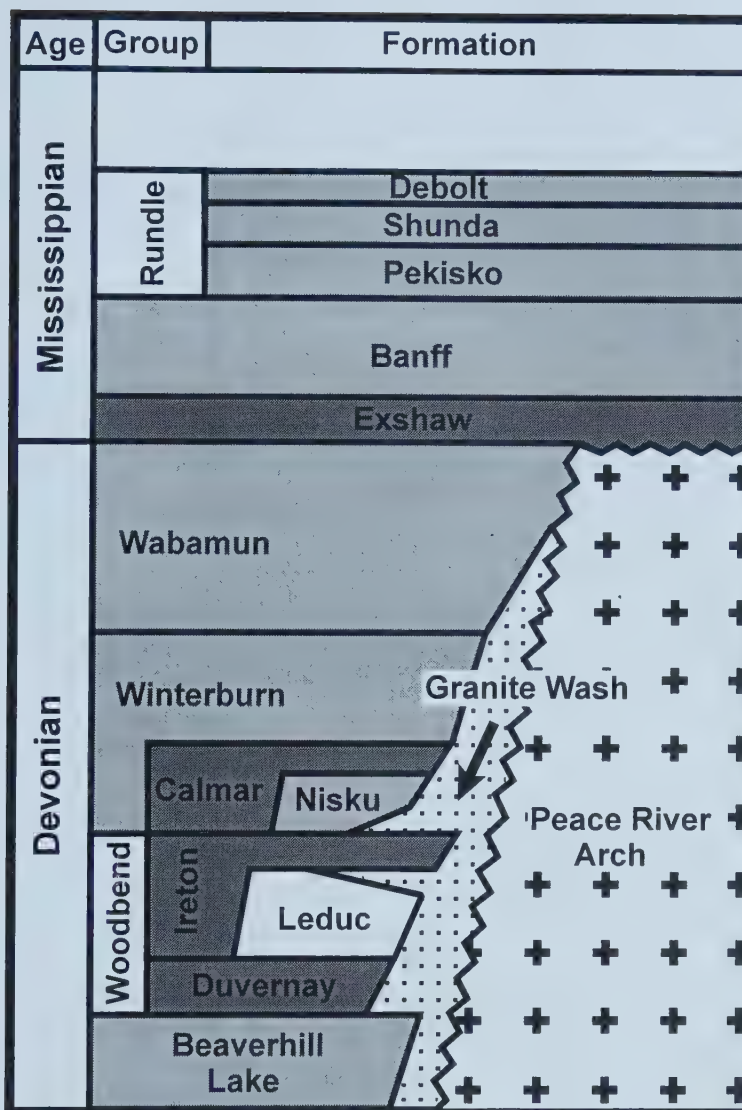


Figure 1.3 – Schematic stratigraphic column showing the Late Devonian and Early Mississippian units and their stratigraphic relationships to the Precambrian aged Peace River Arch. Light grey fill denotes carbonate units, dark grey fill indicates shales and/or marls, and dotted pattern fill indicates siliciclastic units. The Peace River Arch granite landmass is shown by the crossed patterned fill. Modified from Dix (1994).

Table 1.1 - Summary of core examined in the study.

Well Location	Core Interval Logged	No. of metres/feet Logged	No. Samples Taken	Stratigraphic Interval
16-04-65-04/W6	12697-12714 ft	17 ft	1	Nisku
12-22-66-06/W6	12799-12849 ft	50 ft	5	Leduc
11-30-66-07 /W6	13505-13565 ft 13670-13719 ft 13880-13928 ft	157 ft	19	Leduc
11-06-67-26/W6	10421-10588 ft 10641-10650 ft	176 ft	2	Nisku
11-14-67-04/W6	11289-11348 ft	59 ft	2	Leduc
04-34-67-04/W6	11080-11130 ft 11702-11752 ft 12021-12054 ft 12170-12198 ft	161 ft	5	Wabamun & Leduc
06-27-68-05/W6	3505-3508 m	3 m	0	Nisku
13-19-69-08/W6	13095-13146 ft	51 ft	0	Leduc
11-03-70-11/W6	14100-14126 ft	26 ft	3	Leduc
09-31-71-23/W5	8904-8968 ft	64 ft	5	Leduc
02-05-72-23/W5	9322-9372 ft 9468-9564 ft	146 ft	10	Leduc
10-20-73-01/W6	2973-3044 m	71 m	5	Leduc
06-04-74-01/W6	2735-2758 m	23 m	6	Leduc
14-23-74-01/W6	2660-2691 m	31 m	6	Ireton & Leduc
01-26-74-01/W6	2704-2713 m	9 m	4	Leduc
04-34-74-01/W6	9066-9096 ft	30 ft	5	Leduc
12-18-74-02/W6	9435-9461 ft	26 ft	5	Leduc
02-08-76-26/W5	8050-8181 ft	131 ft	13	Leduc
12-11-77-25/W5	7543-7592 ft	49 ft	3	Leduc
14-11-77-25/W5	7545-7588 ft	43 ft	0	Leduc
10-14-77-25/W5	7590-7615 ft	25 ft	5	Leduc
09-06-77-25/W5	7963-7995 ft	32 ft	5	Leduc
02-17-79-22/W5	6782-6805 ft	23 ft	2	Leduc

the area, and since the early 1950's, the PRA has been a target for oil and gas exploration.

The general trend of the uplifted area is NE-SW with an approximate length of 750 km, spanning from 54° to 58° latitude, and 114° longitude to the Cordilleran front ranges in British Columbia (O'Connell, 1994). The PRA is an asymmetrical structure with a steeply dipping northern flank, and a more gently dipping southern flank (O'Connell *et al.*, 1990). It has been estimated that the Precambrian basement rocks in the PRA area have been raised to between 800 and 1000 m above their original elevation (Cant, 1988).

The origin of the PRA structure has yet to be adequately resolved. However, most investigators concur that the arch first rose in the Late Proterozoic (Cant, 1988). The PRA structure does not seem to coincide with any NE-SW trending structural features, or any major structural zone in the Precambrian basement (O'Connell, 1994). Several theories have been proposed over the years to account for the structural high of the arch. These include: 1) potassium metasomatism in the underlying basement gneisses (Burwash and Krupicka, 1970), 2) a mantle hotspot (Stelck *et al.*, 1978), and 3) a failed rift system along the passive continental margin (Cant, 1988). As well, Ross (1990) revealed a series of aeromagnetic and gravity anomalies, and radiometric age data which indicate that the PRA is underlain by three distinct tectonic domains making up the basement rocks: the Buffalo Head Terrane, the Chinchaga Low, and the Ksituan High (Figure 1.4). However, these three domains do not seem to coincide with the NE-SW trend of the arch, but instead are characterized by north trending, curvilinear features (Ross, 1990).

The structural development of the PRA may be divided into three distinct phases. Initial uplift occurred in the Late Proterozoic, as interpreted by the examination of pre-Devonian sedimentary sequences located in the Rocky Mountain Front ranges (McMechan, 1990). However, there is no remaining sedimentological evidence related to the formation of the arch in its early stages. By the Middle Devonian, the arch was an emergent structure located on the edge of a subsiding passive continental margin (Bond and Kominz, 1984). This is interpreted from the onlap of platform carbonates, reef growth, and terrigenous clastic facies surrounding the PRA at that time. Although the exact mechanism for arch burial is unclear, it is known that the PRA was successively

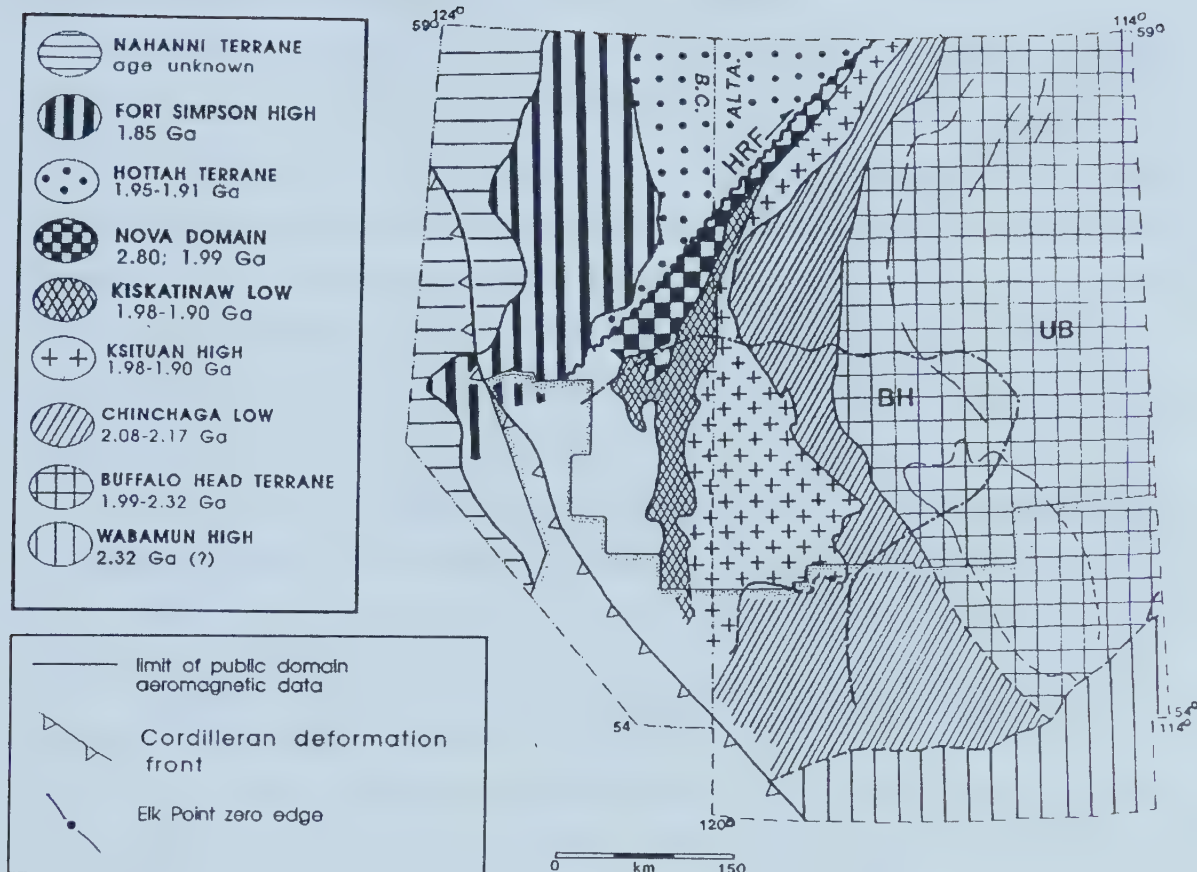


Figure 1.4 – Tectonic domains in the basement of northwestern Alberta and northeastern British Columbia based on interpretations of aeromagnetic anomaly data and U-Pb geochronology. The Elk Point zero edge outlines the Peace River Arch. HRF = Hay River Fault, UB = Utikuma Belt, BH = Buffalo Head High. From Ross (1990).

onlapped and covered by the deeper marine facies of the Exshaw Formation in early Mississippian time. This development reflects an overall eustatic sea level rise, subsidence of the structure, or both (O'Connell *et al.*, 1990).

Extensional tectonics, uplift, and subsidence in the Early Carboniferous resulted in the development of the centrally located Dawson Creek Graben Complex on the crest of the PRA. The accompanying Carboniferous and Permian sediments were deposited as a thickened clastic sequence within the downdropped graben. Finally, an overall regional subsidence in the Late Jurassic affected the extent of the PRA area. This may be attributed to the rejuvenation of underlying basement structures as a result of loading on the continental margin sediments by thrust sheets from the west at the onset of the Laramide Orogeny (O'Connell *et al.*, 1990; Cant, 1988).

Leduc carbonate deposition began to form a fringing structure surrounding the PRA landmass in the Late Devonian. The Leduc Formation fringing the Peace River Arch represents a seaward-thickening carbonate platform comprised of a series of shallow marine carbonates interfingering with siliciclastic terrigenous and nearshore facies eroding off of the emergent arch (Dix, 1993) (Figure 1.5).

Previous research on the Leduc Formation in the Peace River area suggests that several stages of diagenesis have occurred (Dix, 1993). Dolomitization began at shallow depths, and culminated at depths greater than 1 km where deep basinal fluids appear to have been channeled upward through basement fractures. At shallow and intermediate depths dolomitizing fluids may have originated from the diffusion of seawater into the reef carbonates or from chemical compaction, whereas dolomitizing fluids associated with deeper burial include intermixed platform-derived fluids and deep basinal brines (Dix, 1993).

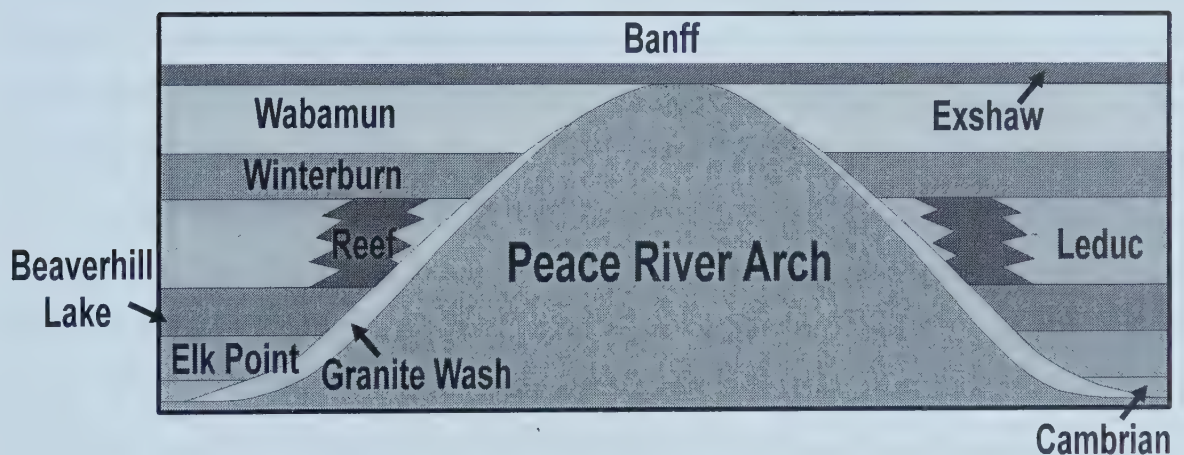


Figure 1.5 - Schematic cross-section through the Peace River Arch showing the onlapping of Devonian carbonates and shale strata onto the granite landmass and the eventual covering of the arch by the Exshaw Formation in Early Mississippian time. The Granite Wash sand interfingers with the Leduc carbonates along the edge of the arch. The Leduc fringing reef is depicted flanking the landmass. Modified from Cant (1988).

CHAPTER 2

THE LEDUC FORMATION

The Leduc Formation has been extensively studied throughout the WCSB. It is largely composed of pervasively dolomitized reef and platform facies, and is part of the Devonian Woodbend Group. The Leduc may be divided into three intervals, each associated with a distinct period of reef growth: the Lower, Middle, and Upper Leduc. These intervals correspond stratigraphically to the Majeau Lake, Duvernay, and Ireton Formations, which represent Leduc-equivalent basinal sediments (Figure 2.1). They are mainly composed of argillaceous carbonate muds and shales with an increased bioclastic component near reef margins, and represent an influx of fine-grained terrigenous material into central Alberta from extra-basinal sources (Stoakes, 1992). Furthermore, the Majeau Lake, Duvernay, and Ireton Formations form effective aquitards and seals for Leduc reef reservoirs where sediment thickness exceeds 10 m, and where not affected by faulting and fracturing (Rostron, 1995; Hearn, 1996). Overall, Woodbend Group strata comprise a single major cycle of deposition made up of a lower transgressive and an upper regressive phase of sedimentation (Stoakes, 1992). Three smaller transgressive-regressive cycles can be identified within the Woodbend Group, each distinguished by a shallow water carbonate (*e.g.* Leduc) that is capped by a deep-basin carbonate mud or shale (*e.g.* Ireton) (Hedinger *et al.*, 1994) (Figure 2.1).

Two comprehensive studies on the PRA have been published by Dix (1990, 1993). A summary of both Dix's work and observations made in this study will be presented here and in the following chapter, with focus on the southwest portion of the PRA Leduc strata, tying in both the Gold Creek, and the top of the Sturgeon Lake Leduc buildups where data are available. Cored wells are indicated on Figure 1.2 in the previous chapter. Most cored wells only penetrate the top of the Leduc. Thus, it is difficult to get a complete picture of Leduc thicknesses and the development of facies within the study area.

2.1 Peace River Arch Leduc Formation Depositional Environments

2.1.1 Stratigraphy

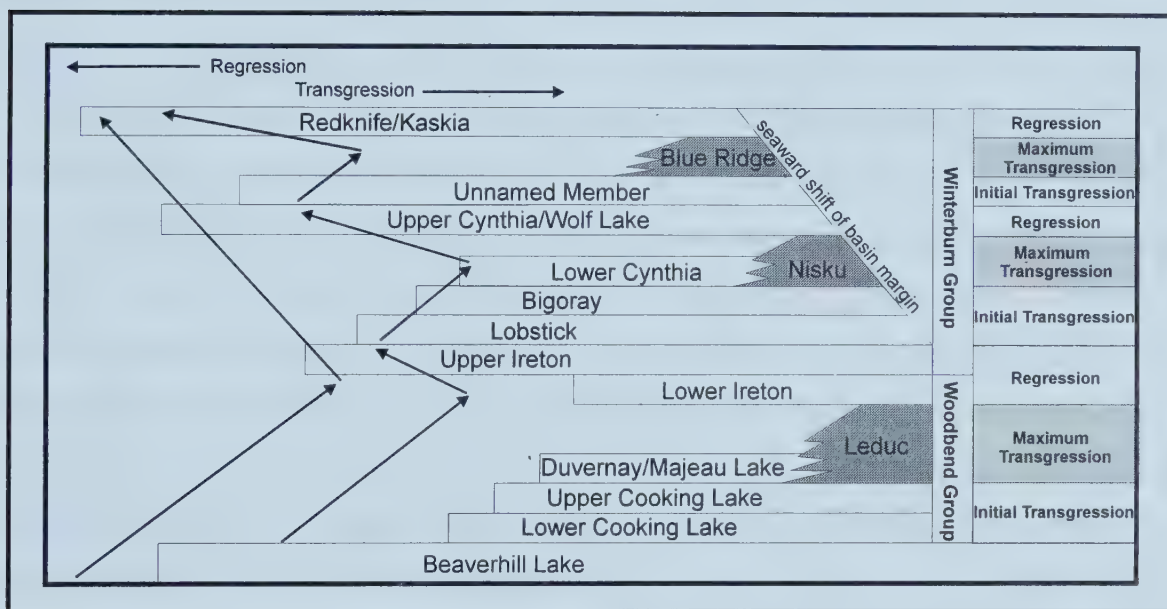


Figure 2.1 – Woodbend & Winterburn Group transgressive-regressive cycles. Modified from Hedinger *et al.* (1994).

The PRA Leduc Formation represents a shallow-water mixed carbonate-siliciclastic platform that onlapped onto the emergent landmass during the Frasnian (367 to 374 Ma). The platform extends from the landmass to a maximum distance of approximately 120 km and thickens to 200-250 m along the basinward margin (Figure 2.2). Along the northern flank of the PRA, the Leduc is relatively narrow in comparison to its eastern and southern flanks. The notable increase in platform width in the east and south may have resulted from the gentler dip of the Precambrian surface along the southern edge of the arch (O'Connell, 1994). The Leduc platform and reef carbonates were deposited disconformably on top the carbonates of the Middle Devonian Beaverhill Lake Group. On their shoreward edge, however, the PRA Leduc dolomites are interbedded with, and lie conformably on top of, terrigenous clastic sediments of the Granite Wash Formation (Hedinger *et al.*, 1994; Dix, 1990). The Granite Wash in the PRA area consists of sandy to conglomeratic, arkosic, clastic units with granite fragments as the major component (Dunham *et al.*, 1983; Dix, 1990; Dec, Hein and Trotter, 1996). Leduc reef facies are stacked one on top of another to form a discontinuous fringing complex surrounding the landmass and the interior carbonate platform. Basinward progradation of the reef complex during times of eustatic sea level fall or stillstand was inhibited due to the lack of basin-fill sediments upon which the reefs could forestep (Hedinger *et al.*, 1994). By the end of the Frasnian, the Leduc platform had backstepped onto the PRA as a response to a major eustatic sea level rise. At this time, the Ireton Formation marls were deposited conformably on top of the Leduc, drowning the carbonate factory of the fringing reef. The Ireton thus represents the highstand at the top of an overall transgressive package. As sea level once again dropped, the argillaceous carbonates and shales of the Winterburn Group were deposited conformably on top of the Ireton Formation.

2.1.2 Structure

Structural contours drawn on the top of the Leduc indicate that there are two distinct sections to the platform, including the northern and southern “arms” and their associated reef facies, that appear to be separated by a southwest-plunging trough. The northern arm of the reef facies slopes to the west at approximately 7m/km, whereas the southern arm is steeper, dipping to the southwest at approximately 12m/km (Dix, 1990) (Figure 2.3). The Sturgeon

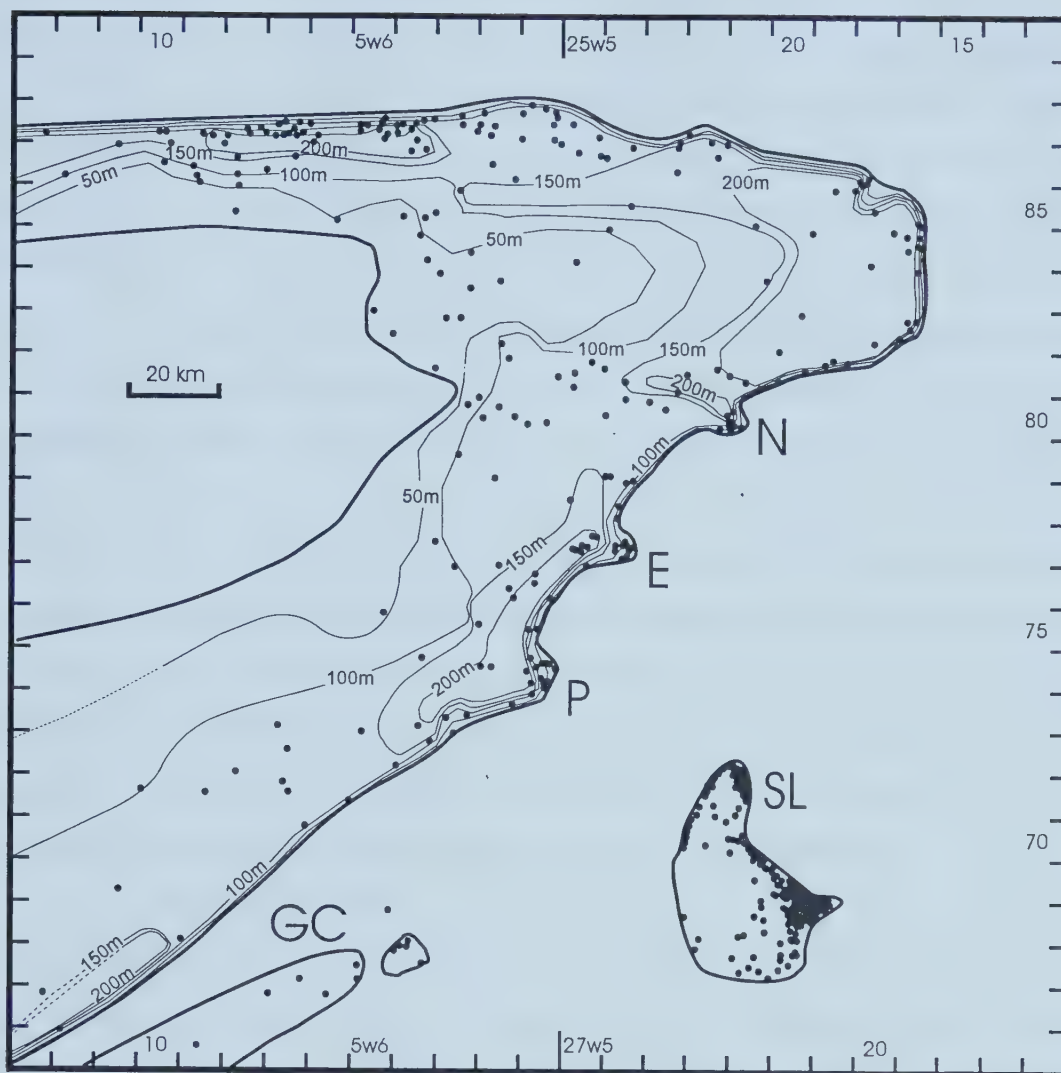


Figure 2.2 – Isopach map of the Devonian Leduc Formation over the Peace River Arch study area. Contour Interval = 50 m, small black dots are well locations that penetrate the Leduc Formation, hydrocarbon fields are noted as P = Puskwaskau Field, E = Eaglesham, N = Normandville, GC = Gold Creek, SL = Sturgeon Lake. Modified after Dix (1990).

Lake and Gold Creek platforms to the south of the PRA follow the same general structural trend as the southwest arm of the arch. Generally, the PRA area Leduc platforms dip to the west-southwest as a result of basin downwarp during the Laramide Orogeny (Hedinger *et al.*, 1994). In the study area, there are also local structural highs at Normandville, Eaglesham, Puskwaskau, and the top of Sturgeon Lake fields that are a result of post-Leduc faulting (Stoakes, 1987), coincident with abundant reef growth in these areas (Dix, 1990). Dix has also noted that pre- and syn-Leduc faulting may have played a role in the modification of Leduc deposition, as suggested by anomalously thickened Leduc sections and changes in carbonate facies distribution that occur across the regional strike of the area. The influence of Precambrian lineaments on facies development is indicated by the distribution of interbedded siliciclastics and carbonates and by the development of local embayments in Middle Leduc time, which seem to coincide with N-NE trending faults (Dix, 1990). Structural contours on the Precambrian surface in the PRA area indicate the presence of NE-SW and NW-SE trending fault zones and accompanying downthrown blocks that are most likely related to the original uplift of the arch (deMille, 1957; O'Connell *et al.*, 1990). The Granite Wash infills the topographic lows created by faulting on the Precambrian surface, making it easy to trace Precambrian structural features in the PRA area (Cant, 1988) (Figure 2.4).

2.1.3 Facies Distribution

Where core is available in the study area, it usually covers the uppermost 50 m of the Leduc Formation, and many cores are very short (< 5 m). Furthermore, the wells are widely spaced, which makes the study of lateral facies changes difficult. Cores also tend to be focused within the three petroleum fields situated along the platform margin on the southwest arm of the arch (refer to Table 1.1 for a summary of the core examined and to Figure 1.2 for locations of cores).

Dix (1990) divided the Leduc platform and reef carbonates into three units, based on core examination and geophysical log signature. PRA Leduc Sequences I, II, and III correspond, respectively, to Upper, Middle, and Lower Leduc units that have been distinguished elsewhere in the WCSB (*e.g.* McCrossan, 1957; Klován, 1964; McGillivray and Mountjoy, 1975; Stoakes, 1980; Wendte, 1987; Hedinger *et al.*, 1994).

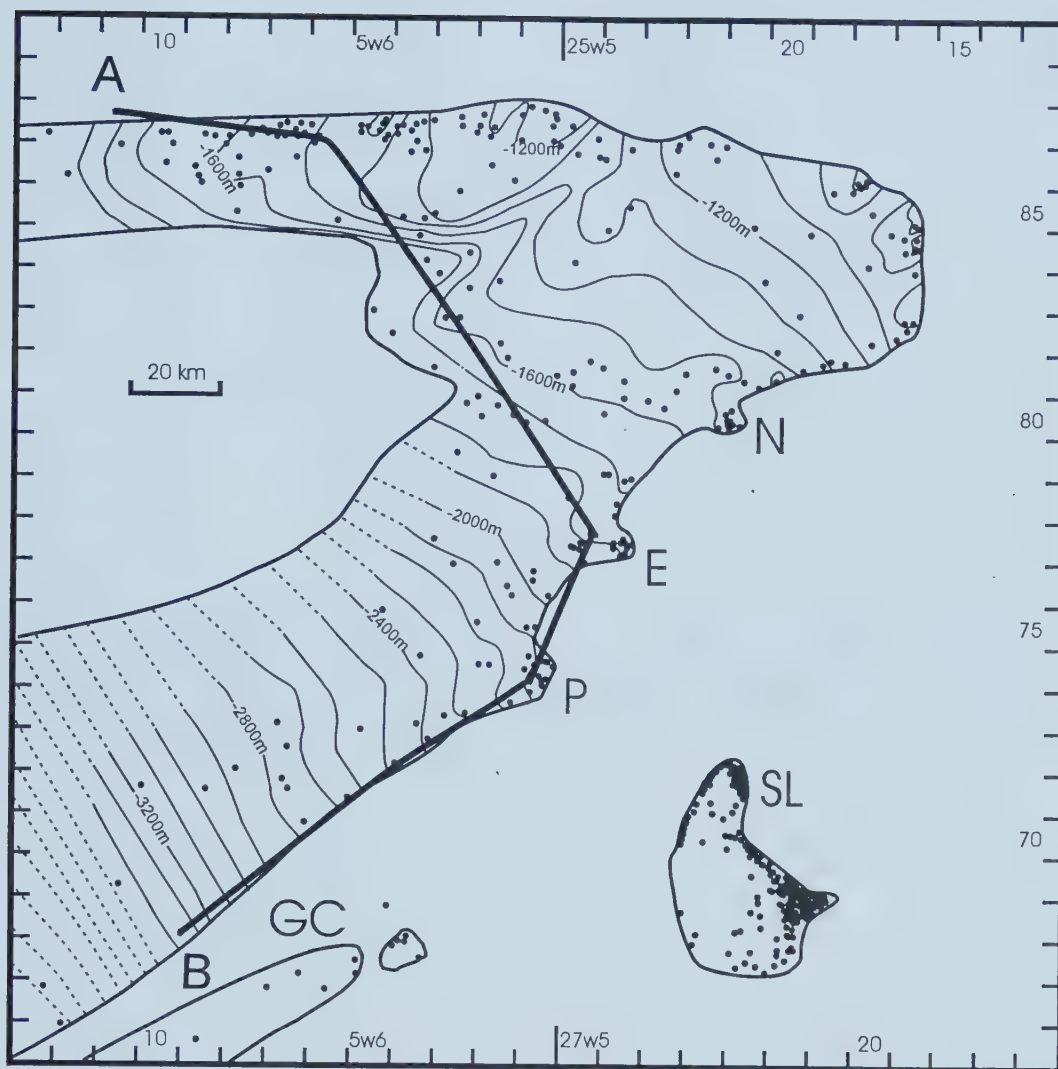
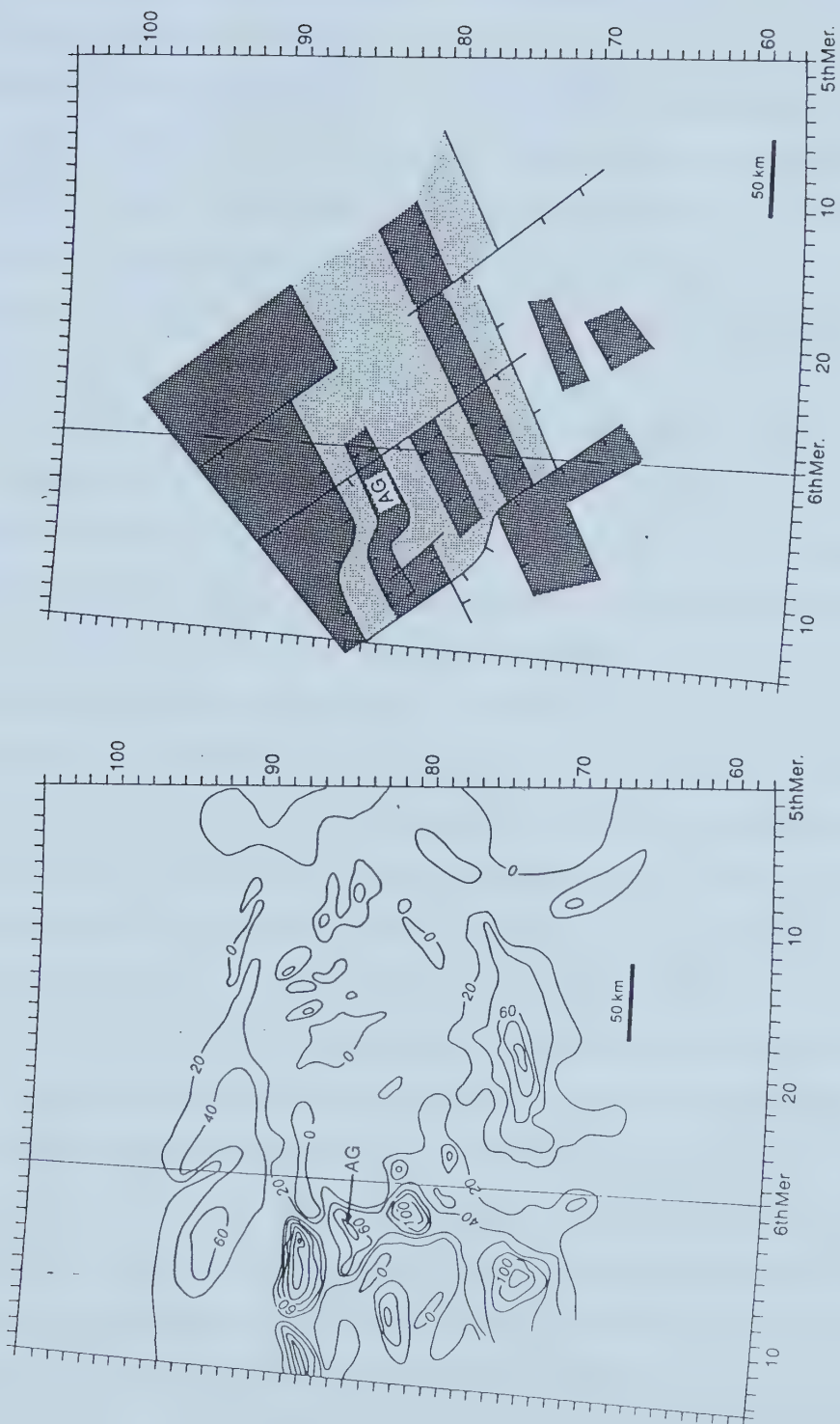


Figure 2.3 – Structural contour map of the Devonian Leduc Formation over the Peace River Arch study area. Contour Interval = 50 m, small black dots are wells that penetrate the Leduc Formation, hydrocarbon fields are noted as P = Puskwaska Field, E = Eaglesham, N = Normandville, GC = Gold Creek, SL = Sturgeon Lake. Cross-section A-B shown in Figure 2.5 is also noted here. Modified after Dix (1990).

Figure 2.4 – a) Isopach map of the Granite Wash Formation indicating where coarse clastic sediments accumulated in fault-bounded depressions. The Axial Graben (AG) shows clearly. b) An interpretive structure diagram of the basement indicating the orientation of major faults (with throws greater than about 40m) over the Peace River Arch. The Axial Graben is labelled AG. From Cant (1988).



Sequence III, lying at the base of the Leduc Formation, has been described by Dix based on geophysical log character only, as there is no core available for petrographic characterization. This unit appears to be composed mainly of argillaceous and arenaceous dolomite, with some relatively clean platform carbonate on the eastern edge of the PRA, interbedded siliciclastics and carbonates along the shoreward margin, and interbedded shales and carbonates along the basinward margin. Sequence III seems to represent a basal transgressive unit, with geophysical data suggesting little relief along the platform margin, analogous to a carbonate ramp setting (Figure 2.5).

The Middle Leduc unit, Sequence II in Dix's 1990 study, documents the greatest vertical aggradation of Leduc sedimentation in this area. This unit is comprised largely of argillaceous and relatively clean platform dolomites, with only localized arenaceous dolomite, and interbedded siliciclastics along its shoreward margin. There are several depositional units within this sequence (Figure 2.5). Dix (1990) suggested that these units might form parasequences as defined by van Wagoner *et al.* (1988). The facies is dominated by shallow water sediments, suggesting that the platform had developed into a shallow rimmed shelf at this time. The carbonates in this unit include peritidal to subtidal wackestone and packstone, laminated to thinly bedded and massive mudstones, and interbedded fossiliferous (stromatoporoid, crinoid, brachiopod) rudstones to floatstones. The latter may represent deeper water shelf sediments and some small organic buildups (patch reefs).

The uppermost Sequence I is composed of basal argillaceous and arenaceous platform dolomites with interbedded siliciclastics, overlain by localized organic buildups and related inter-mound shelf, peritidal, and shoreface strata. This unit represents deposition in a carbonate ramp environment and the maximum back-stepping of the ramp onto the PRA landmass, a concurrent retreat of the basinward margin, and the eventual demise of Leduc reef deposition by the onlap of basinal shales (Figure 2.5). Commonly, Sequence I facies consists of a two-stage deepening upward trend, indicative of an overall transgression. The reef core facies are stromatoporoid, coral, and brachiopod mounds with rudstone, floatstone, and local bindstone textures. Thin, isolated green shale beds are also present, inferring short-term basinal influence.

The majority of the core in the southwest PRA intersects only Sequence I carbonates.

A

B

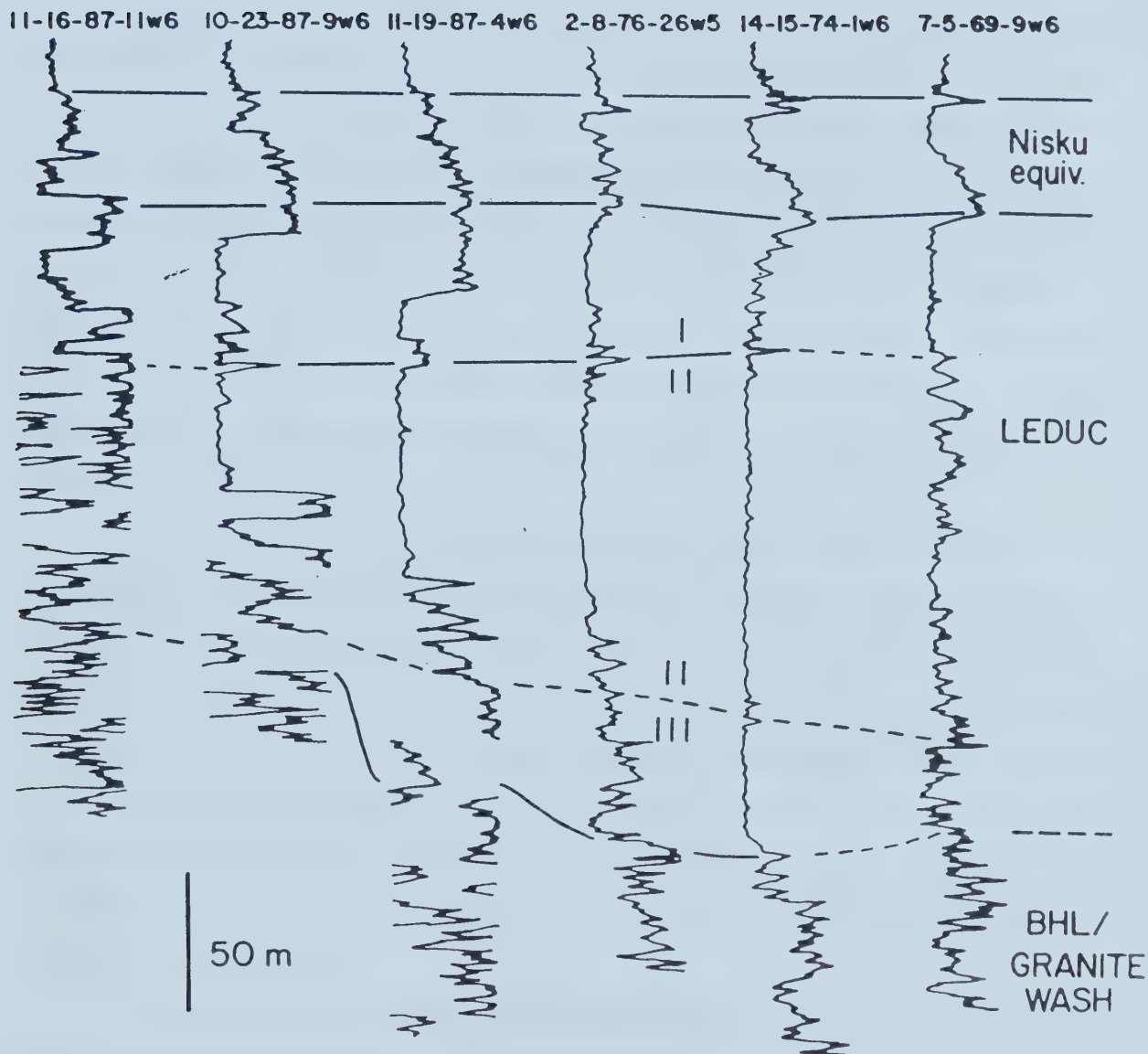


Figure 2.5 – Changing gamma-log characteristics of the three mappable Leduc sequences in the Peace River Arch area. Note the juxtaposition and interfingering of the Granite Wash clastic sediments at wells in Township 87 North.

A few of the cores extend in to Sequence II, however, Sequence III is not cored within the study area. The cores investigated in the present study contain: intertidal to shallow subtidal, lagoon, fore-reef to slope, and deep basin carbonate facies, which have been identified according to Machel and Hunter (1994) and Dunham (1962).

2.1.4 Facies Types

Intertidal to shallow subtidal facies are characterized by buff to light grey dolomitic grainstone and laminated mudstone textures. These are comprised of well-sorted, 1-3 mm coated grains; broken bioclasts, including stromatoporoid, crinoid, solitary coral, and brachiopod debris; and laminated to massive micrite. Sedimentary structures include load and cast structures, occasional burrows, and low angle to horizontal laminations that are common in areas containing abundant micrite. Occasionally green shales are interbedded with grainstones and mudstones, indicating the influence of basin sediment flux during Leduc deposition (Dix, 1990), possibly representing flooding surfaces. Minor moldic, and vuggy to interparticle pore types are found throughout this facies, with an average porosity of about 3% (Figure 2.6).

The most abundant facies observed in the study area is the *lagoonal facies*. It is recognized by light to dark grey, dolomitized *Amphipora* floatstones to rudstones, with lesser amounts of interbedded packstones and wackestones. These dolostones have a very low faunal diversity, dominated by *Amphipora*, with minor amounts of solitary corals, crinoid, brachiopod, and stromatoporoid components. The matrix is commonly micritic, indicating the low energy of the depositional environment. The few sedimentary structures in this facies include occasional geopetal structures, and wavy to horizontal muddy laminations. Porosity varies considerably, from < 1% intercrystalline and minor moldic to 5-7% intercrystalline, moldic, and vuggy porosity (Figure 2.7).

The *fore-reef to slope facies* is the least common facies found in the study area. It is distinguished from other facies by its great faunal diversity, coupled with very poor sorting of grains and angular, broken, detrital, bioclastic material. The main rock types are medium to dark grey dolomitic wackestones and packstones, with lesser amounts of mudstones. Bioclastic components are angular to abraded and include tabular and bulbous stromatoporoid, solitary



Figure 2.6 – Core photographs of *intertidal to shallow subtidal facies*: a) dolomitized fossiliferous grainstone with well-developed moldic (and/or fenestral?) porosity possibly after *Amphipora* ?, b) tight dolomititic grainstone.

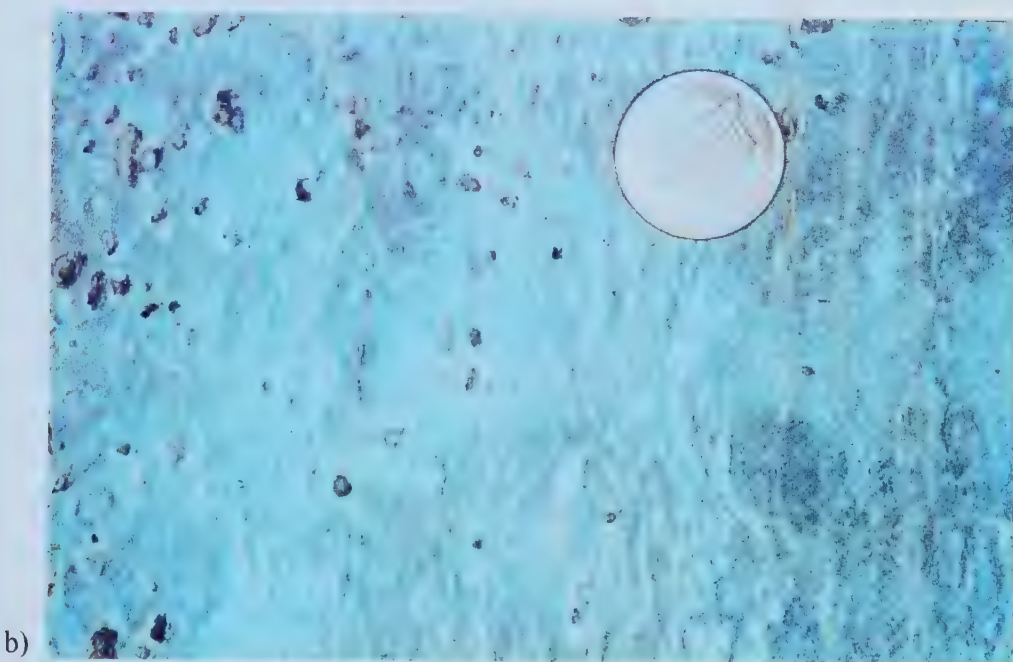


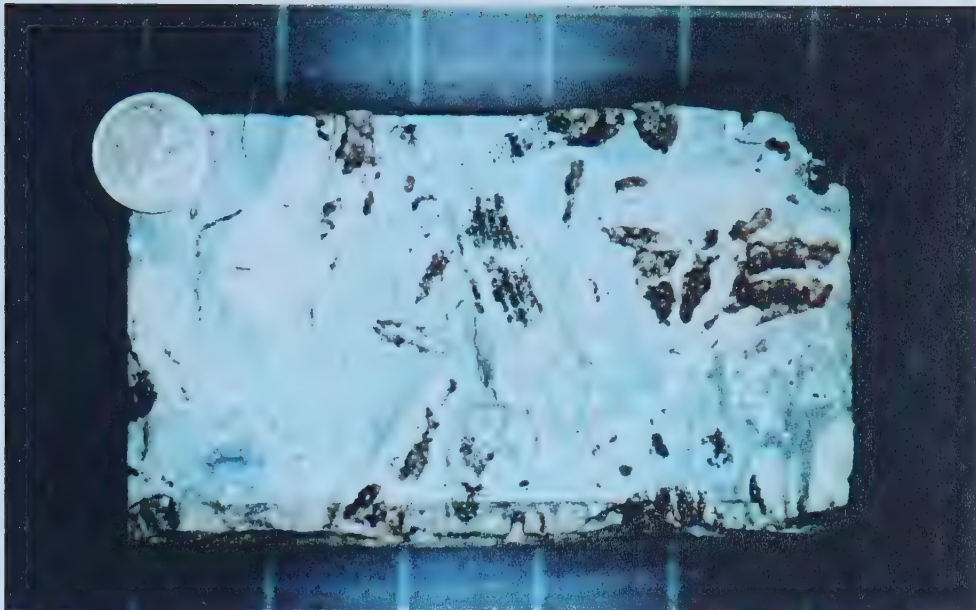
Figure 2.7 – Core photographs of the *lagoonal facies*: a) dark grey *Amphipora* floatstone, and b) close up view of a medium grey *Amphipora* packstone exhibiting moldic porosity.

and colonial corals (most notably *Thamnopora*), crinoids, and brachiopods. The carbonaceous to argillaceous matrix ranges from coarse to finely crystalline. Rare mudstone interbeds occur between the wackestone and packstone zones, with sharp contacts. These zones have less diverse biota, containing only crinoid and brachiopod fragments. Overall porosity ranges from < 1 to 5 %, largely depending on the abundance of bioclastic material. Pore types include moldic, intercrystalline, and vuggy, and less commonly intergranular (Figure 2.8).

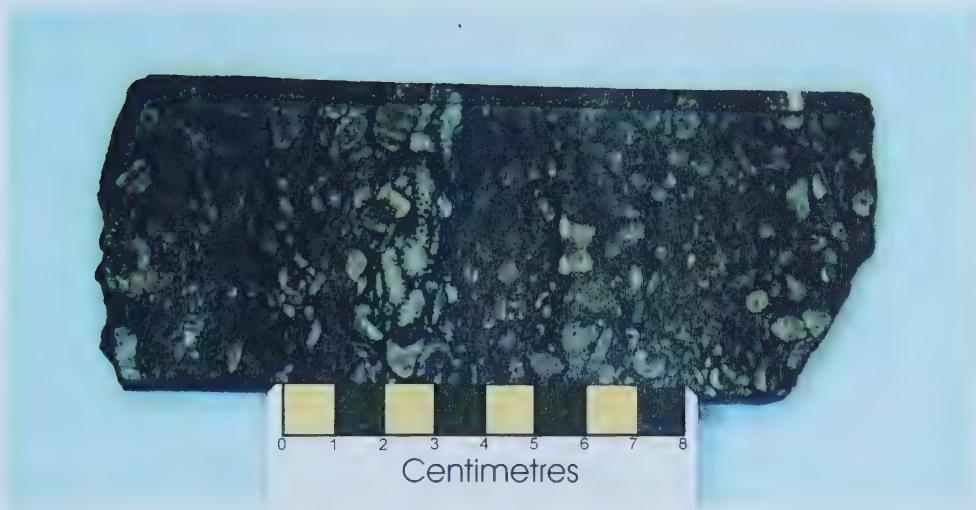
The *slope to basinal facies* is one of the less common facies observed in the study area and tends to be present in those cores that are close to the Leduc platform basinward edge. This facies is made up of medium to dark grey, nodular to thinly bedded, argillaceous carbonate mudstones with a very minor bioclastic component (Figure 2.9). When present, biota includes crinoid fragments and brachiopods. Bedding is low-angle to horizontal, and laminations are common. Some burrows can be seen locally in core where fabrics are well preserved. Porosity is usually < 1% and includes intercrystalline and intergranular pore types. The dark colour and fine grained nature of this facies is representative of a low energy and poorly oxygenated environment.

Brecciated intervals have been noted in all of the facies described above, particularly in wells 04-34-67-04W6, 09-31-71-23W5, 14-23-74-01W6, 01-26-74-01W6, 02-08-76-26W6, and 14-11-77-25W6. Breccias are composed of angular to subrounded, platform-derived dolomite clasts within a muddy matrix (Figure 2.10). They are found mainly in wells that are either close to the basinward edge of the platform, or close to zones where faults are suspected to cross cut the Devonian strata. Dix (1990) inferred that some of these breccias are sedimentary in nature and resulted from syn-depositional slope failure along the platform margin. However, at least some of the breccias could have formed from fault-related movement that occurred post-depositionally. Core for the White Rose *et al.* Smokey River well located at 04-34-74-01W6 contains a thin, fissile shaley zone exhibiting slickensides and a polished surface. However, no brecciated zones were identified in this core.

In summary, although the PRA Leduc Formation has been described in many publications as a "fringing reef" (e.g. Hedinger *et al.*, 1994), no reef facies was seen in the cores investigated in the southwest PRA, Gold Creek, or Sturgeon Lake buildups. The proximity of

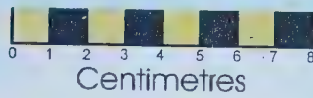
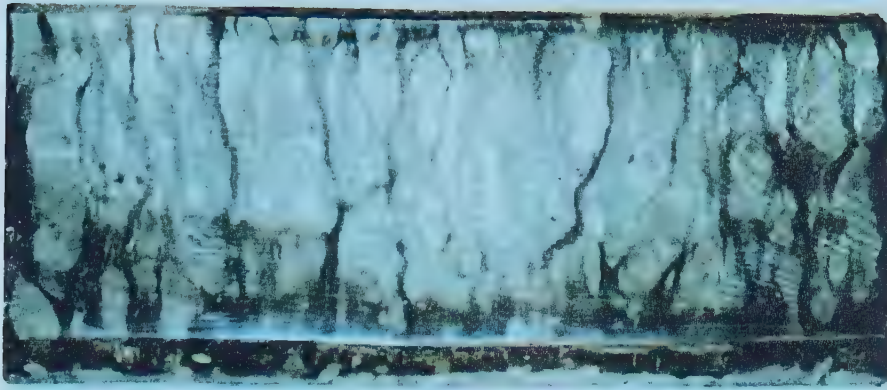


a)

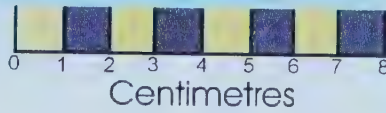
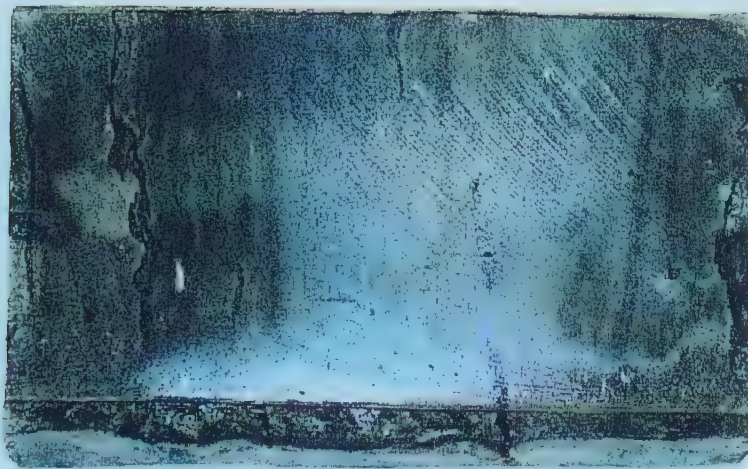


b)

Figure 2.8 – Core photographs, a) and b), of the *fore-reef to slope facies* showing large vuggy and moldic pores after broken bioclastic fragments.



a)



b)

Figure 2.9 – a) *slope* to b) *basinal facies* core photos: a) medium grey nodular dolomitic wackestone, b) dark grey massive dolomitic mudstone.

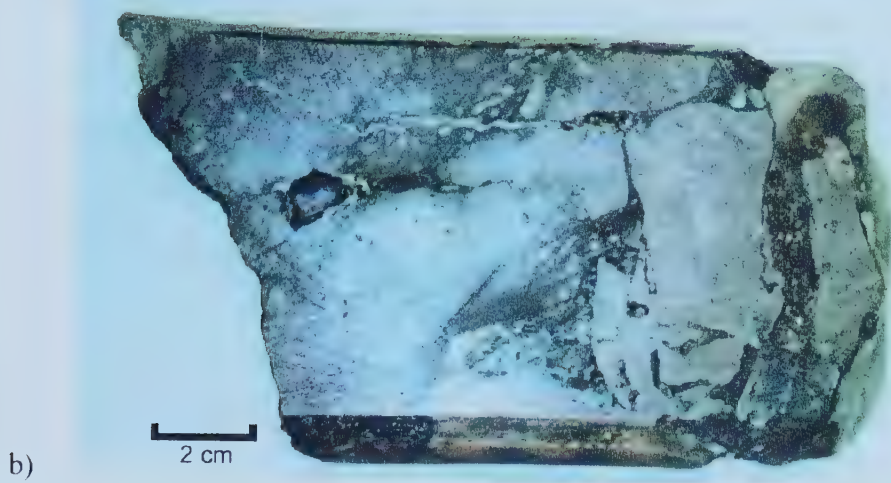


Figure 2.10 – Core photographs of suspected syndepositional breccias in a) well 14-23-70-1W6 and b) well 02-08-76-26W6.

a reef, however, may be inferred by the presence of well-developed back-reef, lagoonal, and fore-reef facies. Stromatoporoid and coral fragments, representing the common reef and mound builders in the Devonian, were observed in several cores. Furthermore, the extent and continuity of the PRA fringing reef facies types cannot be estimated due to the lack of core in the area. Nonetheless, one might imagine that this Devonian fringing reef may have resembled today's modern analogue: the Great Barrier Reef. The PRA Leduc fringing reef complex was likely a discontinuous reef barrier along the basinward edge of a large shallow water carbonate platform.

2.2 Post-Depositional Tectonic Development

In the period lasting from the Middle Cambrian to the Late Devonian, the PRA was transformed from a region of active uplift to a passive, shallow water continental margin setting. The sedimentation history records the gradual onlap and burial of the arch by the beginning of the Mississippian (O'Connell, 1994). High-angle, NW-SE striking faults are well developed in the Normandville, Eaglesham, Puskwaskau, and Sturgeon Lake fields. They cross cut Late Devonian and older strata and may have been conduits for diagenetic and/or hydrothermal fluids (Halbertsma and Meijer-Drees, 1987; Stoakes, 1987; Dix 1990; Mountjoy and Halim-Dihardja, 1991; Packard *et al.*, 1992; Saller and Yaremko, 1994). Movement along the post-Leduc fault lineaments corresponds closely to the underlying Chinhaga-Ksituan basement contact, as well as Precambrian-aged block faults, suggesting an obvious Precambrian influence on the placement of Late Devonian faulting (deMille, 1957; Cant, 1988; O'Connell *et al.*, 1990) (Figure 2.11).

During the Mississippian to the Jurassic, the PRA went through extension, uplift, and eventually subsidence, creating a horst and graben topography over the central axis of the arch. Local syndepositional faults, identified within the Banff and Pekisko Formations, may have been reactivated after Jurassic time to cause further subsidence over the arch (O'Connell, 1994). Isopach maps of the clastics of the Pennsylvanian-aged Stoddard Group and the Permian Belloy Formation reflect a thickening of these sediments of up to 1200 m within the Dawson Creek Graben Complex in the central axis of the PRA (Figure 2.12). The development of the

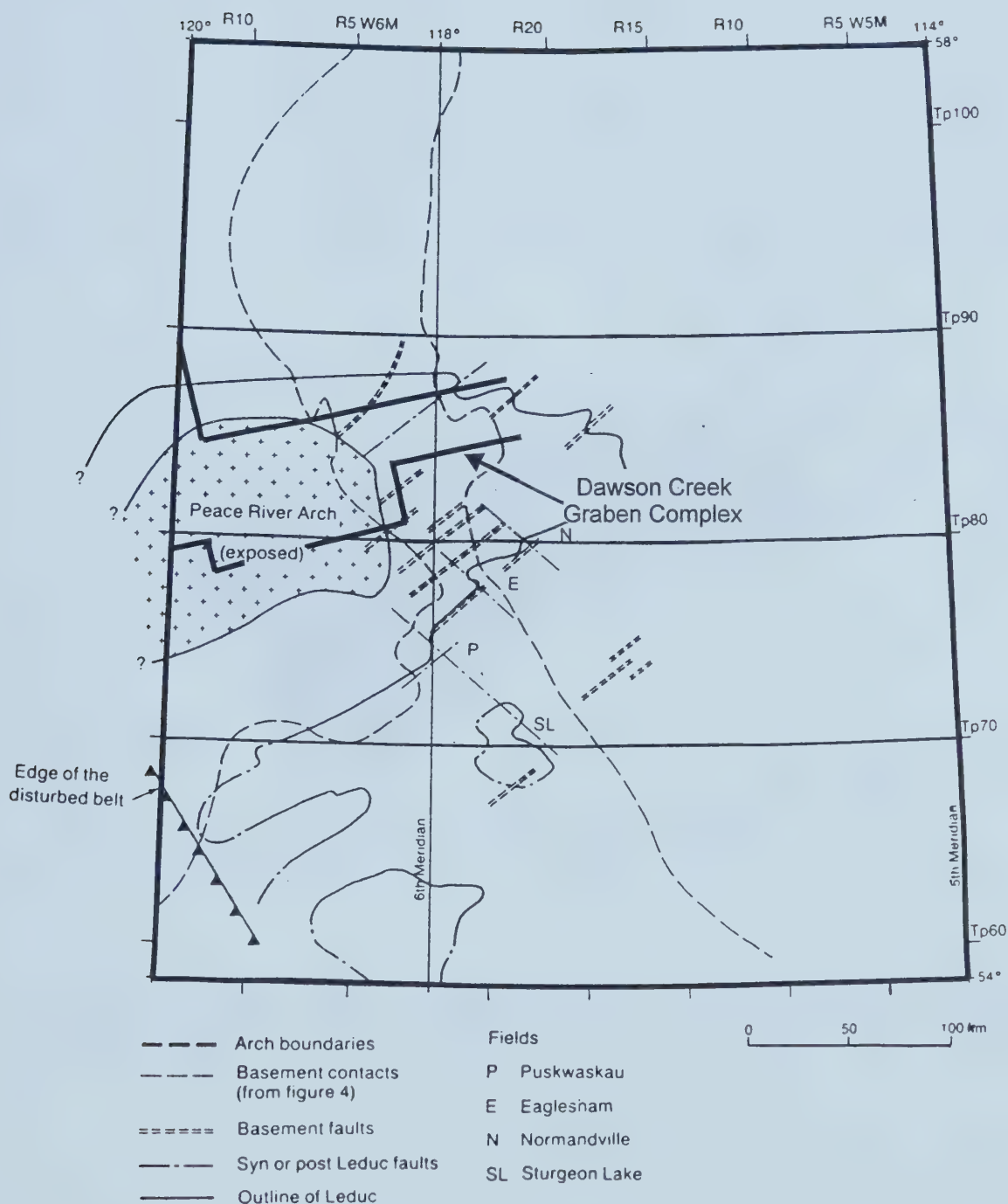


Figure 2.11 – Map showing the locations of Precambrian basement faults, and syn- or post Leduc faults in the Peace River Arch area. The Pennsylvanian-Permian aged Dawson Creek Graben Complex, indicated by thick, solid lines, is shown overlying the arch (O'Connell *et al.*, 1990).

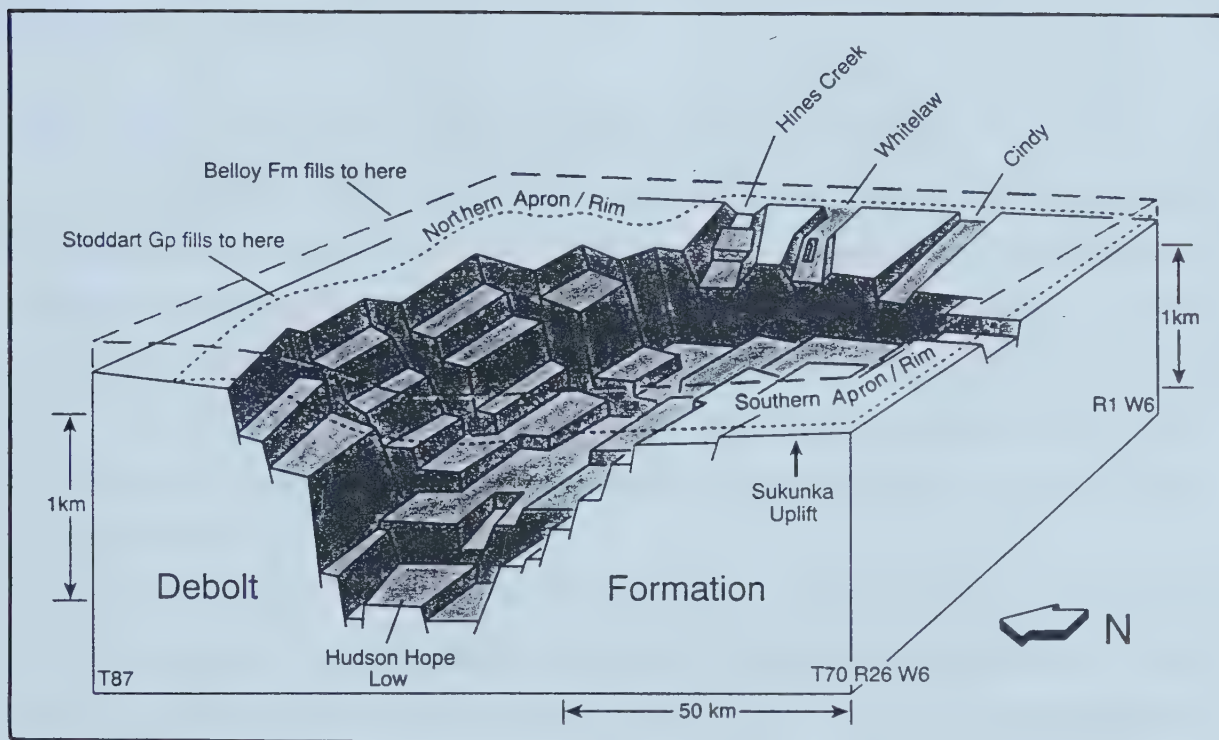


Figure 2.12 – Sketch of the Carboniferous-Permian Dawson Creek Graben Complex highlighting successive infilling of the structural lows by the Stoddart Group and Belloy Formation. Modified from Barclay *et al.* (1990).

Dawson Creek Graben Complex signifies the presence of a local extensional tectonic regime throughout the Pennsylvanian and Permian (O'Connell *et al.*, 1990).

Throughout the Jurassic and Cretaceous, the PRA went through a time of subsidence due to tectonic loading during the Laramide Orogeny. Subsidence appears to have been accommodated by the faults that formed during the Carboniferous, yet not by the older lineaments (O'Connell, 1994). No major fault offsets have been detected on maps of post-Palaeozoic sediments (Cant, 1988).

2.3 Source Rocks, Hydrogeology, and Possible Migration Pathways

Oil and gas in the PRA area are being produced from reservoirs ranging in age from the Middle Devonian through to the Lower Cretaceous. Abundant hydrocarbon source rocks are also found throughout the sedimentary succession (Figure 2.13). Within the PRA area, several studies have attempted to characterize the subsurface hydrogeologic regime on a regional scale (e.g. Toth, 1978; Hitchon, 1990; Hitchon *et al.*, 1990; Bachu and Underschultz, 1992). However, these studies lack the detail required to trace past and present fluid flow locally in the southwest PRA.

The stratigraphic units in the PRA area have been divided into three general hydrostratigraphic groups, made up of complex successions of aquifers (strata that are able to transmit fluids readily), aquitards (strata that retard, but do not prevent the transmission of fluids), and aquicludes (strata that effectively block the transmission of fluids) (Hitchon *et al.*, 1990) (Figure 2.14). The three hydrostratigraphic groups, from oldest to youngest, are as follows: 1) lower Palaeozoic, 2) upper Palaeozoic-lower Mesozoic, and 3) upper Mesozoic-Cenozoic. At the base of the entire sedimentary section is the Precambrian crystalline basement complex, which is assumed to be an aquiclude. The three hydrogeological groups are separated by three regionally extensive aquitards: the Muskeg-Watt Mountain Aquitard, the Ireton Aquitard, and the Clearwater-Wilrich Aquitard. This study concentrates on the lower Palaeozoic hydrogeologic group.

The two main aquicludes within the study area, other than the Precambrian, are the Lower Devonian Aquiclude and the Fort Vermillion Formation. The Lower Devonian

Stratigraphy				Source Rock and Hydrocarbon Type	Initial Volume in Place 10 ⁹ m ³	
System	Group	Formation				
Tertiary		Paskapoo				
Cretaceous	U	Smoky	Wapiti			
			Puskwaskau			
			Bad Heart			
			Muskiki			
			Cardium			
			Kaskapau			
	L	Fort St. John	Dunvegan			
			Shaftesbury			
			Peace River	Paddy	Gas	51.54
				Harmon		
			Split River	Notikewan		
				Falher		
			Wilinch			
			Bullhead	Bluesky	Tar Sands	14.6
Gething						
		Cadomin				
Jurassic	Femie	Nordegg				
Triassic	Schooler Creek	Baldonnel				
		Charlie Lake				
		Halfway				
Permian		Diaber				
Mississippian		Stoddart	Belloy			
			Taylor Flat			
			Kiskatinaw			
		Rundle	Golata			
			Debolt			
	Shunda					
		Pekisko				
		Banff				
		Exshaw				
	Devonian	U	Wabamun			
Winterburn						
Woodbend			Grosmont	Ireton	Tar Sands	>100
			Leduc			
			Cooking Lake			
Beaverhill Lake		Swan Hills	Waterways	Oil and Gas	0.727 + 107.	
		Slave Point				
		Ft. Vermilion				
M		U	Gilwood	Watt Mtn.	Oil	0.240
			Muskeg			
			Keg River			
			Contact Rapids			
L		L	Red Beds	Granite Wash		
			Ernestina Lake			
	Lotsberg					
Cambrian		Red Beds				
PC						

Source Rock

Major Hydrocarbon Resources



Source Rock



Major Hydrocarbon Resources

Figure 2.13 – Stratigraphic column illustrating the correlation between formations, source rocks, reservoirs, and reserves in place in the Peace River Arch area. From Bachu and Cao, (1992).

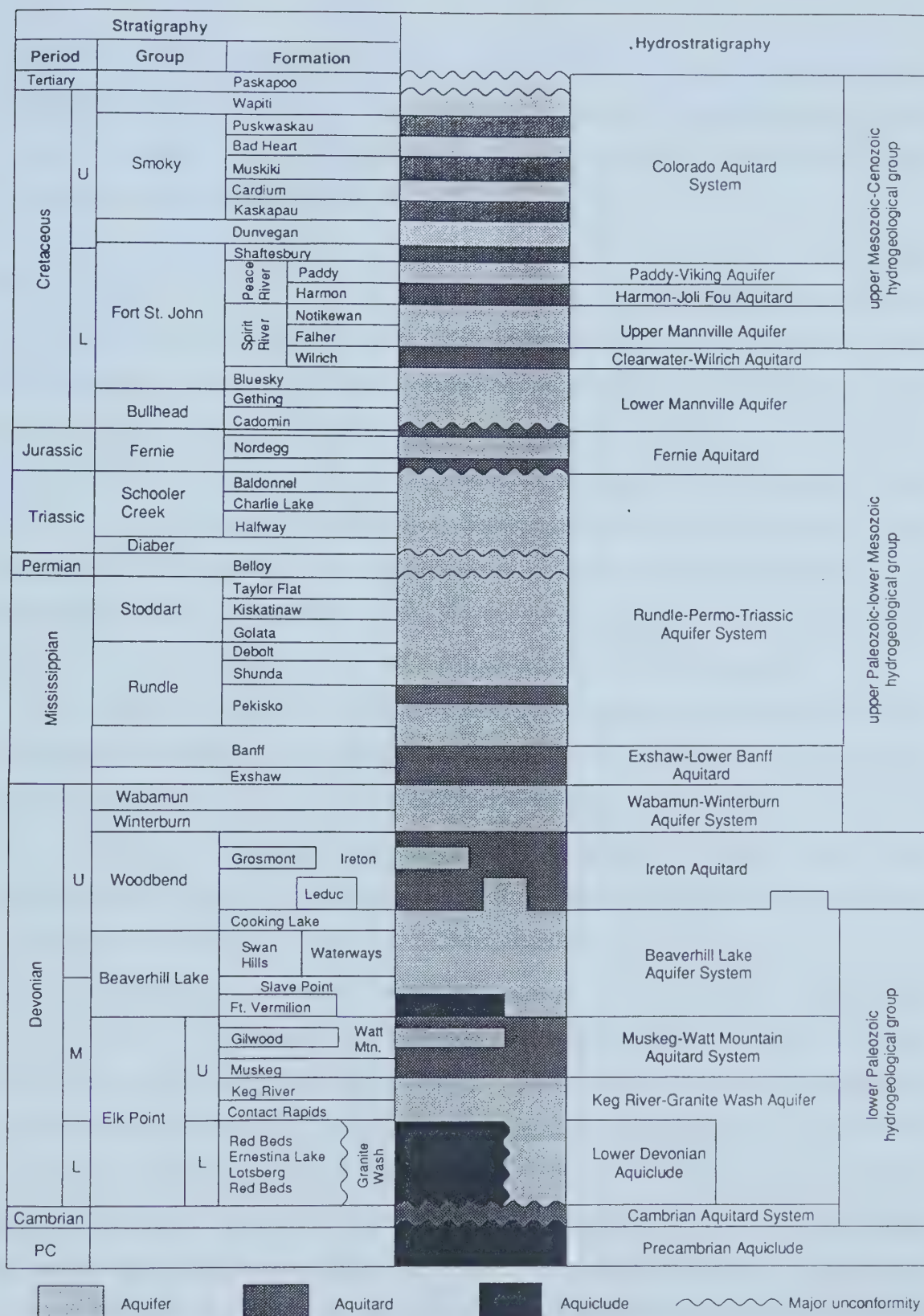


Figure 2.14 – Hydrostratigraphy in the PRA area. The main unit of interest for this study is the lower Paleozoic hydrogeological group (Hitchon *et al.*, 1990).

Aquiclude encompasses the Lower Elk Point Group, which includes halite beds (Hitchon *et al.*, 1989). Where present, the Elk Point salt beds, or any other evaporitic sequences in the stratigraphic column, have a significant effect on increasing the salinity of the formation waters in the adjacent strata (Hitchon *et al.*, 1990).

In the study area, the basal aquifer lying directly above the Precambrian is the Granite Wash Formation (Hitchon *et al.*, 1990). Sedimentological studies by Dix (1990) and Dunham *et al.* (1983) have shown that the Granite Wash lies beneath, and interfingers with, the Leduc and underlying formations along the shoreward edge of the PRA. One can therefore assume lateral and vertical hydrologic continuity between the Granite Wash and the directly overlying units. This package forms the Keg River-Granite Wash Aquifer, the first hydrologic system on top of the Precambrian. This system is separated from the overlying system by the Muskeg-Watt Mountain Aquitard (Figure 2.14). As previously stated, the Beaverhill Lake Group and the overlying Leduc Formation have vertical hydrological continuity and have, therefore, been grouped together by Hitchon *et al.* (1990) to form the Beaverhill Lake Aquifer.

In addition to the two principal Devonian aquifer systems in the study area, it should be noted that the complex tectonic history plays an important hydrogeological role in the PRA area. Pre-, syn-, and post-Leduc faulting and fracturing likely contributed to sub-vertical cross-formational fluid flow, channelling saline formation fluids up and meteoric surface waters down through the sedimentary column. The presence of late stage diagenetic cements in both the Leduc and the overlying Wabamun Formations suggests that post-Wabamun aged fault and fracture systems have also contributed to the fluid systems within the study area (Mountjoy and Halim-Dihardja, 1991; Packard *et al.*, 1990; Dix, 1993). Furthermore, hydrocarbon migration within the area has also been affected by faulting, such that some Devonian reservoirs contain hydrocarbons sourced from a stratigraphically higher level (Creany and Allen, 1989). Therefore, it is quite probable that the various stages of structural development of the PRA have added to the complexity of palaeo-fluid flow pathways within the study area, and cross-formational fluid flow should be taken into account when discerning the diagenetic history of the PRA Leduc Formation. In the following chapters, sedimentological and geochemical evidence from the PRA Leduc Formation will further illustrate the complexity of the diagenetic

fluids, their origins, and the probable migration pathways of aqueous and petroliferous fluids within the study area.

CHAPTER 3

PETROGRAPHY OF DIAGENETIC FABRICS IN THE LEDUC FORMATION

This chapter introduces the diagenetic history of the PRA Leduc. Some observations made by Dix in his 1993 study are also included to compare the study areas, as they overlap to some extent. The data presented here represent the first detailed diagenetic study of late-stage cements that links the southwest PRA, Gold Creek and northernmost Sturgeon Lake Leduc platforms.

The diagenetic and paragenetic history has been determined through detailed core, thin section, and geochemical analysis. Emphasis in this chapter has been placed on the detailed petrographic characteristics of the diagenetic phases. Geochemical data are presented in the following chapter, and a synopsis and discussion of petrographic and geochemical data is presented in Chapters 4 & 5.

Many of the diagenetic phases in the PRA Leduc are similar to those identified by Dix (1993), and Packard *et al.* (1990) in the Leduc and Wabamun Formations to the northeast of the study area. They are presented here in a paragenetic sequence, whereby there is temporal overlap between some cement phases (Figure 3.1).

The methods used to identify and describe diagenetic phases include detailed core and thin section petrography, transmitted light (plane and crossed polarizers) microscopy, cathodoluminescence (CL) microscopy, and observation under ultraviolet light.

Cathodoluminescence microscopy was performed on an Olympus BH-2 microscope with an ELM-3R lumiscope vacuum attachment. Running conditions varied from 30-50 torr, 10-15 kV, and 0.5 mA.

Observation of some samples under ultraviolet (UV) light ($\lambda \sim 10\text{-}400\text{ nm}$) was used to screen samples for the presence of fluorite. Both short and long wavelength UV lamps were used. Fluorite was not present in thin sections due to the rubbly nature of the core where it was found. Furthermore, it was clear and colourless, making it difficult to readily identify in hand samples.

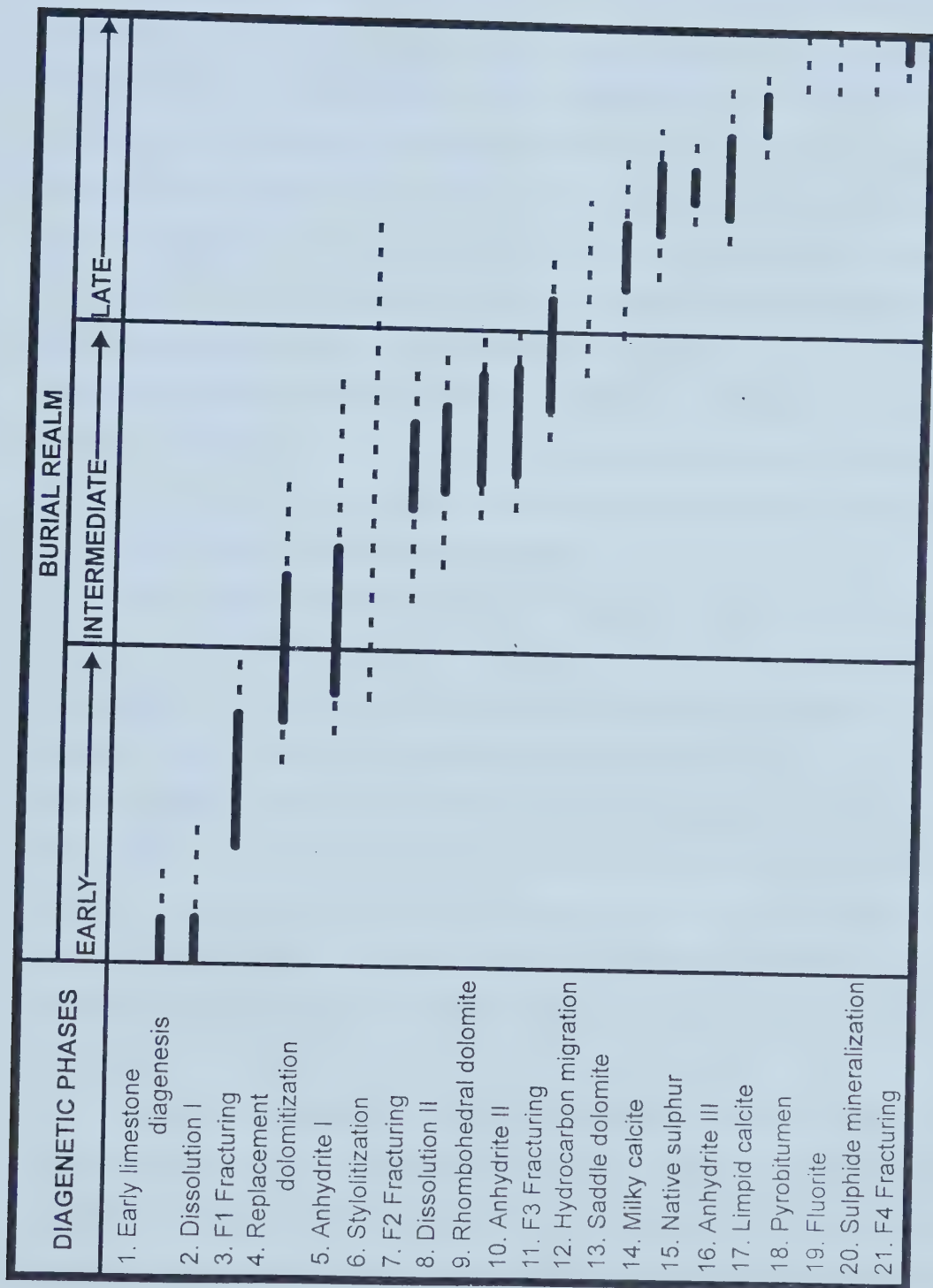


Figure 3.1 – Paragenetic sequence. Uncertainty in the range of an event or mineral phase is indicated by a dashed line.

3.1 Petrography of Diagenetic Phases

3.1.1 Limestones

Limestones are rare in the study area. They have been found only along the northernmost edge of the Sturgeon Lake platform at well 09-31-71-23/W5, and interbedded with dolostones in the Puskwaskau Field, in particular well 14-23-74-01/W6. The main lithologies are wackestone, packstone and grainstone. They are composed of coated grains, bioclastic coral, brachiopod, echinoderm, and crinoid fragments in a micrite matrix. Coated grains are replaced by fine to medium grained blocky, anhedral calcite in many locations. In some intervals, dolomite partially replaced the matrix in irregular patches. The limestone units were not a major focus of this study, as they comprise a very small part of the database and their early diagenesis is not relevant to the objectives of this study. However, early stage diagenesis, including compaction, lithification, and neomorphism, of the original limestone likely occurred prior to replacement by dolomite (*i.e.*, James and Choquette, 1990).

3.1.2 Matrix-replacement dolomites

Matrix-replacive dolomites are the most abundant diagenetic phase in the study area, making up at least 70% of all phases by volume and affecting all limestone. In most wells, replacement dolomitization has been pervasive, and is also a porosity-enhancing phase (Amthor *et al.*, 1994). Four predominant types of matrix-replacive dolomite, and one composite type, were identified. Matrix-replacive dolomites did not show any significant differences in colour when viewed with cathodoluminescence (CL) microscopy. Matrix-replacive dolomites occur as five distinct types, M1-M5, and are classified according to Sibley and Gregg (1987), using both crystal size distribution (unimodal or polymodal) and crystal boundary shape (planar-e [euhedral] or planar-s [subhedral] or nonplanar) to describe the textures.

M1: Fine to medium crystalline (100-200 μm), unimodal, nonplanar dolomite, brown to medium grey in hand sample, forming a mosaic of densely packed, anhedral crystals with sharp extinction (Figure 3.2a). M1 has poorly developed intercrystalline porosity. CL microscopy reveals a uniform, dull red colour throughout M1 dolomite.

M2: Fine to medium crystalline (100-200 μm), unimodal planar-s (e) dolomite,

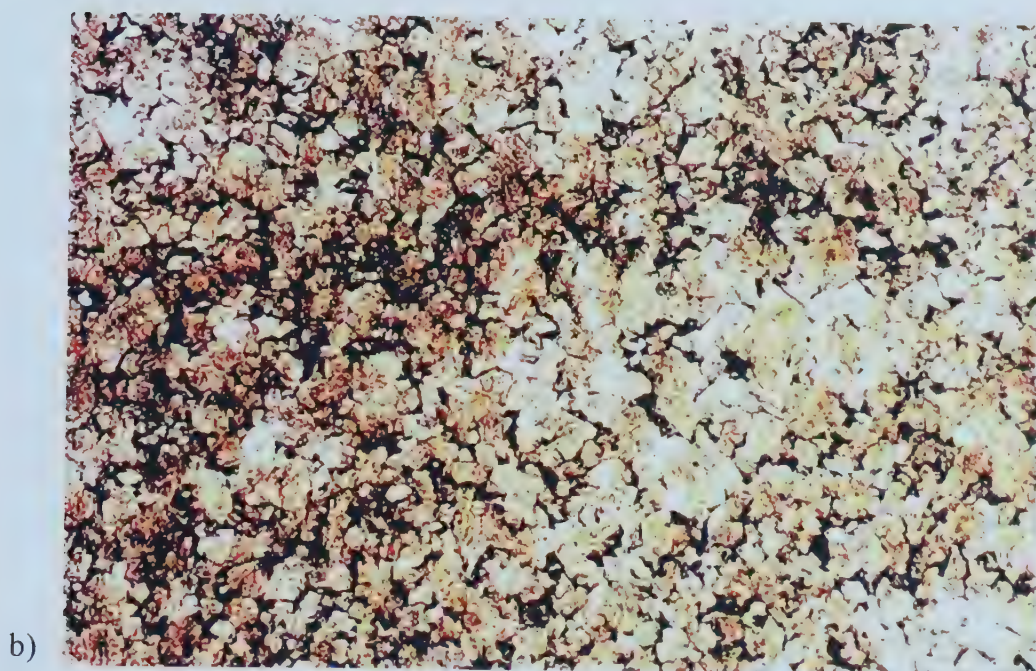


Figure 3.2 – Photomicrographs of different types of matrix-replacive dolomite a) M1, b) M2. Both are shown here in crossed polarizers and have a field of view of 5.5 mm. Note the opaque, black intercrystalline bitumen in b) M2 dolomite.

brown to medium grey in hand sample, forming a loosely packed mosaic of subhedral to euhedral crystals with sharp extinction. Crystals with well-developed faces have distinct cleavage traces. Oil staining is common throughout M2 dolomite, giving the matrix a brown colour when present and indicating the presence of intercrystalline porosity (Figure 3.2b). In addition, M2 dolomite commonly has well-developed vuggy and moldic porosity. M2 dolomite appears dull red with CL microscopy, and ghost textures of coated grains and fine-grained bioclastic material are evident. M2 dolomite cannot be easily distinguished from M1 dolomite either in hand sample, or with CL microscopy. However, these types can be distinguished based on crystal boundary shape (as described by Sibley and Gregg, 1987). M1 dolomite is non-planar, whereas M2 dolomite is planar.

M3: Medium to coarse crystalline (250-500 μm), unimodal planar-s to nonplanar, light brown to grey in hand sample, forming a densely packed mosaic of subhedral crystals with sharp extinction (Figure 3.3a). Crystals with well-developed faces have visible cleavage traces. Intercrystalline porosity is low in M3 matrices, but vuggy and some moldic porosity lined with late-stage cements are common throughout. M3 matrix dolomite destroys all precursor limestone textures. Cathodoluminescence exhibits a dull red colour with local orange-red coloured rims on larger crystals.

M4: Coarse crystalline (>400 μm), unimodal planar-s to nonplanar, grey dolomite with sharp extinction. This is the least common matrix-replacive dolomite identified in the study area. It typically occurs in zones near to M3 dolomite, and is only distinguished because of its coarser crystal size. Thus, M4 dolomite may be a variety of M3 dolomite (Figure 3.3b).

M5: A polymodal mixture of both M2 and M4 dolomites (Figure 3.3c). M5 dolomite may be a transitional type between these two end members. Original textures are completely obliterated in cores with M5 dolomite. Intercrystalline porosity is well developed, and oil staining is common in finer grained (100-200 μm) areas comprised of M2 dolomite rather than the coarser (>400 μm) M4 zones. Enhanced vuggy porosity and late-stage cements are also associated with M5 dolomite. Cathodoluminescence shows a dull red to slightly orange-red colour, similar to that of M3 dolomite.

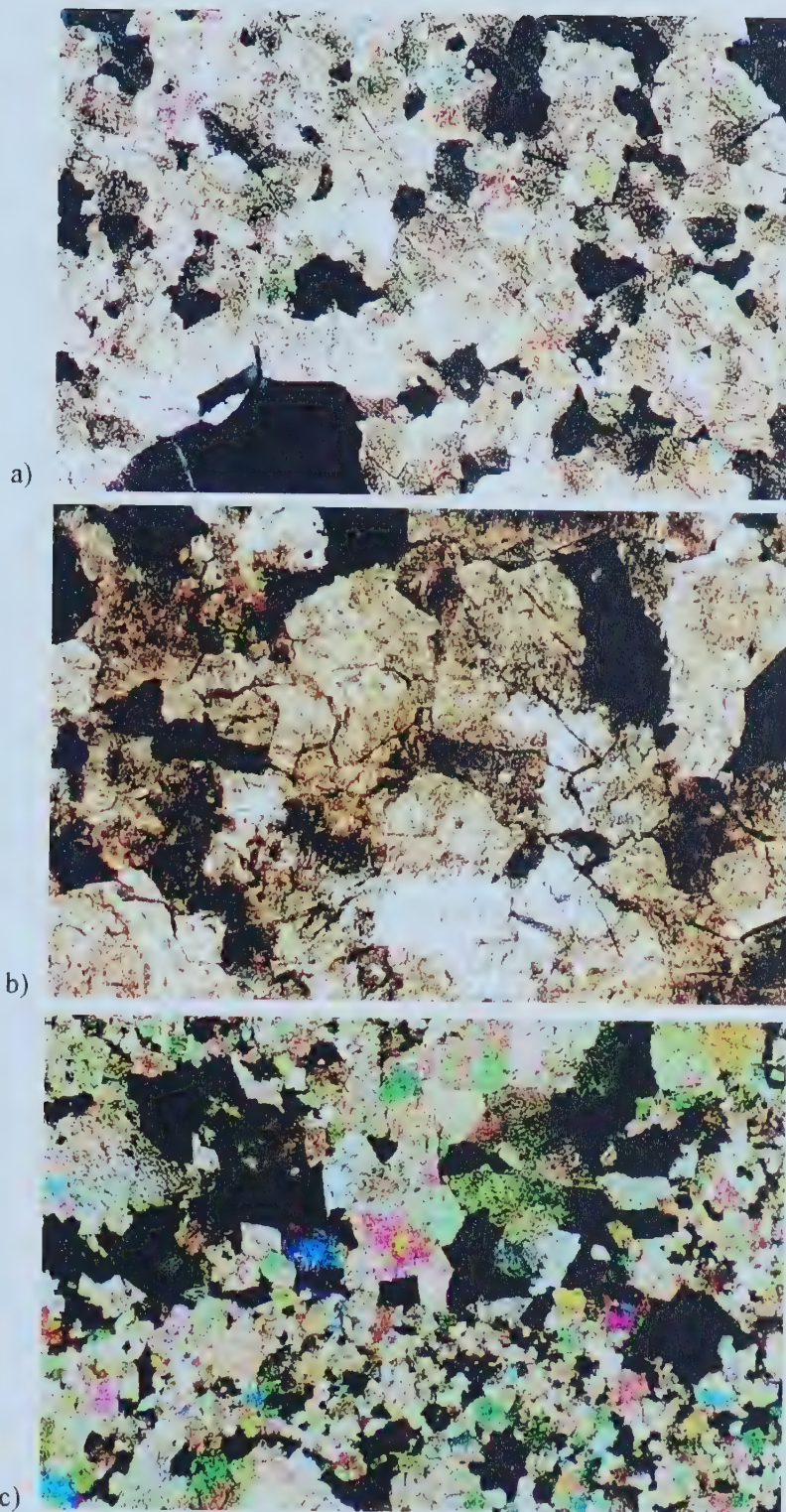


Figure 3.3 – Photomicrographs of matrix-replacive dolomite types a) M3, b) M4, and c) M5. Photos are in crossed polarizers and the field of view is 5.5 mm.

3.1.3 Dolomite cements

Void-filling dolomite cements are a common, but relatively small part of the total diagenetic phases in the study area (≤ 10 vol.%). They are found in almost every core, and post-date all matrix-replacive phases. Two void-filling phases have been identified, with only subtle differences distinguishing the two. However, cathodoluminescence microscopy reveals notable differences between void-filling dolomite and matrix replacive dolomite phases.

Rhombohedral Dolomite: Medium to very coarse crystalline (0.5-6 mm), unimodal planar-e, white to light beige, subhedral and euhedral dolomite rhombohedra with sharp extinction. Rhombohedral dolomite coats macroscopic pore space as a 1-6 mm thick lining, infills thin, 1-2 mm wide fractures, or occurs as single rhombs floating within the finer grained matrix (usually M2) (Figure 3.4a). This is the less common of the two void-filling dolomite types. Its crystals have distinct cleavage traces, and are zoned when viewed in hand sample under magnification, and with CL microscopy. Crystal boundaries between rhombohedral dolomite and all other diagenetic phases are sharp and clear. This dolomite cement only partially occludes porosity in the study area. Crystals have a notable sulphurous odour when crushed for geochemical analysis, and some are associated with black pyrobitumen that coats intercrystalline porosity. Rhombohedral dolomite occurs as the only cement phase, or may be associated with later-stage dolomite, calcite, or anhydrite cements. Its cathodoluminescence ranges from dark red-brown to bright orange zones within individual crystals (Figure 3.4b).

Saddle Dolomite: Coarse to very coarse crystalline (2-6 mm), unimodal non-planar, white to brown, saddle-shaped dolomite with sweeping extinction, comprising 65 vol.% of all dolomite cements. Saddle-shaped crystals have well-developed cleavage traces (Figure 3.5a). Up to 3 stages of zoning may be visible in hand sample, thin section, and with CL microscopy. This dolomite type occurs as the only cement phase lining pores, grown on top of rhombohedral dolomite, or associated with later-stage calcite and anhydrite cements. Crystal boundaries between saddle dolomite and other diagenetic phases are sharp and clear. Saddle dolomite only partially occludes porosity, but when in combination with other



Figure 3.4 – Photomicrographs of rhombohedral dolomite cement shown here in a) crossed polarizers and b) under cathodoluminescence. Note that dolomite precedes limpid calcite cement (pink) in a) and is shown lining open pore space (black) in b). Both fields of view are 5.5 mm.

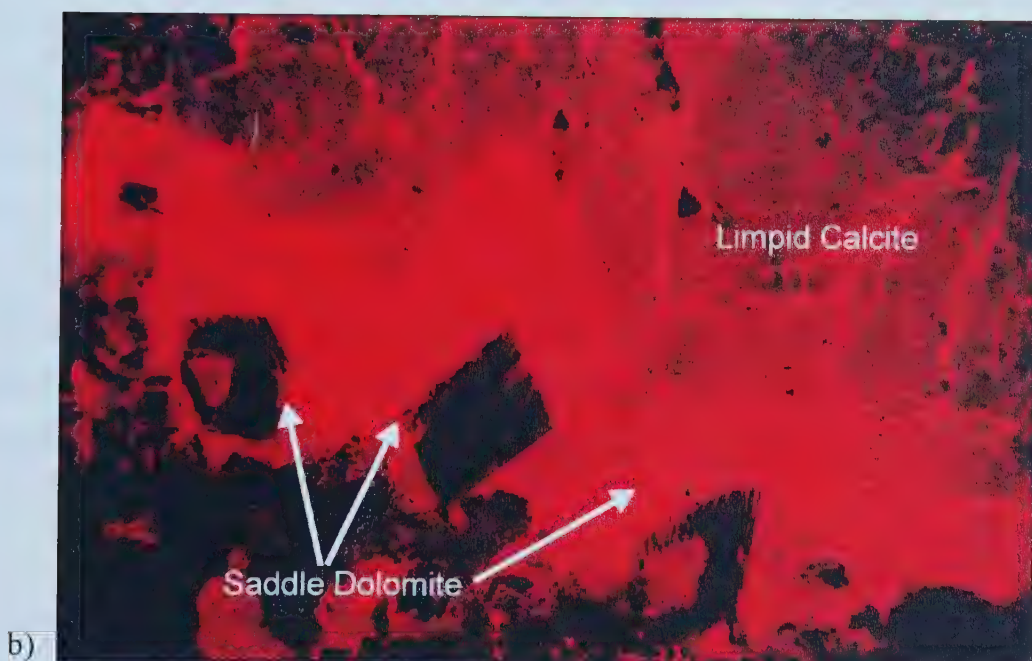


Figure 3.5 – Photomicrographs of saddle dolomite cement shown here in a) plane-polarized light and b) under cathodoluminescence. Note the curved faces and cleavage traces on brown crystals lining a large solution-enhanced vug in a). Dolomite crystals in b) are zoned with dark coloured cores and are shown here preceding limpid calcite. Note that saddle dolomite crystals have a slightly brighter cathodoluminescence than the surrounding calcite. Field of view in both is 5.5 mm.

cements, porosity is greatly reduced. Crystals have a notable sulphurous or hydrocarbon odour upon crushing for geochemical analysis, and some are associated with black bitumen that coats and infills between crystals in pores. Cathodoluminescence reveals dark red-brown to bright orange-red zones within crystals (Figure 3.5b).

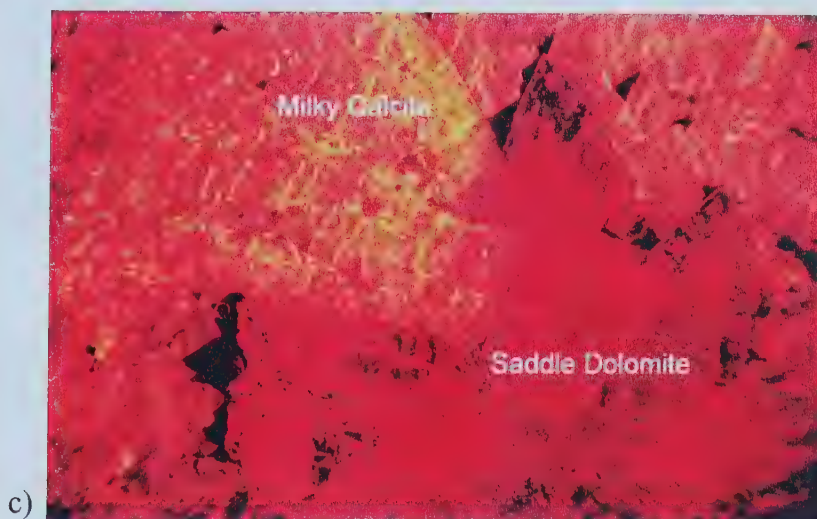
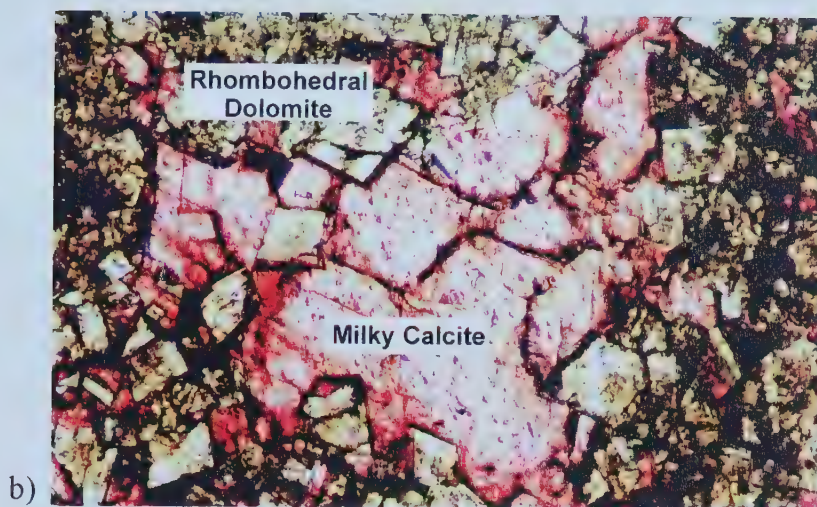
3.1.4 Calcite cements

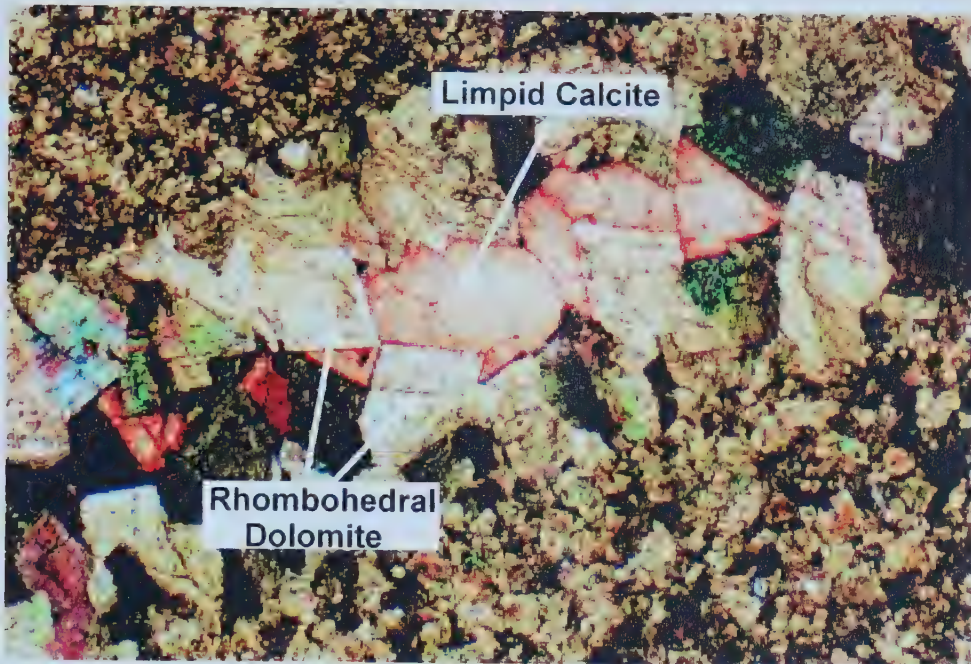
Calcite cements comprise approximately 10% of all cements by volume in the study area. Two types of calcite cement have been identified, based on crystal size, habit, and lithological associations. It is difficult to determine when these two phases formed relative to one another, but both calcite phases post-date all dolomite phases (matrix and void-filling) and can be distinguished from dolomite phases by their cathodoluminescence orange-gold colour.

Milky Calcite: Very coarsely crystalline (7-30 mm), milky white, massive and anhedral blocky, inclusion-rich calcite crystals with sharp extinction, occurring as late-stage cement in large vugs (Figure 3.6a, b) and in fractures. Milky calcite does not occur together with limpid calcite, but is commonly associated with both phases of dolomite cement, as well as minor anhydrite, and is the only phase associated with late-stage fluorite. Milky calcite is the most abundant calcite cement in the study area by volume (70%), but it is restricted to the southwest corner of the study area. Cleavage traces and lamellae are visible in thin section, and crystal boundaries between milky calcite and all other diagenetic phases are sharp and clear. Cathodoluminescence is light orange-gold and uniform with no zonation (Figure 3.6c). Milky calcite has a notable sulphurous smell upon drilling and crushing for geochemical analysis.

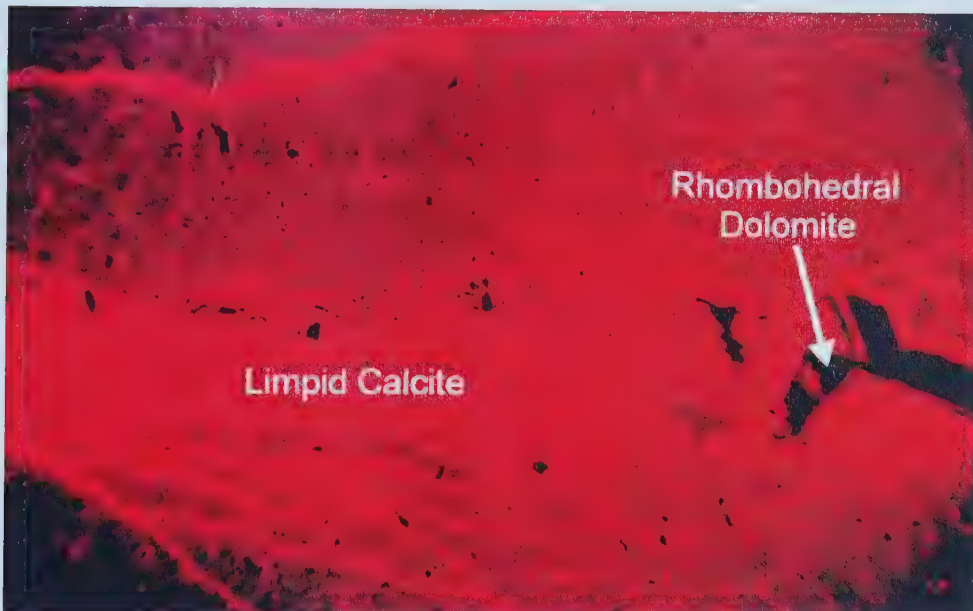
Limpid Calcite: Coarse crystalline (1-10 mm), white to transparent, euhedral to anhedral blocky, inclusion-poor calcite crystals with sharp extinction. Limpid crystals occur as 1) anhedral masses filling thin (1-3 mm wide) fractures or veins; 2) blocky, anhedral to subhedral cement filling shelter and intercrystalline porosity within fine grained (M2) dolomite matrices; or 3) as single, euhedral crystals (up to 4 mm) filling large solution vugs as late-stage cement post-dating dolomite (Figure 3.7a). Limpid calcite comprises about 30 vol.% of all calcite cements and is found throughout the study area. Cleavage traces are

Figure 3.6 – Milky calcite cements. a) Core photo showing white milky calcite completely infilling a vug in well 12-22-66-06W6. b) Photomicrograph in plane polarized light showing inclusion-rich milky calcite (pink) as the last cement phase after rhombohedral dolomite infilling pore space. Field of view is 5.5 mm. c) CL photomicrograph showing saddle dolomite cement (red) and coarsely crystalline milky calcite cement (orange). Field of view is 5.5 mm.





a)



b)

Figure 3.7 – Limpid calcite cements. a) Photomicrograph in crossed polarizers showing limpid calcite (pink) infilling a vug after rhombohedral dolomite. Note the lack of fluid inclusions in the calcite. Field of view is 5.5 mm. b) CL photomicrograph showing dark red matrix dolomite cement and brighter red limpid calcite cement infilling a fracture. Field of view is 5.5 mm.

visible in thin section when crystals are well developed. Crystal boundaries between limpid calcite and all other diagenetic phases are sharp and clear. Cathodoluminescence is bright red and uniform with no zonation (Figure 3.7b) and is slightly brighter than that of milky calcite. Limpid calcite cement is associated with all cement types except fluorite. There is a notable sulphurous smell upon crushing samples of limpid calcite for geochemical analysis.

3.1.5 Anhydrite cement phases

Anhydrite is widespread throughout the study area and is the most abundant cement phase. No primary nodular anhydrite was observed in the Leduc Formation. However, to the eastern end of the study area, primary anhydrite and evaporitic facies occur in the overlying Nisku Formation.

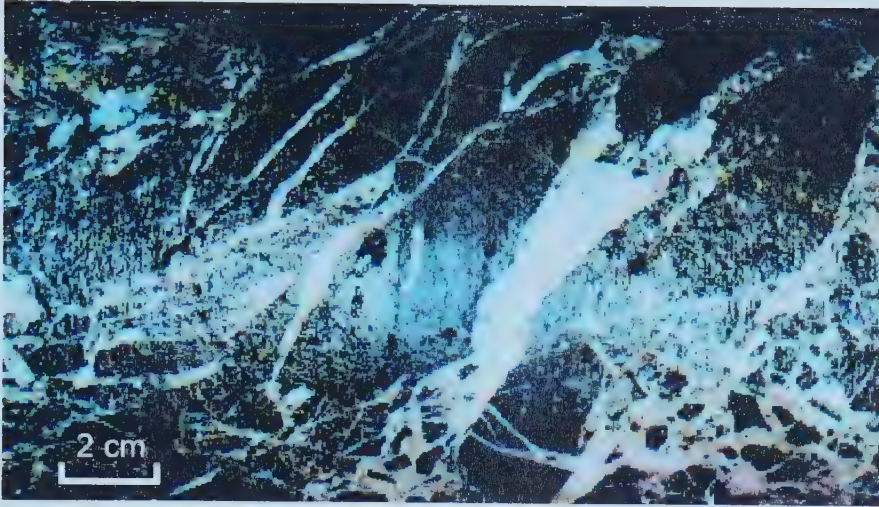
Three different types of anhydrite cement have been identified based on crystal habit, size, and lithological associations. Anhydrite is commonly associated with early fractures that cross-cut matrix dolomite within the study area, but some is also recognized as a late-stage cement, post-dating rhombohedral and saddle dolomite. Paragenetic relationships between anhydrite phases and calcite cements are unclear, as they are not found together in the core. Some anhydrite precipitated prior to all other cements, whereas other anhydrite precipitated syn- and post-formation of dolomite and calcite cements. Anhydrite is rarely found in association with milky calcite, but does occur with all other diagenetic phases.

A1: Finely crystalline (50-100 μm), white, felted anhydrite infilling veinlets, vein networks, and pods in dolomitic matrices, making up about 30 vol.% of the anhydrite cements in the study area. A1 anhydrite post dates matrix dolomitization, but it is unclear if it pre- or post dates any of the other cement phases as it does not occur with any of them (Figure 3.8a).

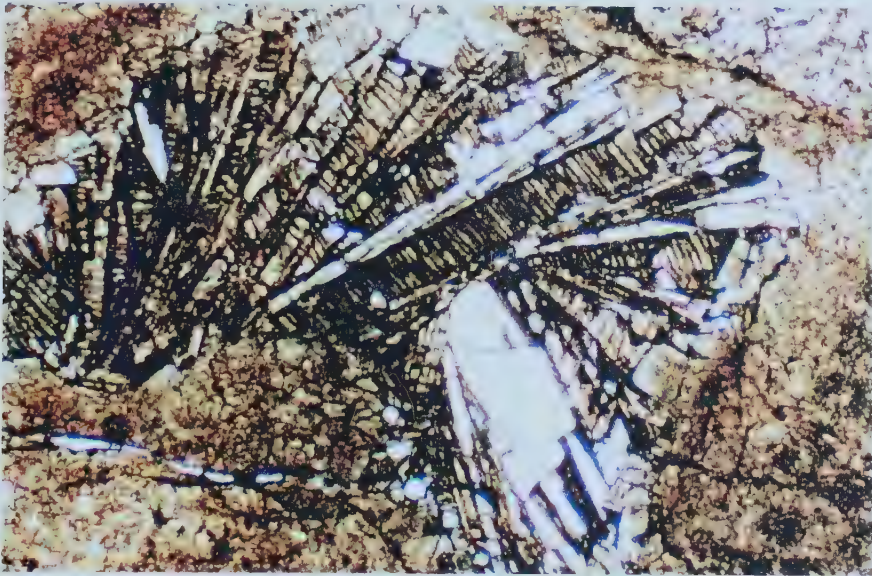
A2: Coarsely crystalline (10-40 mm), white to light grey, fibrous, elongate anhydrite laths. A2 anhydrite is found in 1-2 cm wide veins and vugs with random orientation of crystals, or in larger (4-7 cm wide) solution-enhanced vugs with a radial pattern. It is the least common anhydrite in the study area, accounting for 20 vol.% of all anhydrite cement (Figure 3.8b). A2 anhydrite does not occur with any other diagenetic cements.

A3: Coarsely crystalline (10-60 mm), transparent, white and light grey, blocky to

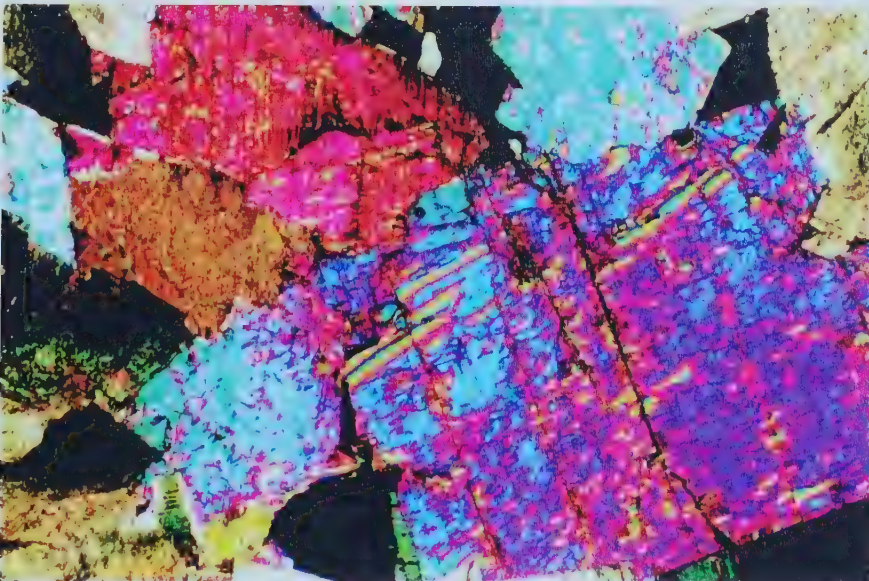
Figure 3.8 – Diagenetic anhydrite cement phases in the Peace River Arch area. a) A1 finely crystalline white anhydrite infilling F2 fractures in the lagoonal facies in well 11-14-67-04W6. b) Photomicrograph in crossed polarizers of A2 radial splays of anhydrite infilling a vug. Field of view is 5.5 mm. c) Photomicrograph in crossed polarizers of coarsely crystalline, blocky A3 anhydrite. Field of view is 5.5 mm.



a)



b)



c)

tabular anhydrite crystals. These occur as late-stage void-filling cements post-dating dolomite and calcite phases, or as coarse (2-4 cm wide) vein filling cements. Occasional, single laths occur in intercrystalline porosity in M2, M3, M4, and M5 dolomitic matrices. A3 anhydrite is the most common anhydrite in the study area, making up 50 vol.% of the anhydrite cements. It is not commonly associated with calcite cements (Figure 3.8c).

3.1.6 Fluorite

Fluorite is found only in well 11-30-66-07/W6, which lies on the Gold Creek platform in the study area. At this location, fluorite is found throughout a 400 foot cored interval, where it post-dates all other cements, but is only a minor constituent of the total rock volume. Overall, fluorite accounts for <1 vol.% of all diagenetic cements. Fluorite crystals are coarse (7-40 mm), euhedral, prismatic to anhedral, blocky, colourless to white in colour (Figure 3.9), and were identified by X-Ray diffraction. They do not fluoresce under short or long wavelength ultraviolet light, which infers only very small amounts, if any, of trace or rare earth elements in the crystal lattice (Gleason, 1972). Fluorite of this variety has been described by Aulstead and Spencer (1985) as a late stage cement in the Keg River Formation in the northwest corner of Alberta. Other occurrences of colourless fluorite in the WCSB are rare. Since fluorite is so rare within the study area, it has not been further investigated.

3.1.7 Other diagenetic cements

Several other minor cement contributors (totalling <1 vol.%) are evident in the study area. Bright yellow sulphur is present in sour-gas producing wells, particularly in well 11-30-66-07/W6. In these cores, amorphous blebs of sulphur are intergrown with milky calcite and fluorite, indicating that it is a late-stage cement (Figure 3.10).

Other cements found in the study area are disseminated sulphide minerals (pyrite and sphalerite), and black, vitreous pyrobitumen. Of the two sulphide minerals, pyrite is more common, found in small amounts throughout most wells. Pyrite occurs disseminated throughout the matrix, and along thin veinlets where it is associated with rhombohedral dolomite. Sphalerite, on the other hand, is found in very small amounts intergrown with limpid calcite in veins, and is always a late stage cement. Pyrobitumen clogs

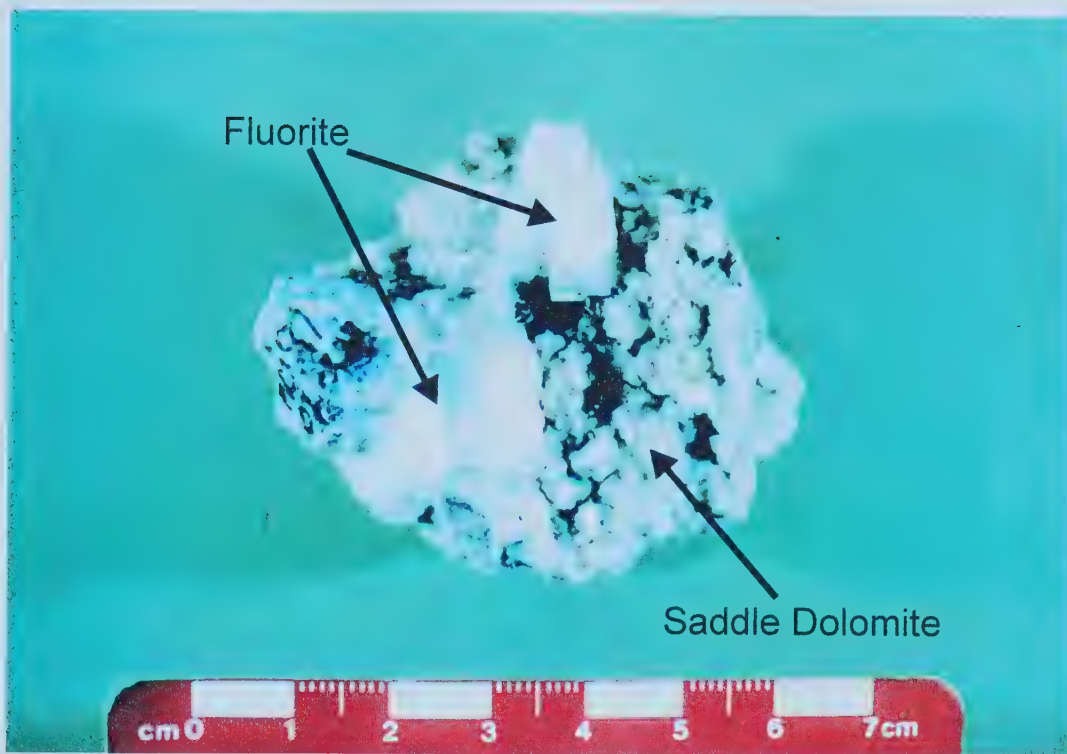


Figure 3.9 – White blocky fluorite cement after saddle dolomite, infilling a large solution vug in well 11-30-66-07W6.

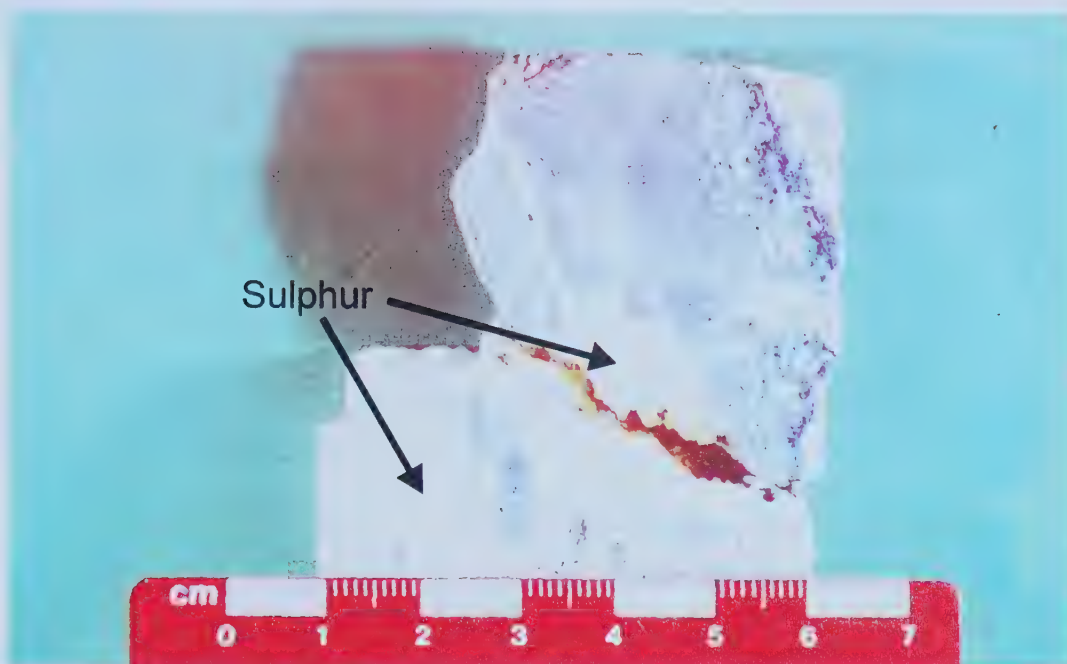


Figure 3.10 – Yellow native sulphur infills porosity as the latest cement phase. Core photograph from well 11-30-66-07W6 intergrown with white milky calcite.

intercrystalline, moldic and vuggy porosity, and coats early to late-diagenetic dolomite (rhombohedral and saddle), calcite (limpid), and anhydrite (A3) cements.

3.2 Other Diagenetic Features

Several other mega and microscopic diagenetic features were observed in the Leduc Formation and warrant discussion at this time. Stylolites and at least four discernible fracture sets are present in the core and may be placed in the paragenetic sequence based on their cross-cutting relationships with other diagenetic phases.

3.2.1 Stylolites

Stylolites in the Leduc Formation are black to brown, wispy to high amplitude, organic and clay-rich seams. Stylolites are either sutured, with a jagged appearance, or non-sutured and wispy. The relationship between stylolites and other diagenetic phases is varied. Stylolites cross-cut all matrix dolomite and clearly offset an early fracture set. However, stylolites are themselves cross-cut and displaced by at least 3 other fracture sets and the cement phases that fill them.

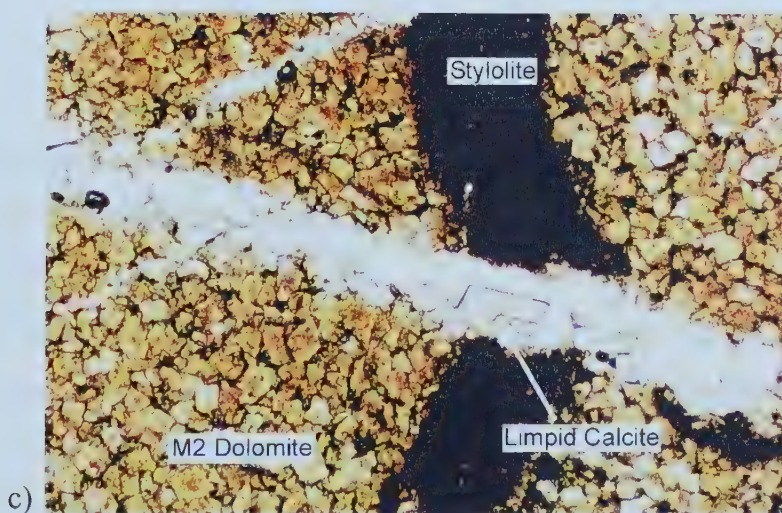
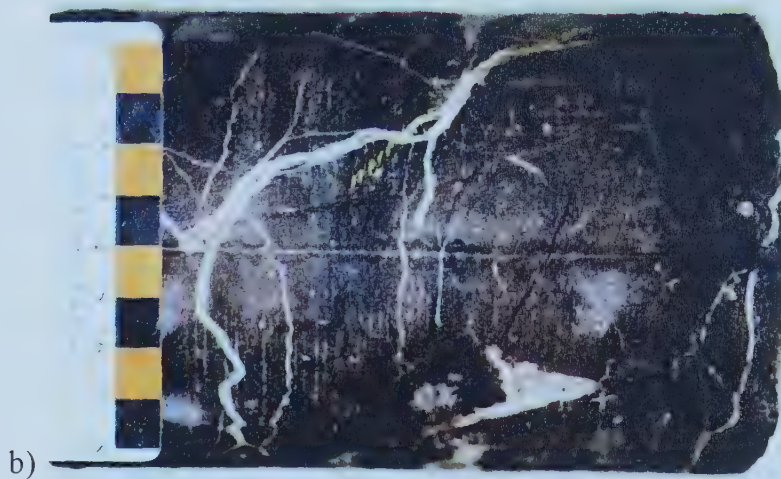
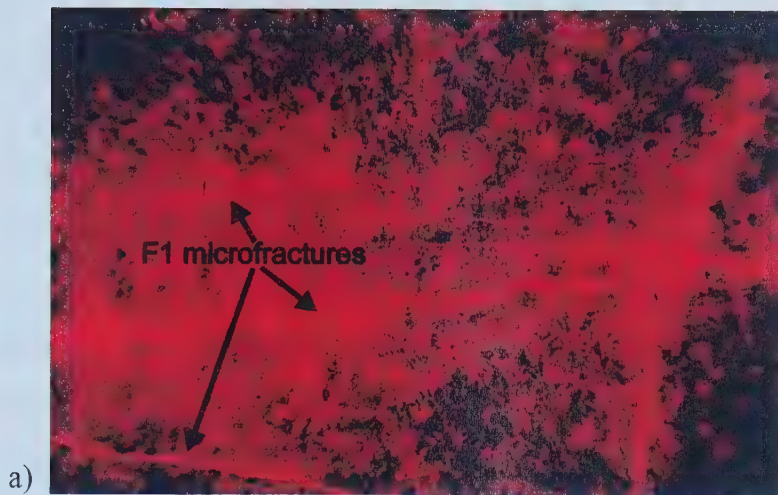
3.2.2 Fractures

Four main fracture sets that cross-cut the matrix replacive dolomite have been observed in the study area: **F1**, filled with early (matrix?) dolomite; **F2**, filled with anhydrite; **F3**, partially filled with rhombohedral dolomite, minor saddle dolomite, and limpid calcite; and **F4**, unfilled. Fracture sets F2, F3, and F4 are all associated with dissolution and vug creation.

F1 microfractures are recognized only with cathodoluminescence microscopy. They are sub-vertical, <1 mm wide, display *en echelon* fabric in some wells, and are recognized by their brighter red colour in comparison to the dull red matrix (Figure 3.11a). F1 fractures likely occur early in the paragenetic sequence as they are offset by wispy stylolites which have been shown to form at relatively shallow burial depths (Lind, 1993; Machel, 1999). As well, F1 fractures cannot be distinguished from the matrix dolomite with a petrographic microscope. These fractures likely formed syn- to post-dolomitization of the Leduc.

Fracture types F2 and F3 are much more difficult to rank in the paragenetic sequence.

Figure 3.11 – Fracture sets in the Leduc Formation. a) CL photomicrograph of F1 fractures (bright red) in matrix-replacive dolomite (dark red). These fractures are undetectable under plane or polarized light. Field of view is 5.5 mm. b) Core photograph of well 11-14-67-04W6 showing extensive anhydrite-filled F2 fracture network. c) Photomicrograph in plane polarized light showing a partially filled F3 fracture cross-cutting M1 dolomite (light brown) and a stylolite (dark brown). The fracture is partially filled with small, clear limpid calcite rhombohedral crystals. Field of view is 5.5 mm.



These fracture sets propagate in three different directions (sub-horizontal to sub-vertical), cross-cutting, and occasionally displacing, each other, and may be 2 mm to several cm's wide (Figure 3.11b,c) fractures are anhydrite filled, and form extensive networks and anhydrite pods (1-7 cm wide) (3.11b). Where F2 fractures are large, pieces of the host dolomite are incorporated into the anhydrite cement forming “crackle” breccias. F3 fractures, on the other hand, are completely or partially filled with rhombohedral dolomite +/- limpid calcite and saddle dolomite. They are 2-7 mm in width, sub-vertical in orientation, and are less abundant than F2 fractures (Figure 3.11c). When trying to place these two fracture sets into the paragenetic sequence, cross-cutting relationships alone are problematic. F2 fractures have 3 subsets which cross-cut each other. Thus, they had several periods of emplacement. F3 fractures typically cross-cut F2 fractures, however, some may be cross-cut by F2 sets. Both fracture sets cross-cut F1 microfractures. Furthermore, F2 and F3 sets may be found cutting through, or being displaced by stylolites. Therefore, these fractures cannot be constrained to a narrow time range in the paragenetic sequence, as their timing of emplacement overlaps both with each other, and with stylolitization.

Fracture set F4 cross-cuts all diagenetic products, and is one of the latest stages to develop. It is solution-enhanced and remains unfilled by any cements.

3.3 Summary

All diagenetic products identified and described here (dolomitization, void-filling cements, stylolites, fractures) may be placed in a preliminary paragenetic sequence, based on their lithological associations (e.g. cross-cutting relationships) relative to one another. Geochemical characteristics (to be discussed in Chapter 4) will further constrain their positions in the paragenetic sequence.

Pervasive matrix dolomitization of the platform and reef carbonates was the first observed diagenetic event to occur in the study area. Rhombohedral dolomite, saddle dolomite, milky calcite, limpid calcite, anhydrite cements, fluorite, sulphur, sulphide minerals, and pyrobitumen infill vuggy and moldic pores and fracture sets. A1 anhydrite infills small fracture networks, whereas A2 anhydrite is found in fractures or pores. Neither

A1 nor A2 anhydrite is associated with any other cement. Where A2 anhydrite is not present, rhombohedral or saddle dolomite are typically the earliest cements that line pores. Milky calcite, A3 anhydrite, and limpid calcite are later-stage precipitates that line pores after dolomite. These cements never occur with A1 or A2 anhydrite. All other cements are minor constituents that have been emplaced either syn- or post-precipitation of anhydrite or calcite phases. Stylolitization occurred throughout most of the early and intermediate diagenetic realm, cross-cutting all matrix dolomites and one early fracture set that is only detectable with CL microscopy. Stylolites are cross-cut and displaced by at least three sub-horizontal to sub-vertical fracture sets. Each fracture set was likely accompanied by a phase of dissolution. F2 fractures are completely filled by A2 anhydrite, whereas F3 fractures are partially filled by either type of dolomite +/- limpid calcite cement. Fracture set F4 remains completely open.

CHAPTER 4

GEOCHEMISTRY

4.1 Introduction

Geochemical techniques have been widely used to 1) interpret the environment of deposition of carbonate rocks, 2) identify authigenic minerals or recrystallized reaction products, and 3) understand the fluid-rock interactions that occur in the diagenetic realm (e.g. Aulstead, Spencer and Krouse, 1987; Carpenter and Lohmann, 1988; Allan and Wiggins, 1993; Machel and Burton, 1996; Machel, Cavell and Patey, 1996; Mountjoy *et al.*, 1997; Duggan and Mountjoy, 1998). Carbon and oxygen stable isotopic ratios are frequently used in sedimentological studies because of their abundance in the sedimentary rock record and in the earth's hydrosphere, and because they are easily fractionated by a number of diagenetic processes. Radiogenic strontium (^{87}Sr) has been used effectively to characterize and trace subsurface fluids (e.g. Mountjoy, Quing and McNutt, 1992; Allan and Wiggins, 1993; Banner, 1995; Machel, Cavell and Patey, 1996; Machel and Cavell, 1999).

Stable isotope values are expressed as the ratio of a heavy to a light isotope (R) of a sample relative to that of a standard. The resulting notation, δ -value, is expressed in parts per thousand (or permil, denoted by the symbol ‰) for a given sample:

$$\delta_{\text{sample}} = \left(\frac{R_{\text{sample}} - R_{\text{standard}}}{R_{\text{standard}}} \right) \times 10^3$$

Carbon isotopes are generally compared to the Peedee Belemnite (PDB) standard, whereas oxygen isotopes may be compared to either the PDB or Standard Mean Ocean Water (SMOW) standards. It is common to use the PDB standard for both carbon and oxygen isotopes when working with carbonate minerals (e.g. Allen and Wiggins, 1993).

Measurable stable isotopic variations occur because isotopes undergo a partial separation, or fractionation, during chemical and physical processes. Fractionation occurs because bond energies of atoms vary with respect to their weights, thus, the lighter elements C, H, O, N, and S are more easily fractionated. A substance is enriched (has a positive δ -

value) with respect to an isotope if it contains more of the heavy isotope than the standard ($R_{\text{sample}} > R_{\text{standard}}$). Conversely, a substance is depleted (has a negative δ -value) with respect to an isotope if it contains less of the heavy isotope than the standard ($R_{\text{sample}} < R_{\text{standard}}$).

The carbon isotopic ratio $^{13}\text{C}/^{12}\text{C}$ reflects the source of carbon that is involved in a mineral-forming reaction. If carbon derived from the breakdown of organic matter is incorporated into a carbonate precipitate, a negative $\delta^{13}\text{C}$ value may result for that mineral. However, if inorganic carbon derived from pre-existing rocks and sediments is the dominant carbon species, a $\delta^{13}\text{C}$ value close to zero is expected. Generally, the lighter C^{12} isotope is preferentially fractionated in biochemical reactions, whereas C^{13} is preferential in inorganic chemical reactions.

Carbon isotopes may also be used to ascertain if bacterial or thermal methanogenesis have occurred, and/or if bacterial sulphate reduction (BSR) or thermochemical sulphate reduction (TSR) have occurred since these processes occur in mutually exclusive thermal and burial regimes (Machel *et al.*, 1995b). Isotopic ranges for methane produced from microbial reactions during methanogenesis are characteristically $< -65\text{‰}$. Methane produced from the thermal maturation of hydrocarbons also has a depleted carbon signature, but it is in the range of -30 to -35‰ . Carbonate cements crystallized in sour gas reservoirs under TSR conditions commonly have a $\delta^{13}\text{C}$ range between normal marine and negative values due to mixing between the carbon produced from TSR reactions, and the pre-existing carbon in the reservoir.

The oxygen isotope ratio, $^{18}\text{O}/^{16}\text{O}$, may be used either to distinguish the type of water (meteoric, marine, or evaporitic in origin) that was involved in mineral precipitation or recrystallization reactions during diagenesis, or it may be used to estimate the temperature of formation of mineral phases. Many researchers have attempted to experimentally derive equations to approximate replacement dolomitization temperatures of formation of carbonate cements in the diagenetic environment (*i.e.* Epstein *et al.*, 1953; Craig, 1965; Fritz and Smith, 1970; Friedman and O'Neil, 1977; Land, 1983 and 1985; Fisher and Land, 1986). The following equations can be used for calcite and dolomite:

$$1) \delta^{18}\text{O}_{\text{calcite}} - \delta^{18}\text{O}_{\text{fluid}} = 2.78 \times 10^6 T^{-2} - 2.89 \quad \text{Friedman and O'Neil (1977)}$$

(for temperatures from 0 – 500 °C)

$$2) \delta^{18}\text{O}_{\text{dolomite}} - \delta^{18}\text{O}_{\text{fluid}} = 2.78 \times 10^6 T^{-2} + 0.11 \quad \text{Fritz and Smith (1970)}$$

(for temperatures from 25 – 78.6 °C)

$$3) \delta^{18}\text{O}_{\text{dolomite}} - \delta^{18}\text{O}_{\text{fluid}} = 2.78 \times 10^6 T^{-2} - 0.91 \quad \text{Land (1985)}$$

(for temperatures up to 200 °C),

where $\delta^{18}\text{O}$ values are in SMOW and T is temperature in Kelvin. These equations have three unknowns: 1) the temperature at which the mineral phase formed, 2) the $\delta^{18}\text{O}$ of the parent fluid, and 3) the $\delta^{18}\text{O}$ of the mineral. The $\delta^{18}\text{O}$ of the mineral is easily obtained from laboratory analysis. It then becomes necessary to estimate either the temperature of formation, or the $\delta^{18}\text{O}$ of the parent fluid in order to solve the equation. The temperature of formation of the mineral phase can be determined using fluid inclusion homogenization temperatures obtained from a sample for which $\delta^{18}\text{O}$ is known. The $\delta^{18}\text{O}$ value for the parent fluid can then be calculated. The $\delta^{18}\text{O}_{\text{fluid}}$ may then be used to "back-calculate" the temperatures of formation for other samples that lack fluid inclusion data.

Strontium isotopes occur as four species with varying proportions within the crust: ^{84}Sr (0.56), ^{86}Sr (9.87), ^{87}Sr (7.04), and ^{88}Sr (82.53). Of these, only ^{87}Sr is radiogenic, forming from the decay of the parent isotope ^{87}Rb . The stable isotope ^{86}Sr is used as the reference isotope because its abundance is similar to ^{87}Sr , thus making the $^{87}\text{Sr}/^{86}\text{Sr}$ ratio practical for use in isotopic comparisons. Unlike stable isotopes, when Sr is incorporated into a crystal lattice during a chemical reaction, it is a direct function of the species available in the fluid involved in the reaction. Strontium isotopes are not fractionated by variations in other conditions within a system (*i.e.* temperature or pressure). Thus, the Sr isotopic composition of marine carbonates is assumed to be a reflection of the Sr composition of the seawater at the time of precipitation. The strontium isotope ratio in the oceans is relatively constant at any given time (*i.e.*, on a time scale over a few Ma), balanced by the processes of weathering, and the formation of volcanic rocks on the seafloor. However, the $^{87}\text{Sr}/^{86}\text{Sr}$ ratio for the oceans has varied throughout the Phanerozoic (Burke *et al.*, 1982). The estimated $^{87}\text{Sr}/^{86}\text{Sr}$ ratio for the oceans in the Late Devonian during Leduc deposition is

between 0.7080 and 0.7085 (Burke *et al.*, 1982; Smalley *et al.*, 1994) (Figure 4.1).

A preliminary paragenetic sequence has been presented in Chapter 3 (Figure 3.1). In the following discussion, geochemical signatures will be used to further distinguish the various diagenetic phases. Two phases of dolomite (rhombohedral and saddle), two types of calcite (limpid and milky), and three types of anhydrite can be distinguished based on their geochemical compositions. Matrix dolomite, “fracture-related” dolomite, and “fracture-fill” dolomite cements from Dix’s (1993) study of the northern and eastern parts of the PRA have been incorporated for comparison with the data gathered in this study.

4.2 Methodology

X-ray diffraction (XRD), $\delta^{18}\text{O}$ and $\delta^{13}\text{C}$ analyses, $^{87}\text{Sr}/^{86}\text{Sr}$ analyses, and fluid inclusion heating/freezing microthermometry were the geochemical techniques used in this study. The complete geochemical data set obtained in this study is listed in Appendix A.

A total of 35 samples were analysed for stable and strontium isotope ratios. An additional 17 samples were processed for their strontium ratio alone. These additional 17 samples consist of calcite, dolomite, anhydrite, and fluorite. Five samples were selected for fluid inclusion microscopy from those that had stable isotope data. A total of 86 two-phase inclusions were analysed.

Samples were first cleaned by hand and using a sonic bath in order to remove any residual drilling mud caked on crystals in large pore spaces. Individual minerals were extracted from whole rock samples with the use of a dental drill. If possible, at least 200 mg of powder was extracted from each sample to produce a single homogeneous sample for use in all geochemical analyses. However, some cement phases did not have enough material to yield 200 mg of powder and a complete geochemical data set could not be obtained for these samples. Samples were crushed to a uniform powder for stable, radiogenic and XRD analyses. XRD analysis was performed with a Rigaku Geigerflex ($\text{Co K}\alpha = 1.79026 \text{ \AA}$).

Carbon and oxygen isotope analyses of carbonate cements were carried out by standard methods of CO_2 extraction using phosphoric acid at 25°C (McCrea, 1950; Epstein *et al.*, 1964) and analysed on a Finnegan Mat 252 Gas Chromatograph Mass Spectrometer

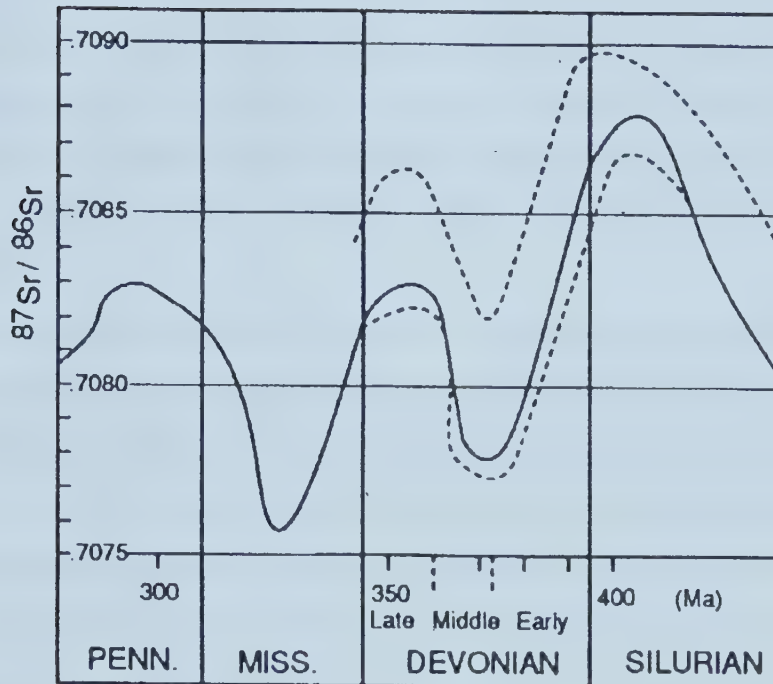


Figure 4.1 – Interpreted $^{87}\text{Sr}/^{86}\text{Sr}$ curve for seawater from the Silurian to the Pennsylvanian Periods. Dashed lines represent outer limits of data. Modified from Burke *et al.* (1982).

(GCMS). The samples were not roasted prior to analysis. Carbon and oxygen isotopic ratios have an analytical precision of $\pm 0.1\text{‰}$.

Strontium was extracted from calcite, dolomite, anhydrite, and fluorite mineral phases following the procedures as outlined in Appendix B. There was no laboratory protocol for the extraction of strontium from fluorite. Therefore, the procedure outlined herein was specifically designed for this study by the author with assistance from Dr Pat Cavell and Dr. Robert Creaser at the University of Alberta. All samples were processed on a VG 354 multi-collector Thermal Ionization Mass Spectrometer (TIMS). The samples were loaded as a phospho-tantalate gel on a single Re ribbon bead assembly. Values for $^{87}\text{Sr}/^{86}\text{Sr}$ were corrected to N.B.S. SRM-987 for which repeated analytical runs during the course of this study gave a value of 0.71020. Analytical precision on individual runs was better than 0.00007 (2σ).

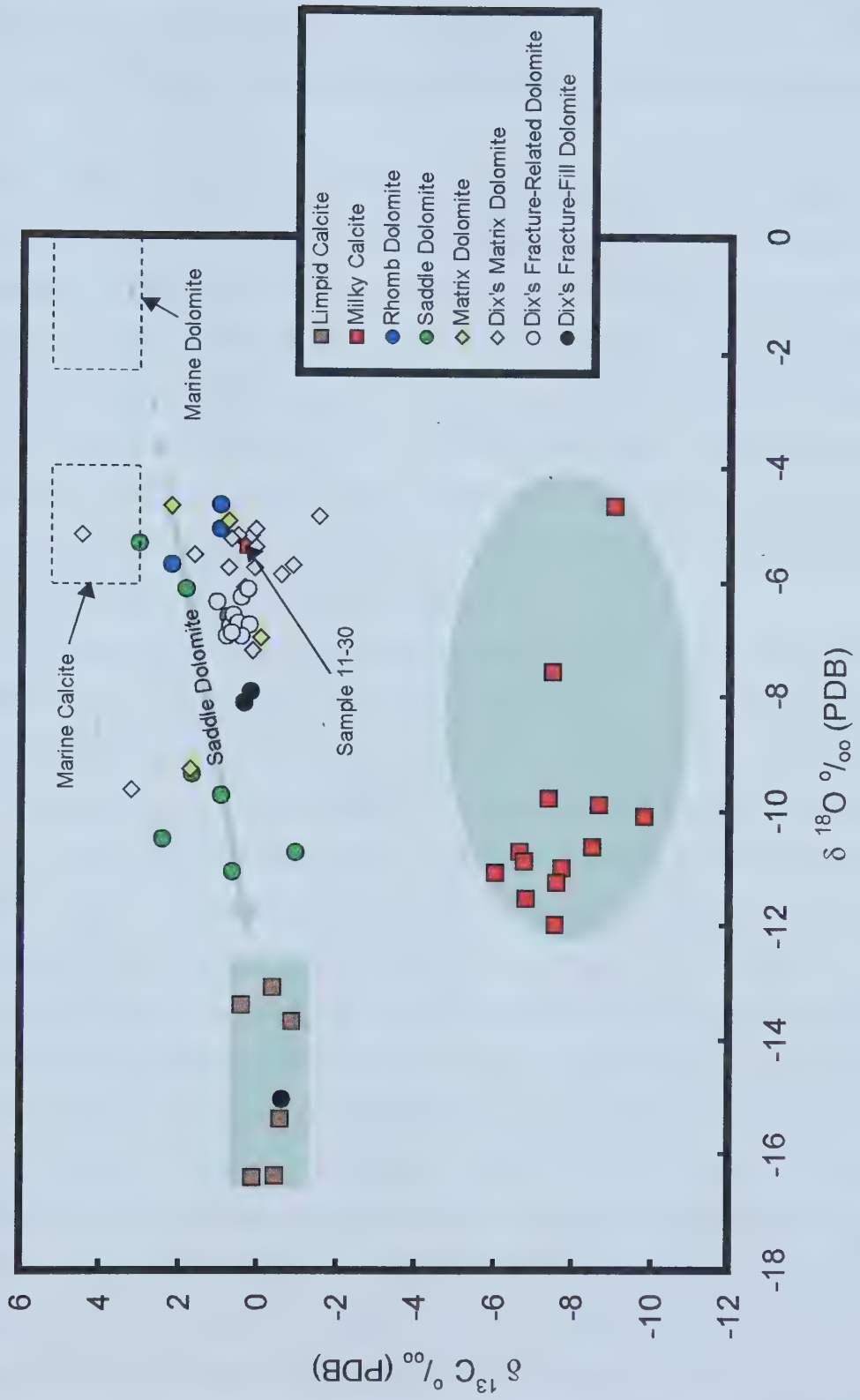
Sixteen polished sections were prepared for fluid inclusion analyses. Of these only 5 were selected for microthermomic analysis based on the amount, size, and type (2-phase primary) of fluid inclusions. Temperatures of homogenization (T_h), freezing (T_f), melting (T_m), and eutectic (T_e) were all measured on a gas-flow heating-cooling stage. At least 3 measurements were repeated for each fluid inclusion, and temperatures were repeatable to $\pm 1^\circ\text{C}$ for individual inclusions. The greatest variation in temperatures within individual crystals was in T_h values ($\pm 30.7^\circ\text{C}$).

4.3 Stable Isotopes

Carbon and oxygen isotopic ratios were determined for matrix dolomite, rhombohedral dolomite, saddle dolomite, limpid calcite, and milky calcite cements from the study area. All $\delta^{18}\text{O}$ and $\delta^{13}\text{C}$ values reported herein are relative to the PDB (Peedee Belemnite) standard. In a standard $\delta^{18}\text{O}$ versus $\delta^{13}\text{C}$ plot, the data define several fields (Figure 4.2). Matrix dolomite and fracture-fill dolomite cement samples from Dix's (1993) study on the Leduc in the PRA area have also been included here for comparison. The estimated range of values for marine calcites and dolomites that would have formed in equilibrium with Late Devonian seawater at 25°C are also displayed. Estimated Late

Figure 4.2 – Stable isotope plot for Leduc carbonate cements. The dashed boxes indicate estimated ranges for marine calcite and dolomite that would have formed in equilibrium with Late Devonian seawater. Light grey shading highlights fields for cement phases.

Oxygen Vs. Carbon



Devonian marine calcite values used herein are -5.0 ± 1.0 ‰ for $\delta^{18}\text{O}$ and 2.5 ± 1.0 ‰ for $\delta^{13}\text{C}$, whereas estimated Late Devonian marine dolomite values are -2.4 to 0.0 ‰ for $\delta^{18}\text{O}$ and 2.5 ± 1.0 ‰ for $\delta^{13}\text{C}$ (Land, 1985; Carpenter and Lohmann, 1989; Hurley and Lohmann, 1989).

Matrix dolomite samples have $\delta^{18}\text{O}$ values ranging from -4.7 to -9.3 and $\delta^{13}\text{C}$ values from 2.2 to 0.0 ‰ PDB. The $\delta^{13}\text{C}$ values are slightly depleted from marine values. However, these fall into the same range as matrix dolomite samples from across the WCSB (i.e. Mountjoy *et al.*, 1991; Amthor *et al.*, 1993; Patey, 1995; Drivet and Mountjoy, 1997; Duggan, 1997). However, the $\delta^{18}\text{O}$ values are equal to or lower than those of most matrix dolomites found elsewhere in the basin. These $\delta^{18}\text{O}$ values indicate temperature-induced recrystallization of matrix dolomite at depth (Machel *et al.*, 1996), which seems to be common in the deepest part of the basin (Machel and Cavell, 1999). Dix's matrix dolomite samples also have the same range of stable isotope data.

Dolomite cements have $\delta^{18}\text{O}$ values that range from -4.7 to -11.1 ‰ PDB and $\delta^{13}\text{C}$ values that fall between 3.1 and -0.9 ‰ PDB. In Figure 4.2, the fields for matrix dolomite, rhombohedral dolomite cements, and some saddle dolomite cements are found to overlap significantly. Similarly, Dix's "fracture-related" and "fracture-fill" dolomites also fall into these ranges. Therefore, the dolomite cements cannot be distinguished from one another based on stable isotope data alone. However, the strontium isotope signatures of the dolomite cements may also be used to differentiate between them (see next section). The overlapping fields of matrix, rhombohedral, and Dix's dolomite samples suggest that these cements may have been derived from the same fluid. However, although some of the saddle dolomite samples fall into the same field for $\delta^{13}\text{C}$, the $\delta^{18}\text{O}$ values form a linear trend becoming increasingly more depleted (as shown in Figure 4.2). Hence, saddle dolomite cements likely formed from a different fluid than matrix and rhombohedral dolomites, and the trend shown in Figure 4.2 represents various ratios of fluid mixing, or the fluid forming saddle dolomite may have evolved over a wide temperature range. Thus, saddle dolomite may have formed over a widespread range of burial depths in the study area.

Two distinct populations of calcite cements may be differentiated based on their

stable isotope ranges. Milky calcite is significantly depleted with respect to both carbon ($\delta^{13}\text{C} = -6.0$ to -9.0‰ PDB) and oxygen ($\delta^{18}\text{O} = -4.7$ to -12‰ PDB) and may be grouped in a well-defined field with the exception of one sample (Figure 4.2). The depleted carbon signature unique to milky calcite cements in this study reflects that the parent fluid for these cements likely tapped into a different source of C^{13} than the other diagenetic phases. This may have occurred locally where there was an influx of organic carbon in the system. The process of TSR is known to generate cements that have depleted $\delta^{13}\text{C}$ values (*i.e.* Machel *et al.*, 1995b). Moreover, the higher temperatures (about 100 to 140 °C) required for TSR would also result in the cement having depleted $\delta^{18}\text{O}$ values. This is consistent with the geochemical signature of the milky calcite.

A single sample of milky calcite exhibits higher stable isotope values ($\delta^{18}\text{O} = -5.4\text{‰}$ PDB, $\delta^{13}\text{C} = 0.3\text{‰}$ PDB) than the other milky calcites. This sample is from well 11-30-66-07W6; a known sour gas well. This sample is intergrown with native sulphur cement, indicating that it formed in a zone where TSR was occurring. Several other milky calcite samples were also taken from this well, all of which plot in the defined field for milky calcite. A likely explanation for this anomaly in the data set is the heterogeneity of the carbonate reservoir during TSR. Reactions associated with thermochemical sulphate reduction in sour gas pools have been shown to vary locally within reservoirs (Machel *et al.*, 1995b; Simpson *et al.*, 1996). Specifically, the factors that contribute to the onset of TSR, such as the distribution of anhydrite, wettability, composition of the hydrocarbons, dissolution rate, migration/diffusion rates, and catalysts, may vary within a single pool (Machel, 1998). The variability of the many factors governing TSR, coupled with the heterogeneous porosity and permeability distributions in carbonate reservoirs, may create localized "bubbles" within the TSR system that could harbour different geochemical conditions. Thus, petrographically equivalent mineral phases within a reservoir could exhibit varying geochemical signatures.

On the other hand, the limpid calcites have carbon isotope values that are only slightly depleted relative to Late Devonian marine values ($\delta^{13}\text{C} = 0.4$ to -0.8‰ PDB), but characteristically have a depleted oxygen signature ($\delta^{18}\text{O} = -13.1$ to -16.4‰ PDB). Since

limpid calcite samples have more depleted $\delta^{18}\text{O}$ values than saddle dolomite, and $\delta^{18}\text{O}$ depletion occurs coincident with increasing temperature, these cements may have formed at a higher temperature range (deeper burial depth) than did the saddle dolomite cement. On the other hand, the near-marine $\delta^{13}\text{C}$ values of limpid calcites indicate that these cements formed after TSR had ended, *i.e.*, when no more oxidized organic carbon was available.

4.4 Strontium Isotopes

Strontium isotope ratios were determined for matrix dolomite, rhombohedral dolomite, saddle dolomite, milky calcite, limpid calcite, anhydrite, and fluorite cements in the study area. The $^{87}\text{Sr}/^{86}\text{Sr}$ ratios were plotted versus $\delta^{13}\text{C}$ (Figure 4.3) and $\delta^{18}\text{O}$ (Figure 4.4) wherever possible.

The isotopic ratios determined for the Leduc cements in the study area may be compared to the MAXimum Strontium Isotope Ratio in BASinal Shales, or MASIRBAS (Cavell and Machel, 1997; Machel and Cavell, 1999), as indicated on the isotope plots in Figures 4.3 and 4.4. MASIRBAS has been determined experimentally by the stepwise leaching of strontium from basinal shale and outcrop slate samples (Figure 4.5). The sample set analyzed includes Devonian aged basinal shales from 1) the Duvernay Formation in the Kaybob field, 2) the Ireton Formation in the Obed field, and 3) the Cynthia Formation from the centre of the West Shale Basin (Twp 49, Rng 12 W6). As well, metamorphic slate samples from the Proterozoic Miette Group, outcropping in the Rocky Mountain Front Ranges, were analyzed. The combined data set defines the highest possible strontium ratio that can be derived from basinal shales under diagenetic temperature and pressure conditions that have affected the WCSB, and those strontium ratios that are characteristic of metamorphic (extra-basinal) sources. MASIRBAS is defined as 0.7120 (Cavell and Machel, 1997; Machel and Cavell, in press). Strontium isotope ratios higher than MASIRBAS indicate a basement or extra-basinal source.

Leduc matrix and rhombohedral dolomite samples fall below MASIRBAS, whereas most saddle dolomite and all limpid and milky calcite samples lie above this value. Matrix dolomite samples have $^{87}\text{Sr}/^{86}\text{Sr}$ ratios that range from 0.7087 to 0.7100 (Figures 4.3 and

Figure 4.3 – Carbon versus strontium isotope plot for Leduc carbonate cements. The MAXimum Strontium Isotope Ratio in Basinal Shales (MASIRBAS) = 0.7120. Light grey shading highlights isotopic fields for cement phases.

Carbon Vs. Strontium

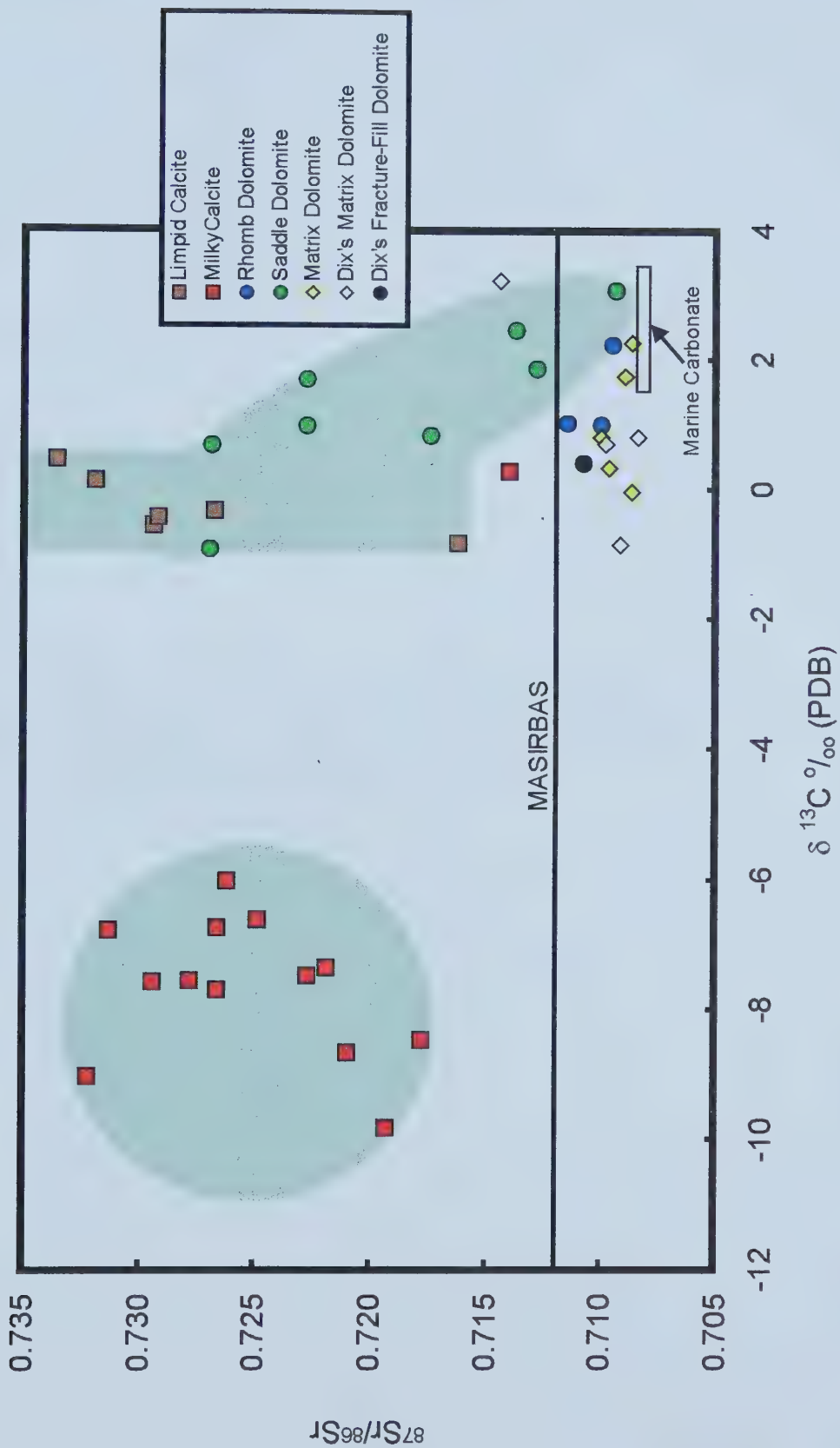
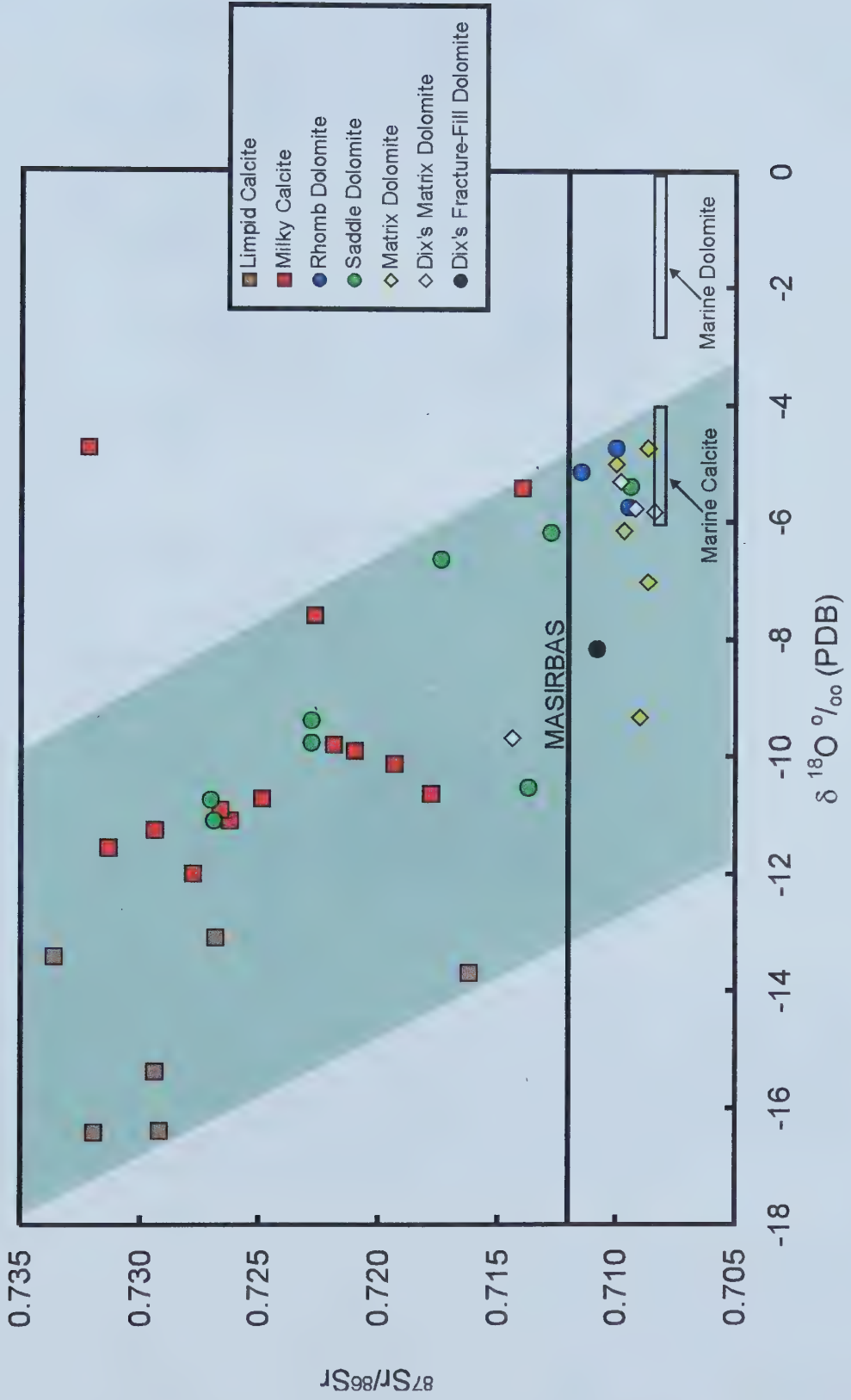


Figure 4.4 – Oxygen versus strontium isotope plot for Leduc carbonate cements. The MAXimum Strontium Isotope Ratio in Basinal Shales (MASIRBAS) = 0.7120. Light grey shading indicates the general isotopic trend for cement phases highlighting a correlation between oxygen depletion and increasing radiogenic strontium.

Oxygen Vs. Strontium



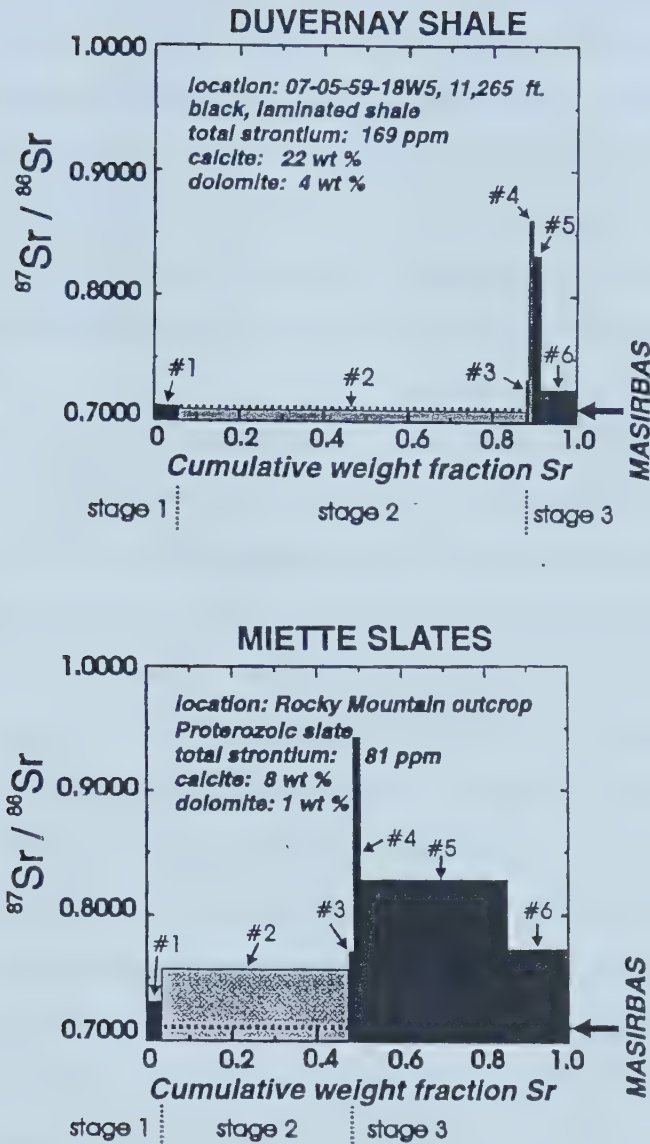


Figure 4.5 – Plots of the cumulative weight fraction of Sr versus the $^{87}\text{Sr}/^{86}\text{Sr}$ ratios from each sample from a) the Devonian Duvernay basinal shale and b) the Proterozoic Miette slate. The Sr released in solutions #1 and #2 can be used to approximate subsurface diagenetic conditions. In a), solutions #1 and #2 define MASIRBAS at 0.7120. In b), the $^{87}\text{Sr}/^{86}\text{Sr}$ ratios of solutions #1 and #2 considerably exceed MASIRBAS. Stages refer to increasing sample dissolution. Modified from Machel and Cavell, 1999.

4.4). Generally, these values are marginally higher than estimated Late Devonian seawater ratios (0.7080 to 0.7085), and are in the same range as matrix dolomites reported from across the WCSB (e.g. Mattes and Mountjoy, 1980; Kaufman *et al.*, 1990; Laflamme, 1990; Mountjoy and Halim-Dihardja, 1991; Patey, 1995; Duggan, 1997). Dix's matrix dolomite samples also fall into this field. In combination with the stable isotope data, these data support the earlier interpretations of the matrix dolomites, i.e., they formed from slightly modified seawater at burial depths of about 500 to 1500 m (Amthor *et al.*, 1993; Mountjoy and Amthor, 1996).

Rhombohedral dolomite samples have a wider, and slightly higher, range of $^{87}\text{Sr}/^{86}\text{Sr}$ than matrix dolomite, with values from 0.7095 to 0.7103 (Figures 4.3 & 4.4). Furthermore, the relative spread of $\delta^{13}\text{C}$ and $\delta^{18}\text{O}$ values over the strontium isotopic range is small. Due to the small number of samples analysed, there is not an apparent trend in this data set.

In contrast, saddle dolomite samples have a wide spread of strontium isotope ratios from a minimum value of 0.7094 to a maximum value of 0.7337, well above MASIRBAS. Again, not all of the $^{87}\text{Sr}/^{86}\text{Sr}$ values can be plotted in Figures 4.3 and 4.4 as they lack stable isotope values. Moreover, the saddle dolomite cements have a relatively wide spread of $\delta^{18}\text{O}$ with a characteristically depleted signature (Figure 4.4). The data indicate a crude correlation between strontium and oxygen such that highly radiogenic strontium ratios are coupled with a depleted oxygen signature. In comparison, there is a less pronounced correlation between strontium and carbon (Figure 4.3) and much less variation in $\delta^{13}\text{C}$ than in $\delta^{18}\text{O}$ over the wide range of $^{87}\text{Sr}/^{86}\text{Sr}$ values. As well, the saddle dolomite field overlaps with the limpid calcite field in Figure 4.3 and with the milky calcite field in Figure 4.4, suggesting that these cements formed either from mixing of two types of diagenetic fluid and/or from a progressively evolving fluid.

Calcite cements have the highest Sr isotope values in the data set ranging well above MASIRBAS. The lowest measured value for calcite cements is 0.7140, higher than the highest measured $^{87}\text{Sr}/^{86}\text{Sr}$ values in all other carbonate mineral phases except saddle dolomite. There is no significant difference between the two calcite cement types. Milky calcite ranges from 0.7178 to 0.7335, whereas limpid calcite has a range for $^{87}\text{Sr}/^{86}\text{Sr}$ from

0.7140 to 0.7336. Although, when coupled with stable isotope data, two distinct populations of calcite are apparent. Both calcite cements have a narrow range of $\delta^{13}\text{C}$ values over a wider range of $^{87}\text{Sr}/^{86}\text{Sr}$. However, limpid calcite carbon values are close to that of Late Devonian marine calcite, whereas milky calcite carbon values are significantly depleted. When comparing the relationship between $\delta^{18}\text{O}$ and $^{87}\text{Sr}/^{86}\text{Sr}$, both calcite cements have the same data trend as saddle dolomite cements, suggesting that these phases may have formed from the mixing of two diagenetic fluids and/or from a single, evolving fluid. Some limpid calcite cements have more depleted $\delta^{18}\text{O}$ and higher $^{87}\text{Sr}/^{86}\text{Sr}$ values than milky calcite samples, suggesting that the limpid calcite formed from a more evolved fluid than the milky calcite.

Several types of anhydrite were also analyzed (Figure 4.6). These included A2 and A3 anhydrite cements, as well as primary anhydrite from the Nisku Formation at the eastern end of the study area. Both primary anhydrite samples have a $^{87}\text{Sr}/^{86}\text{Sr}$ ratio of 0.7082. These samples formed in a restricted basin from the direct evaporation of Late Devonian seawater, thus a marine $^{87}\text{Sr}/^{86}\text{Sr}$ ratio is expected. On the other hand, the anhydrite cement phases have a wide range of $^{87}\text{Sr}/^{86}\text{Sr}$ values from 0.7092 to 0.7316. Generally, A2 cements have strontium ratios that are lower than A3 cements. This suggests that the two phases may have formed from different and/or evolving fluids during diagenesis: A2 cement from similar fluids that precipitated both matrix and rhombohedral dolomites, and A3 cement from the fluids associated with the precipitation of saddle dolomite and both calcite cement phases.

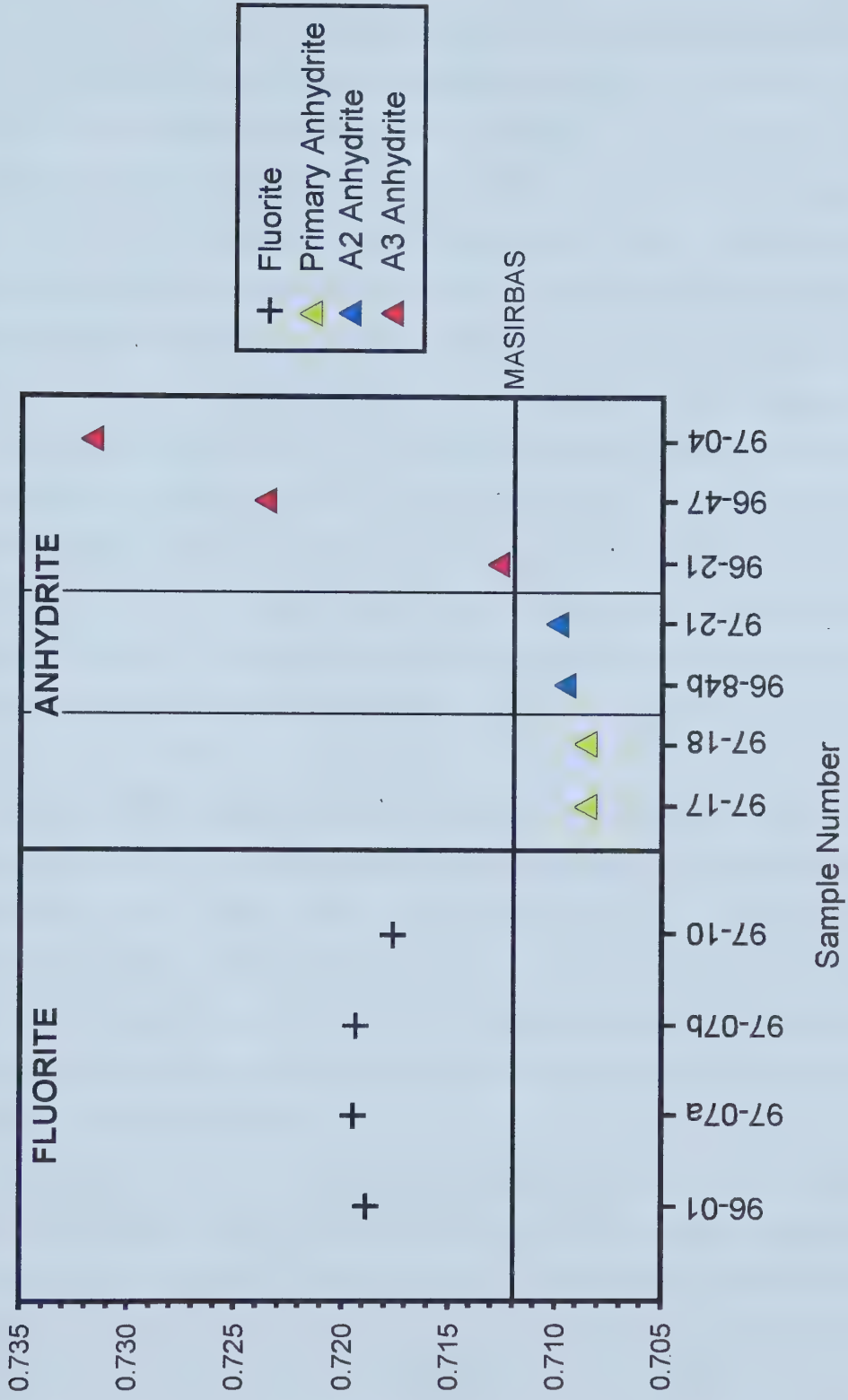
Finally, four samples of fluorite were also analyzed. The $^{87}\text{Sr}/^{86}\text{Sr}$ range for fluorite cements is narrow, varying between 0.7175 and 0.7193. Although, this cement phase formed after both calcite phases, the overall $^{87}\text{Sr}/^{86}\text{Sr}$ values are lower. However, fluorite cement does have radiogenic strontium values well above MASIRBAS, suggesting a correspondence with the highly radiogenic fluids that precipitated the saddle dolomite, and both types of calcite cement.

4.5 Fluid Inclusion Microthermometry

Eighty-seven two-phase (aqueous liquid-vapor) fluid inclusions were analyzed from 5 calcite samples (2 limpid, 3 milky calcite) in three wells. Inclusions were identified as

Figure 4.6 – Strontium isotope ratios for fluorite and anhydrite cements in the Leduc Formation. Sample numbers are indicated on the x-axis (*i.e.* 96-01), and correlate with those in Table A-1 in Appendix A. The MAXimum Strontium Isotope Ratio for BASinal Shales (MASIRBAS) = 0.7120.

$^{87}\text{Sr}/^{86}\text{Sr}$ of Fluorite and Anhydrite Cements



primary (those that form at the time of crystal growth) by the criteria listed in Roedder (1981). All inclusions chosen for analysis had the same liquid to vapor ratio (approx. 85 vol.% liquid:15 vol.% vapor). Inclusions were observed to be one of two basic shapes: 1) irregularly shaped or 2) negative crystal, and ranged in size from 5 μm to 50 μm . Vapor bubble diameters in the inclusions ranged in size from 1-12 μm . Relatively large and abundant inclusions were observed in the milky calcite samples, while limpid calcite samples tended to have smaller and fewer inclusions. Although coarse saddle dolomite crystals are inclusion-rich, the inclusions were not practical for analysis due to the “cloudiness” of the individual crystals and the small size ($< 5 \mu\text{m}$) of the inclusions. Separate inclusions were chosen for heating and freezing runs in each sample in order to minimize the error caused by stretching and/or leakage of the inclusions during analysis. Inclusions were then re-run in the opposite procedure to check values and to maintain homogeneity in the data set. Inclusions that did not yield repeatable temperatures, or had obvious physical changes (*i.e.* stretching of the vapor phase) after one heating/cooling run, were discarded from the sample set.

Homogenization temperatures may be used as an approximation of the temperature of formation of a crystal. Most milky and limpid calcites have high average homogenization temperatures of 137.3 $^{\circ}\text{C}$ and 141.7 $^{\circ}\text{C}$ (Figure 4.7) respectively. These estimates of temperature of formation would be higher if corrected for pressure, assuming that maximum burial was 1-2 km higher than today’s depths. Nonetheless, the high T_h for both cements indicates that they likely formed at great depths (3-4 km) near to the maximum burial depth of the Leduc Formation in the study area.

Supercooling fluid inclusions to their freezing point and observing melting behavior can yield two important properties of the crystallizing fluid: the salt system of the fluid, and an indication of the total salinity. When melting begins, first melt at T_e can be indicative of the salt system in the inclusion. However, it can be very difficult to see the subtle changes that mark this phase transition because of the small amount of initial fluid. Eutectic, or first melt, temperatures for some common salt systems, taken from Crawford (1981), are as follows:

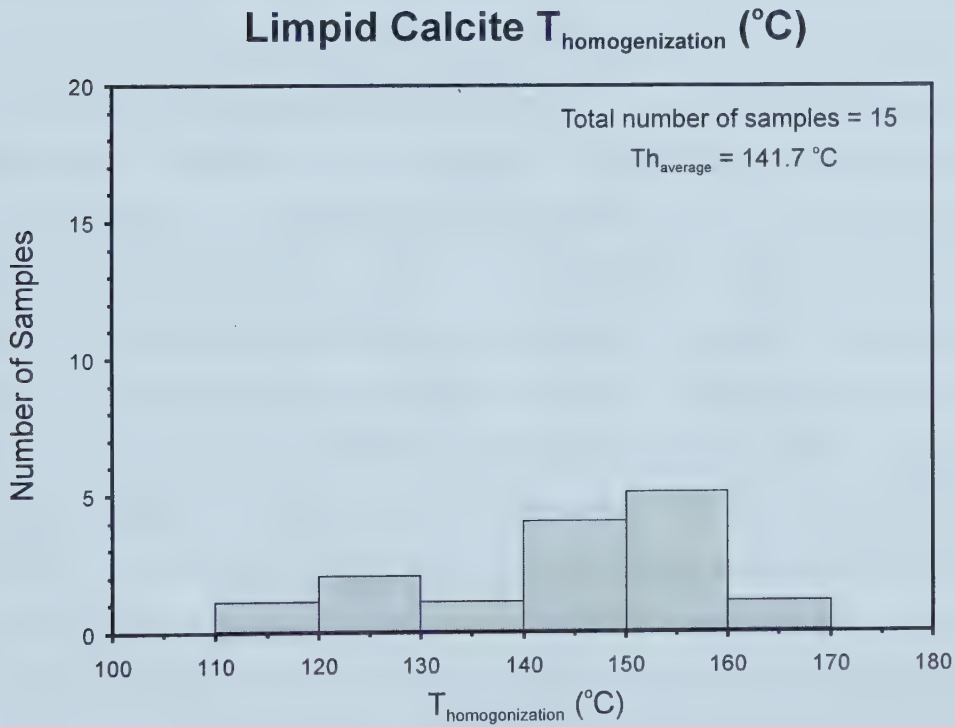
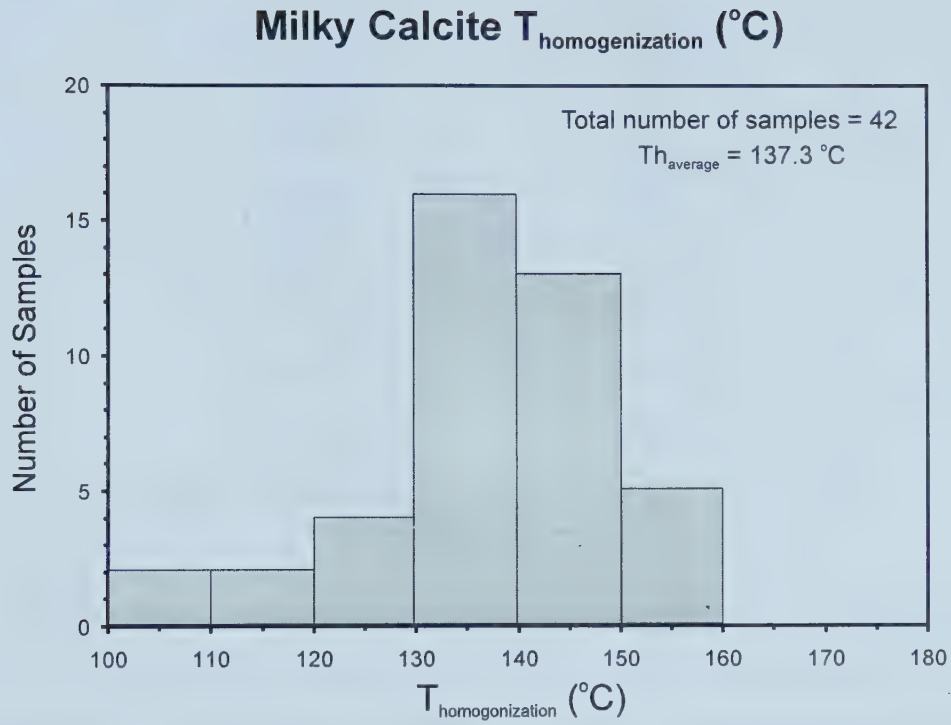


Figure 4.7 – Homogenization temperature histograms for milky and limpid calcite cements.

Salt System	Eutectic Temperature (°C)
KCl	-10.6
NaCl	-20.8
KCl-NaCl	-22.9
MgCl ₂	-33.6
MgCl ₂ -NaCl	-35.0
CaCl ₂	-49.8
CaCl ₂ -NaCl	-52.0
MgCl ₂ -CaCl ₂ -NaCl	-57.0

There are two distinct populations of T_e values in the milky calcite data set: one with a median at $-49\text{ }^{\circ}\text{C}$, and the other median closer to $-54\text{ }^{\circ}\text{C}$ (Figure 4.8). $T_e = -49\text{ }^{\circ}\text{C}$ corresponds to a CaCl salt system, whereas $T_e = -54\text{ }^{\circ}\text{C}$ corresponds to a more complex mixture of salts, such as CaCl₂-NaCl or MgCl₂-CaCl₂-NaCl. Furthermore, the inclusions with a distinctly lower average T_e are from the same milky calcite sample, taken from a TSR reservoir, that exhibits anomalous stable isotope data when compared to the rest of the milky calcite samples. It would not be unreasonable to attribute the variability of the salt system found in this sample to a spatially heterogeneous TSR system in the reservoir. Brines in localized "bubbles", which may or may not contain additional H₂S liberated during TSR (e.g. Machel, 1998), may not have the same composition of the "connate" fluids elsewhere in the reservoir. Thus, inclusions from crystals that formed in "bubbles" would exhibit a different salinity and, in some cases, a different combination of salts, perhaps due to the local dissolution of sulphates or clay minerals. Limpid calcite inclusions have an overall average T_e of $-54.8\text{ }^{\circ}\text{C}$, which falls in between the CaCl₂-NaCl and MgCl₂-CaCl₂-NaCl systems. In this case, a more complex salt solution was likely the parent fluid for this cement type.

Milky calcite inclusions have a broad range of final melting temperatures, T_m , with an overall average of $-16.9\text{ }^{\circ}\text{C}$ (Figure 4.9). Generally, this average melting temperature corresponds to a salinity of about 21 wt.% NaCl (Figure 4.10). On the other hand, limpid calcite has a much narrower range of T_m values with an average temperature of $-20.9\text{ }^{\circ}\text{C}$.

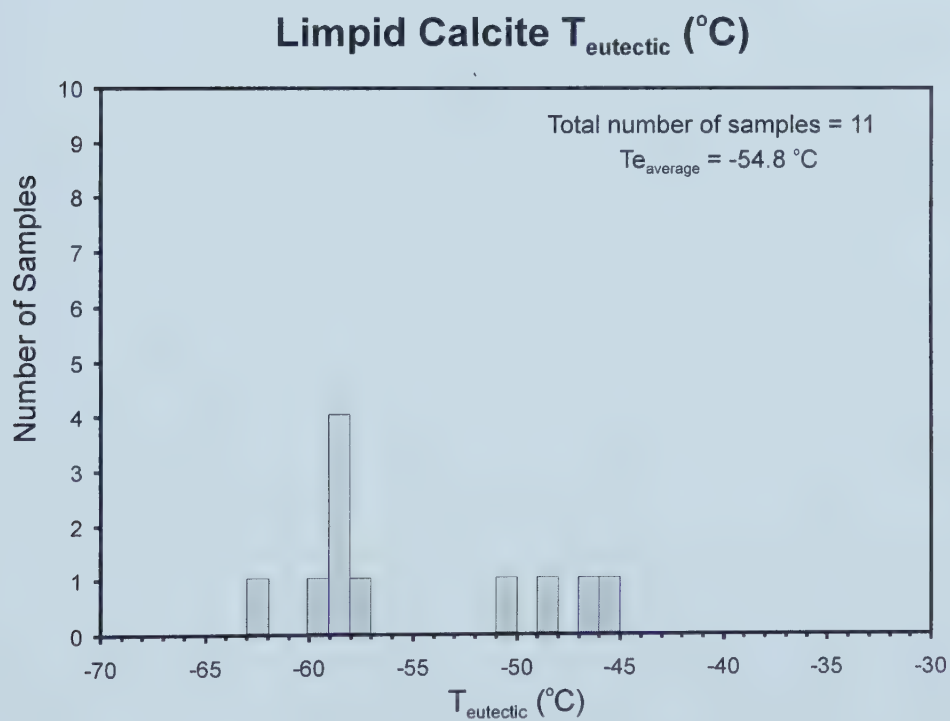
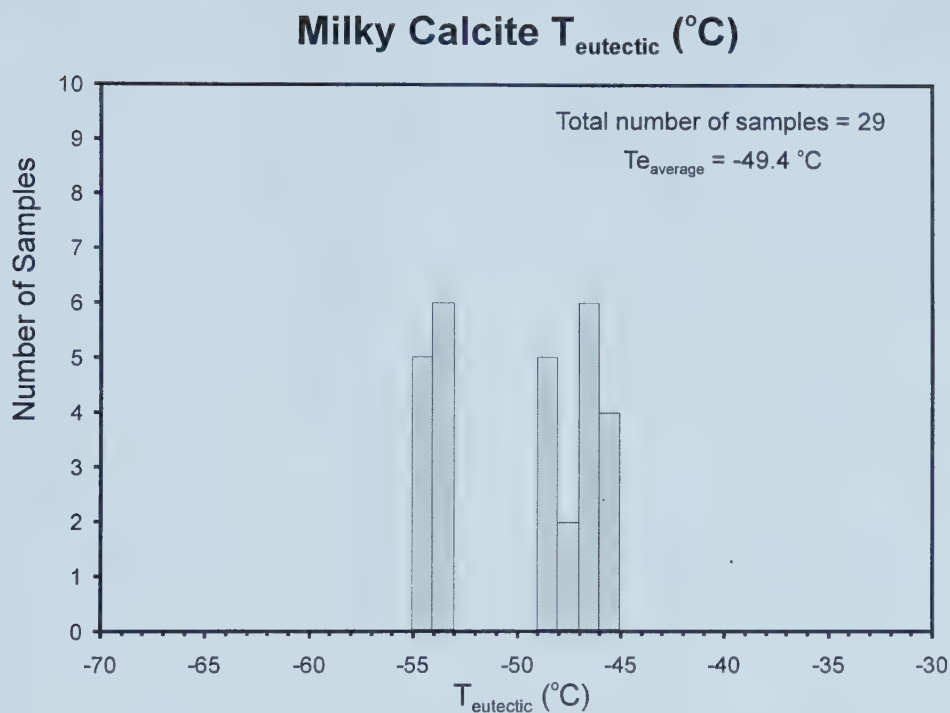


Figure 4.8 – Eutectic temperature histograms for milky and limpid calcite cements.

This average T_m corresponds to a fluid with a salinity of 21-23 wt.% NaCl equivalent.

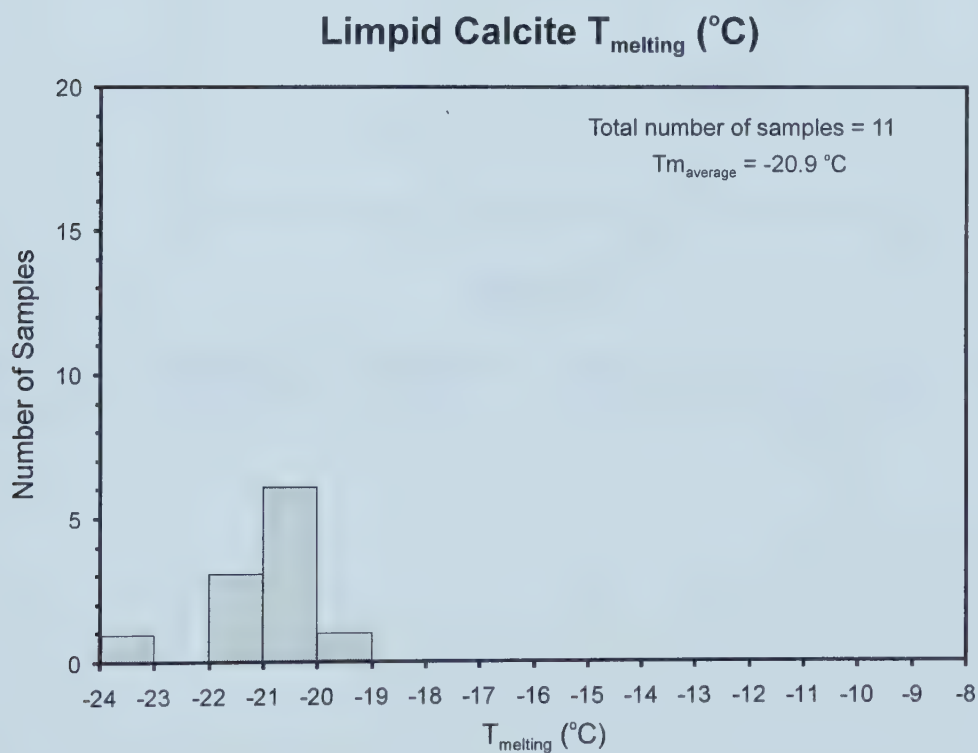
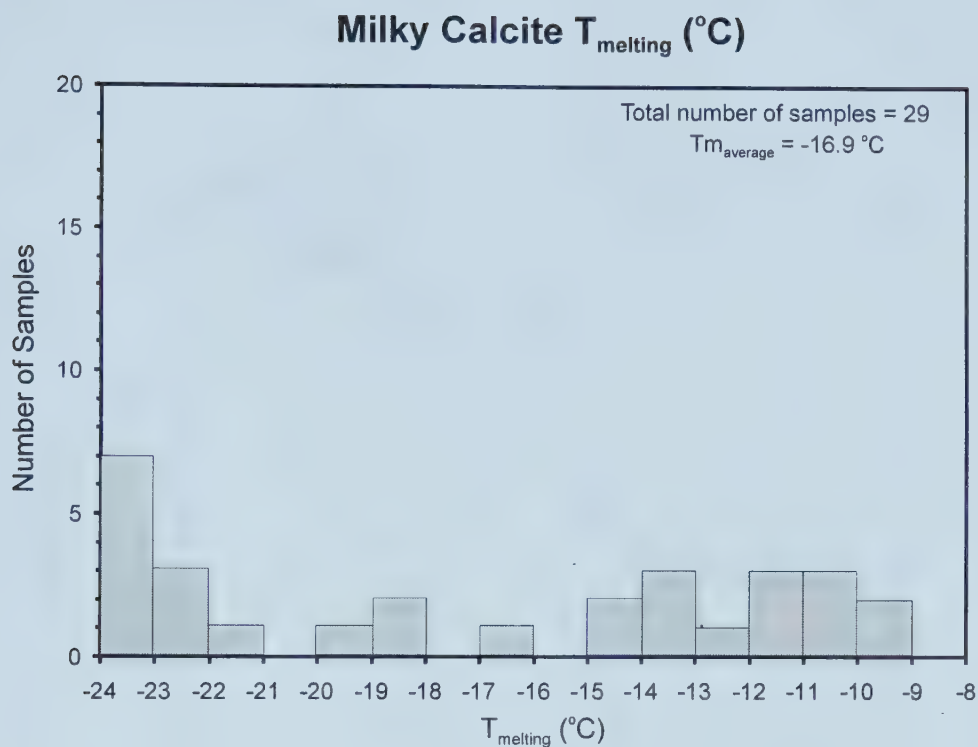


Figure 4.9 – Final melting temperature histograms for milky and limpid calcite cements.

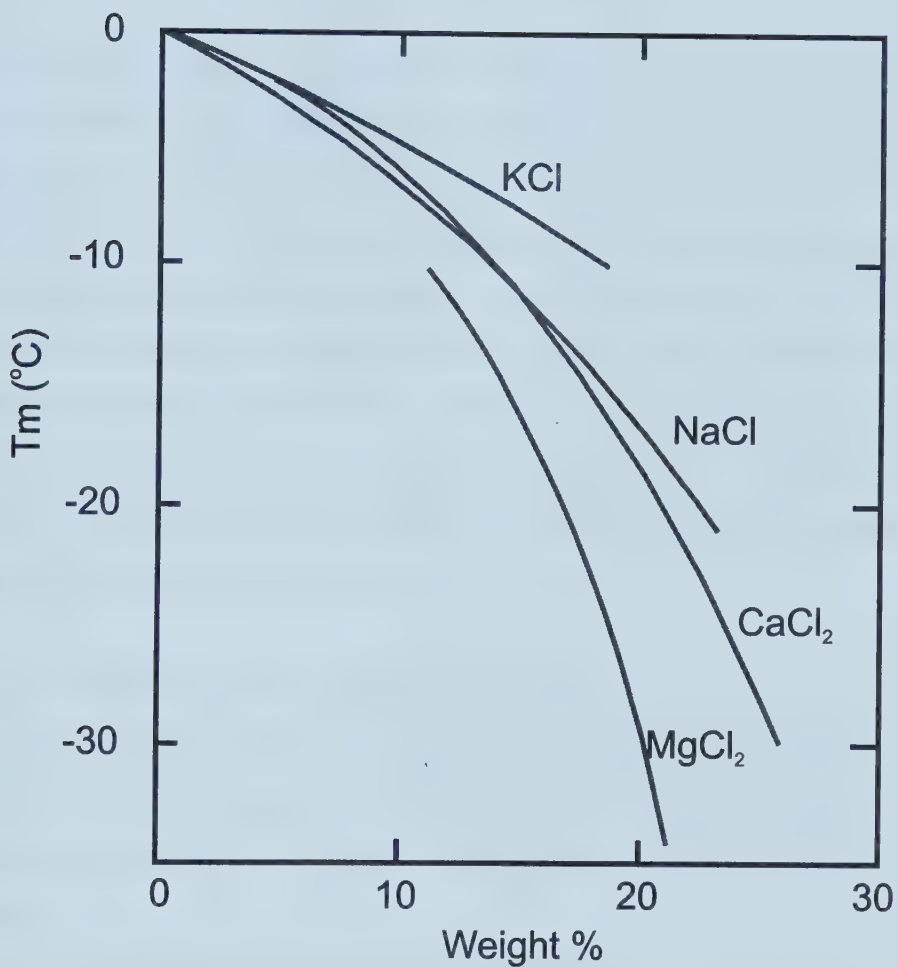


Figure 4.10 – Freezing point depression of water for NaCl, KCl, CaCl_2 , and MgCl_2 solutions. Data from Linke (1958, 1965). Modified from Crawford (1981).

CHAPTER 5

DISCUSSION

The Peace River Arch area has undergone a tectonic evolution that is very different than the rest of the Western Canada Sedimentary Basin. This unique geological environment gave rise to numerous and varied fluid pathways while fostering the development of distinct stratigraphic relationships. Geochemical analyses of the mineral phases in the Leduc Formation indicate that the diagenetic history of these Late Devonian sediments is complex and involved many stages. The diagenetic mineral phases identified in the study area each have a distinctive geochemical signature that reflects the timing of emplacement and the nature of the source fluids. The Leduc Formation has undergone a complex diagenetic history influenced by reoccurring regional tectonism, localized faulting, and fluid movements.

5.1 Diagenetic Fluids and Burial History

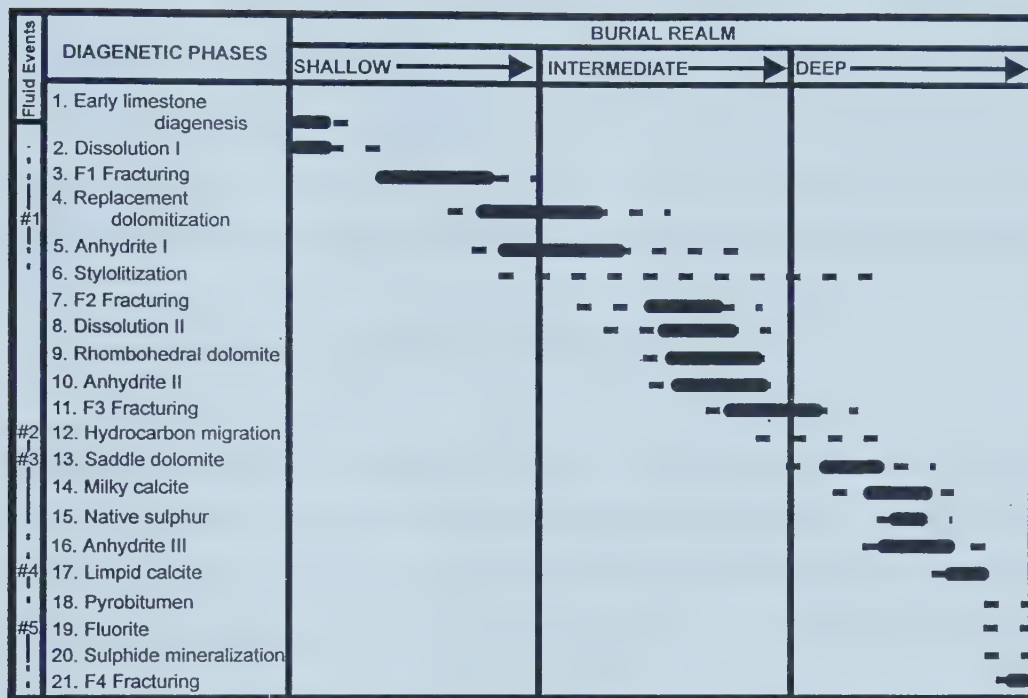
Geochemical data presented to date suggest that at least five major fluid events were involved in the diagenetic evolution of the Peace River Arch area. The fluid events may be characterized by their diagenetic products, each with distinctive geochemical signatures.

5.1.1 Fluid event #1: matrix dolomitization

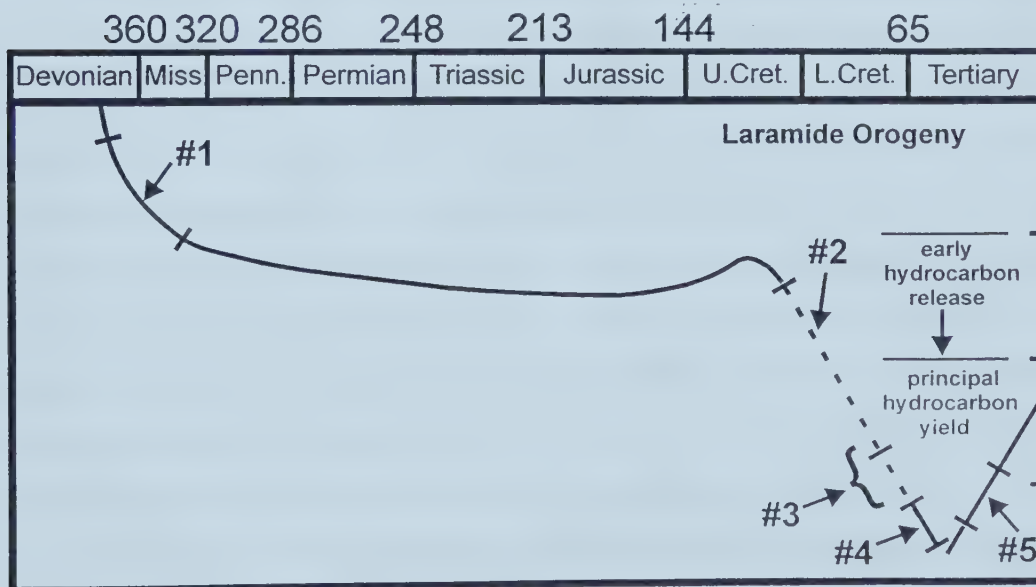
Pervasive matrix-replacive dolomite is thought to form in the subsurface in the shallow and intermediate burial realms from limestone precursors. The Leduc Formation in the Peace River Arch area is pervasively dolomitized throughout most of the carbonate platform and reefal buildups indicating that 1) there was ample dolomitizing fluid available and 2) the carbonates must have formed a relatively continuous, porous and permeable conduit.

This first major fluid event led to the formation of matrix-replacive dolomite types M1 to M5 (Phase 4, Figure 5.1). Their stable isotope δ -values ($\delta^{13}\text{C} = 0.0$ to 2.2‰ PDB, $\delta^{18}\text{O} = -9.3$ to -4.7‰ PDB) indicate that these types likely formed from chemically modified Late Devonian seawater. Petrographically similar matrix dolomite

Figure 5.1 – a) Southwest Peace River Arch paragenetic sequence including interpreted fluid events and their relative timing. Solid lines indicate the probable range of an event, whereas dashed lines indicate uncertainty in that range. b) Burial history profile of the Leduc platform based on vitrinite reflectance. Burial depths below 1 km are poorly constrained. Dashed lines indicate uncertainty in the burial position of the Leduc. The timing of the Laramide Orogeny and hydrocarbon generation in the area are also indicated. Modified from Dix (1993).



Million Years



samples from across the WCSB have this same range of stable isotope ratios. - Strontium ratios released from basinal shales during the relatively early stages of diagenesis are in the range of 0.7090 to 0.7095 (Cavell and Machel, 1997; Machel and Cavell, 1999). These values match the average matrix dolomite $^{87}\text{Sr}/^{86}\text{Sr}$ value of 0.7092 and are below MASIRBAS. If the matrix dolomite was formed during burial diagenesis at depths between 300 to 500 m, temperatures from 50 to 80 °C would be expected based on an average geothermal gradient of 30°C/km and an estimated surface temperature of 25°C, as estimated using the dolomite-water fractionation equation of Fritz and Smith (1970):

$$\delta^{18}\text{O}_{\text{dolomite}} - \delta^{18}\text{O}_{\text{fluid}} = 2.78 \times 10^6 \cdot T^{-2} + 0.11$$

By assuming that the $\delta^{18}\text{O}_{\text{fluid}}$ was that of seawater, varying between 0 to - 2.5 ‰ SMOW (Popp *et al.*, 1986; Gregory, 1991; Holmden and Muehlenbachs, 1993), the temperature of formation for matrix dolomite lies between 49 and 80 °C. This is an appropriate range for early matrix-replacive dolomite that is known to have formed in shallow and intermediate burial depths throughout the WCSB.

Moreover, the rhombohedral dolomite crystals (Phase 9, Figure 5.1) are similar to matrix dolomite in terms of their stable isotopic range, but have slightly higher strontium ratios. Petrographically, these dolomites appear to have formed after both matrix dolomite and fracture event #2. However, the similarity of stable isotopic ranges suggests that rhombohedral dolomite crystals formed from the same parent fluid as the matrix dolomite. Using the same $\delta^{18}\text{O}_{\text{fluid}}$ as that of matrix dolomite (seawater range) and the dolomite-water fractionation equation from Fritz and Smith (1970), a temperature range of 47 to 54 °C results for the rhombohedral dolomite cements. Although this temperature range is narrower than that calculated for matrix dolomite, it is reasonable for the precipitation of cements at shallow to intermediate burial depths.

The higher average strontium value (0.7103) for rhombohedral dolomite is the only known geochemical parameter to differentiate it from matrix dolomite. However, this value is still below MASIRBAS, indicating that there was not likely an extra-basinal influx of ^{87}Sr when rhombohedral dolomite cements formed.

Similarly, A2 anhydrite cements (Phase 10, Figure 5.1) have a strontium isotope average of 0.7095 and are interpreted to have formed early in the paragenetic sequence associated with F2 fractures. It is likely that A2 cements also formed from chemically modified seawater. Leaching of primary sulphates by seawater percolating through the overlying strata of the Nisku Formation and the re-mobilization of sulphate into the Leduc would result in the precipitation of secondary anhydrite infilling fractures and pores.

5.1.2 – Fluid event #2: hydrocarbon migration

The second major fluid event in the Peace River Arch area occurred after F3 fractures and constitutes hydrocarbon generation and migration (Phase 12, Figure 5.1). The timing of hydrocarbon generation in a basin can vary depending upon the type of kerogen involved and the geothermal gradient of the area. However, the top of the oil window is generally considered to be at a depth between 2-3 km (~100 °C) (Hunt, 1996). This depth interval corresponds to the deepest burial of the Leduc strata in the PRA area as a result of basin downwarping during the Laramide Orogeny (Figure 5.1).

5.1.3 Fluid event #3: TSR and initial injection of ⁸⁷Sr-enriched brines

Fluid event #3 occurred immediately following hydrocarbon migration, and corresponds to the deep burial of the Leduc in the PRA area as well as the Laramide Orogeny (Figure 5.1). This fluid event resulted in the precipitation of saddle dolomite and milky calcite cements. Saddle dolomite was the first phase to be precipitated from this fluid. Saddle dolomite crystals emit a sulphurous odour upon crushing, and some are coloured brown by the abundance of hydrocarbon fluid inclusions within them. Therefore, fluid event #3 likely overlaps, in part, with the end of fluid event #2.

Saddle dolomite cements (Phase 13, Figure 5.1) have carbon isotope values that correspond to Late Devonian marine dolomite. However, they exhibit an oxygen isotope trend toward increasingly negative $\delta^{18}\text{O}$ ($\leq -10.8\text{‰}$) values. This observation indicates that saddle dolomite formed either over a range of temperatures or during an influx of meteoric water into the system. It is highly unlikely that meteoric water was a contributing factor to the fluid system, given the depths that saddle dolomite was formed. It does not seem probable that meteoric water could percolate down through 2 km of

strata without considerable mixing and water-rock interaction. If meteoric water did reach the Devonian strata, it would not likely have retained a true "meteoric" signature and would have had much less of an effect on the oxygen isotopic signature of cement phases.

On the other hand, since temperatures would be elevated at this depth in the subsurface, it is reasonable to attribute the depleted oxygen trend to an elevated temperature range. Saddle dolomite cements have been interpreted to form at elevated temperatures and in the intermediate to deep burial regime throughout the WCSB (Mountjoy *et al.*, 1991; Amthor *et al.*, 1993; Patey, 1995; Drivet and Mountjoy, 1997; Duggan, 1997). At approximately 2-3 km depth, one would expect temperatures to reach $\geq 100^{\circ}\text{C}$, assuming an average geothermal gradient of $30^{\circ}\text{C}/\text{km}$ and a surface temperature of 25°C .

Fluid inclusion homogenization temperatures for milky calcite (Phase 14, Figure 5.1) indicate its formation to be at an average temperature of 137.3°C which corresponds to intermediate and deep burial depths in the study area. Using the calcite-water fractionation equation of Friedman and O'Neil (1977):

$$\delta^{18}\text{O}_{\text{calcite}} - \delta^{18}\text{O}_{\text{fluid}} = 2.78 \times 10^6 T^{-2} - 2.89$$

a calculated $\delta^{18}\text{O}_{\text{fluid}}$ value of approximately $+10.1\text{‰}$ is derived for its parent fluid. It is clear that this parent fluid is not marine. Furthermore, fluid inclusion melting temperatures indicate that these fluids were brines with a salinity up to 21 wt.% NaCl equivalent. This salinity is about six times as concentrated as seawater.

Thermochemical sulphate reduction (TSR) occurred concurrently with or shortly after milky calcite precipitation, as indicated by the characteristic negative carbon signature in these cements, as well as their petrographic relationship to native sulphur in the sour gas reservoirs. TSR could not have occurred without hydrocarbons first being present in the reservoir, thus it must have occurred after fluid event #2. However, there appears to be some temporal overlap between hydrocarbon migration, saddle dolomite precipitation, and the start of TSR (Figure 5.1). Saddle dolomite crystals do not exhibit

the same negative shift in $\delta^{13}\text{C}$ as does milky calcite, suggesting that saddle dolomite formed prior to both TSR and milky calcite precipitation. On the other hand, saddle dolomite crystals smell sulphurous upon crushing, suggesting the presence of H_2S when they formed.

Strontium isotope ratios for both saddle dolomite and milky calcite are well above MASIRBAS, indicating that radiogenic Sr was injected into the fluid system in the Leduc at about the time saddle dolomite and milky calcite cements formed during intermediate to deep burial. Sr-bearing fluids may have been continuously injected into the Devonian aquifer system, or fluid injection may have occurred in two or more pulses, coincident with the formation of the two cements. There may have been a mixing of two separate fluids: 1) a brine carrying a non-marine stable isotope signature, and 2) a fluid with a radiogenic strontium component.

The latest phase of anhydrite cement to precipitate, type A3 (Phase 16, Figure 5.1), also exhibits a highly radiogenic range of $^{87}\text{Sr}/^{86}\text{Sr}$ ratios from 0.7125 to 0.7316. A3 anhydrite cannot be definitively placed in the paragenetic sequence, because it lacks petrographic relationships with other cements, except that it post-dates rhombohedral and saddle dolomites. Thus, it may have formed from fluid event #3, or coincident with limpid calcite during fluid event #4. Anhydrite was not present alongside milky calcite since anhydrite is one of the reactants in TSR reactions. Thus, one would not expect to find abundant anhydrite in an area where TSR has occurred.

5.1.4 Fluid event #4: main injection of ^{87}Sr -enriched brines

The next fluid event is characterized by limpid calcite cements (Phase 17, Figure 5.1). They have distinctly higher $^{87}\text{Sr}/^{86}\text{Sr}$ ratios than any of the other diagenetic phases. These strontium isotope ratios reflect continued and/or repeated injection of strontium into the fluid system. Additionally, the petrography of the limpid calcite cements suggests much lower levels of supersaturation and slower growth rates. This petrographic difference to milky calcite cements, as well as the near marine $\delta^{13}\text{C}$ values, suggest a significant hiatus between these two calcite types. Unlike saddle dolomite and milky calcite, limpid calcite forms a distinct, non-overlapping field on a plot of oxygen vs. strontium (Figure 4.4). The strontium isotopic ratios are well above MASIRBAS,

indicating that the strontium-bearing fluids could not have been derived from basinal shales and were more likely injected from an extra-basinal source. The average homogenization temperature of 141.7 °C may also be used to estimate the probable $\delta^{18}\text{O}_{\text{fluid}}$ of the parent fluid that the late-stage limpid calcite was precipitated from. Using the calcite-water fractionation equation:

$$\delta^{18}\text{O}_{\text{calcite}} - \delta^{18}\text{O}_{\text{fluid}} = 2.78 \times 10^6 \text{ T}^{-2} - 2.89$$

of Friedman and O'Neil (1977), the calculated $\delta^{18}\text{O}_{\text{fluid}}$ is +2.1‰. This is the signature of a water that is only slightly enriched in O^{18} as compared to seawater. Moreover, the average T_e and T_m for limpid calcite indicates that it formed from a complex salt brine with salinity reaching 23 wt.% NaCl equivalent, *i.e.*, a different fluid than that which formed saddle dolomite and milky calcite.

Furthermore, an average T_h of 141.7 °C corresponds to a depth of formation for the limpid calcite between 3-4 km with a normal geothermal gradient, indicating that there was not a thermal anomaly associated with the injection of the ^{87}Sr -rich brines.

5.1.5 Fluid event #5: relaxation of ^{87}Sr -enriched brine injection and re-equilibration

A final fluid phase may be distinguished based on the latest forming cements identified and analysed in the study. There is some question as to the exact timing of this fluid event as the latest cement phases are not constrained on their upper limit of formation by other diagenetic phases. Fluorite (Phase 19, Figure 5.1), disseminated sulphide minerals (Phase 20, Figure 5.1), and black pyrobitumen (Phase 18, Figure 5.1) are all found as the latest stage cements after the major porosity-occluding phases. Although fluorite and the sulphide minerals are volumetrically a very small part of the diagenetic phases, they do indicate that fluids with unique chemistries affected the Devonian strata, and suggest that different fluid sources and more complex migration pathways existed in the PRA than elsewhere in the WCSB.

Fluorite cement appears only in one well in the study area; however, its presence does suggest that a late stage fluid event, though limited in extent and/or amount of fluid,

affected the Devonian system. Strontium isotopic ratios for fluorite samples ($n = 4$) are all above MASIRBAS, but much lower than that of the limpid calcite. Fluorite precipitation occurred from a fluid enriched in radiogenic strontium that likely had, however, already passed through its maximum injection period.

Pyrobitumen is the solid residue left behind upon final cracking of oil to dry gas in a reservoir. Its timing of emplacement in the study area is interpreted as late and at maximum burial depth because of its paragenetic association, and by the temperature range required to crack oil to dry gas in the subsurface (150-225 °C) (Hunt, 1996). Dry gas formation is associated with the latest stages of petroleum generation in the subsurface, occurring at depths below 4 km (Hunt, 1996). The emplacement of pyrobitumen may have been prior to or later than fluorite precipitation in the Leduc.

Lead/zinc sulphide mineralization is also attributed to late stage fluids in the study area. These are very minor cement components in the study area and there are no known basinal sources for lead or zinc. Either there was input from an extra-basinal fluid, perhaps igneous or metamorphic in origin, or base metals were leached out of the nearby Granite Wash Formation.

5.2 Sources and Migration Pathways of Strontium Bearing Fluids

In the previous section, a highly radiogenic strontium component was identified in fluid events 3 to 5. Since this strontium has isotope ratios much higher than MASIRBAS, the excess ^{87}Sr cannot have come from the basinal shales. Therefore, potential sources of radiogenic strontium in the Peace River Arch area include: 1) the sediments overlying or underlying the Leduc Formation, 2) the Granite Wash Formation, 3) Precambrian igneous and metamorphic basement rocks, and 4) the metamorphic and volcanic rocks exposed in the Rocky Mountains.

The first possibility can be evaluated using a study to determine the geochemical characteristics of the rocks and formation fluids in the strata of the WCSB by Connolly (1990) and Connolly *et al.* (1990a and b). The formation fluids analysed in the shallow Jurassic, Cretaceous and Tertiary feldspathic sandstones all had measured strontium ratios below MASIRBAS. Furthermore, several of these samples exhibited some of the

lowest $^{87}\text{Sr}/^{86}\text{Sr}$ ratios (as low as 0.7057) documented in the WCSB. Additionally, a geochemical study by Armstrong *et al.* (1998) on the Upper Cretaceous Milk River Group (including sandstones, the surrounding shales, and the overlying glacial till) revealed that these sediments also fell well below MASIRBAS with $^{87}\text{Sr}/^{86}\text{Sr}$ ratios between 0.7069 and 0.7082. Thus, the overlying Mesozoic and Cenozoic sediments are an unlikely source of highly radiogenic fluids in the Devonian reservoirs. However, there are no analyses of Cambrian formation fluids at this time, thus there is no way to positively discount the strontium contribution from Cambrian clastic sediments in the PRA area. Three Cambrian shale samples were analysed by Connolly *et al.* (1990b) which have $^{87}\text{Sr}/^{86}\text{Sr}$ ratios between 0.7431 and 0.7757. However, the analysis was not done by a stepwise leaching process, thus, these strontium values represent the total radiogenic strontium component in the shales, as opposed to the total radiogenic strontium that would be released from the shales under conditions of normal basinal diagenesis.

The second possible source is the Granite Wash sand, derived from the erosion of the exposed Peace River Arch landmass during the time of Leduc sedimentation. In the study area it is known to interfinger with the Leduc Formation on its shoreward margin (Figure 2.5), forming a continuous fluid pathway between the two formations (Dix, 1994; Dec, Hein, and Trotter, 1996). Although no isotopic strontium data from the Granite Wash have been collected or analysed to date, it is possible that these feldspathic sands are a viable source for the highly radiogenic fluid component known to have affected Leduc diagenesis. Locally, fluids could have moved through the Granite Wash Formation and into the Leduc, carrying with them enough radiogenic strontium to result in the precipitation of late-stage calcite cements with the observed high $^{87}\text{Sr}/^{86}\text{Sr}$ ratios. If so, one might also expect that a highly radiogenic strontium signature was prevalent in all of the diagenetic phases in the Leduc, including matrix dolomite. However, it is possible that an early release of strontium from the Granite Wash at the time of pervasive matrix dolomitization was negligible due to the shallow depths and lower temperatures encountered at this stage in the diagenetic history of the Leduc Formation.

A third possible source for radiogenic strontium in the study area is the Precambrian basement. In the PRA area, local syn- and post-Leduc faulting has been recognized at Tangent, Normandville, Eaglesham, Puskwaskau, and the top of Sturgeon Lake fields (Stoakes, 1987; Packard *et al.*, 1990; Mountjoy and Halim-Dihardja, 1991). The influence of Precambrian lineaments on local faulting has been recognized as NE-SW and NW-SE trending basement-derived fault zones that can be seen underlying the Palaeozoic strata on structural contour maps of the area (Figure 2.11) (O'Connell *et al.*, 1990). In studies on Devonian strata to the south of the PRA, late-stage cements with high strontium ratios have been attributed to deeply-circulating, radiogenic brines derived from the Precambrian and channelled upward through basement faults (*i.e.* Green *et al.*, 1997). A study by Duggan (1997) on the Swan Hills Simonette field identified late dolomite and calcite cements with highly radiogenic strontium isotopic values (dolomite = 0.7100 to 0.7350, and calcite = 0.7200 to 0.7369). The fluids that precipitated these highly radiogenic cements have been attributed to Precambrian basement faulting in the Simonette area. Similarly, Green and Mountjoy (1997) and Green (1999) identified radiogenic ($^{87}\text{Sr}/^{86}\text{Sr} = 0.7088$ to 0.7310) late carbonate and anhydrite cements associated with basement faulting in the Leduc and Wabamun Formations at Pine Creek field and in the Swan Hills Formation at Kaybob South field (Figure 1.1).

Geochemical analyses of the Precambrian basement rocks from outcrop in the Canadian Shield yield $^{87}\text{Sr}/^{86}\text{Sr}$ values ranging from 0.7065 to 0.7400 (McNutt *et al.*, 1990; Franklyn *et al.*, 1991). Thus, the Precambrian basement is a potential source of the radiogenic strontium carried by the late fluids in the Leduc Formation during deep burial, late-stage cementation. However, one must also consider the amount of mixing and water-rock interaction that basement-derived brines would have undergone prior to the precipitation of cements in the Leduc. The highest strontium ratio obtained from late-stage cements in the study area is 0.7337, and the highest $^{87}\text{Sr}/^{86}\text{Sr}$ ratio of Precambrian samples is 0.7400. If a fluid with a maximum $^{87}\text{Sr}/^{86}\text{Sr}$ ratio of 0.7400 was to move up through the strata to reach the Devonian, some of the strontium would be lost *en route*, due to water-rock interaction with the underlying strata, and mixing with the connate

formation waters would result in values between the marine (0.7080) and radiogenic (0.7400) end members.

The fourth possible source for the highly radiogenic strontium found in the late stage cements is in the Rocky Mountains. Stepwise strontium extraction from metamorphic slate samples from Proterozoic-aged Miette Group metasediments has yielded $^{87}\text{Sr}/^{86}\text{Sr}$ ratios much higher than MASIRBAS (as high as ~0.9400 from the final solution) (Cavell and Machel, 1997; Machel and Cavell, 1999). Radiogenic strontium within the Miette metasediments would be liberated as fluids passed through them during metamorphism because the strong bonds holding Sr to silicate lattices in the rock-forming minerals would have been broken down at metamorphic temperatures. Moreover, calcite veins cross-cutting the Miette Group clastic and carbonate sediments near Jasper, Alberta have been interpreted as Laramide in age by Koffeyberg (1994), who measured the $^{87}\text{Sr}/^{86}\text{Sr}$ ratios of the veins between 0.7560 to 0.7783 in the clastics, and 0.7335 to 0.7355 in the carbonates. These data indicate that highly radiogenic strontium was present in the pore fluids of the Miette Group when calcite veins formed therein.

Highly radiogenic strontium in carbonate cements identified in the Obed gas field (Machel *et al.*, 1996) are thought to have precipitated, in part, from the same ^{87}Sr -bearing fluids that formed the calcite veins in the Miette Group. It has been argued that fluids entered the Southesk-Cairn carbonate platform from the edge of the disturbed belt on the western margin of the basin, migrated eastward through the carbonate aquifer, and mixed locally with connate brines. The occurrence of the highest strontium ratios in cements in the westernmost wells (Patey, 1995; Buschkuehle *et al.*, 1998) and lower ratios to the east, suggests that there was a general west to east flow through the aquifer (Machel *et al.*, 1996; Machel and Cavell, 1999) (Figure 5.2).

Although no west to east lateral trend in $^{87}\text{Sr}/^{86}\text{Sr}$ ratios with respect to distance from the disturbed belt was observed in the wells in the PRA study area, late stage carbonate cements have the same geochemical signatures and petrographic characteristics as those found at Obed. One explanation as to why fluid pathways may have been different in the PRA is the complexity of the tectonism that occurred here, as opposed to through much of the Mesozoic (O'Connell *et al.*, 1994), creating many fluid pathways

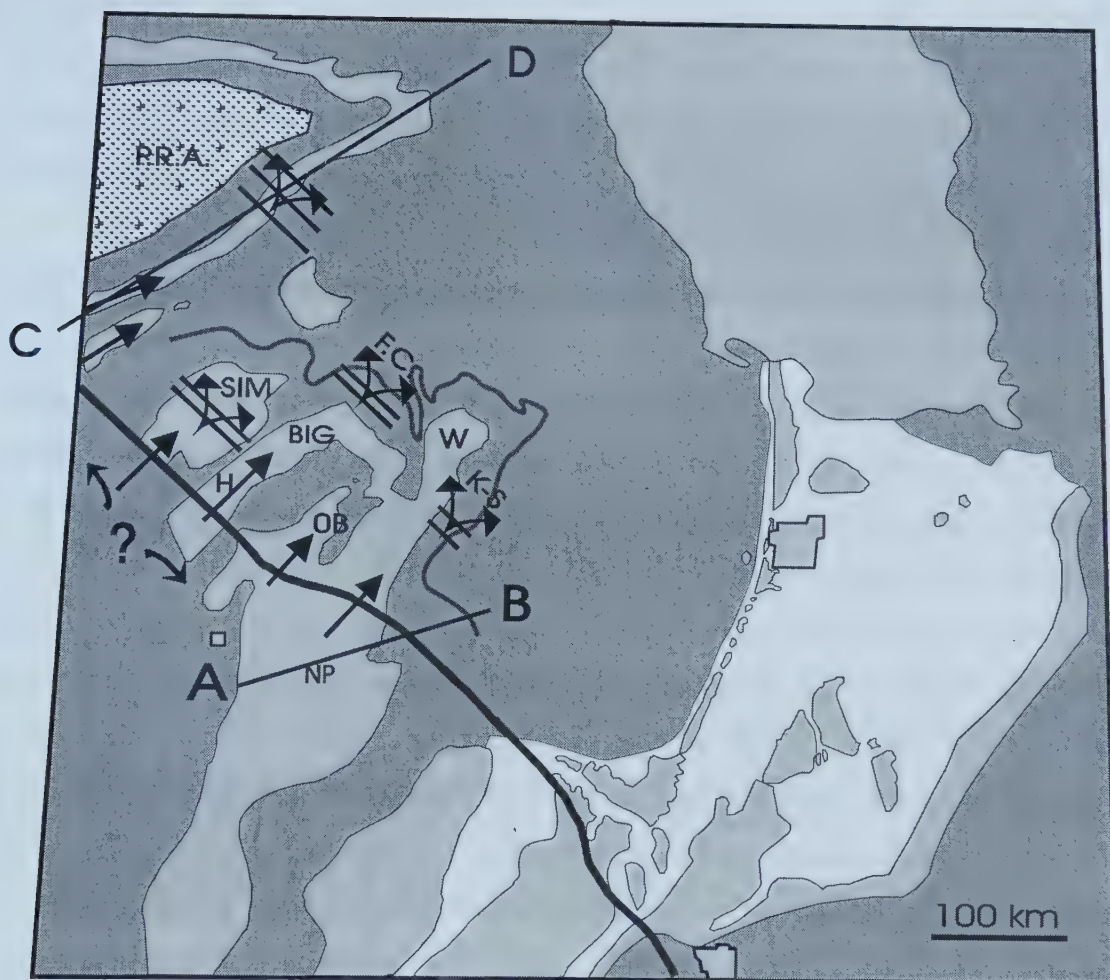


Figure 5.2 – Plan view of inferred tectonically induced flow (black arrows) on a simplified distribution map of Devonian platform and reef carbonates of the Woodbend Group in the Alberta. P.R.A. = Peace River Arch fringing reef; SIM = Simonette; F.C. = Fox Creek; K-S = Kaybob South; OB = Obed; BIG = Bigstone; H = Harley; W = Windfall; NP = Nigel Peak. Cross-sections A-B, and C-D are shown in figures 5.3 and 5.4. Modified from Machel and Cavell (1999).

and connecting stratigraphic intervals vertically. Fluids injected from the Rocky Mountains may have taken any number of pathways in the PRA area instead of that at Obed. Localized faulting has been re-activated throughout the Palaeozoic and continuing along the lateral path provided by the regional Cooking Lake aquifer underlying the Southesk-Cairn platform.

Finally, the presence of fluorite and sulphide minerals, albeit rare in most wells, further suggests that late-stage fluids with unique chemistries occurred in the diagenesis of the Leduc Formation in the study area. Late-stage magnesite, and some of the hydrothermal dolomite and late calcite, in the southern Rocky Mountains contain high concentrations of fluorine in fluid inclusions (Nesbitt and Prochaska, 1997). These authors postulated that the addition of fluorine to the system at the time of late-cement crystallization came from a distal source, possibly of igneous origin. This fluid entered Cambrian-aged carbonates in the Rockies and mixed with brines to form the late cements. In most sedimentary basin brines, fluoride concentrations are low and ocean water is considerably undersaturated with respect to fluorite (Möller *et al.*, 1980). Thus, to precipitate fluorite from a normal marine brine, and additional source of fluorine or a geochemical process that causes F⁻ enrichment in normal ocean water, must be found. No local source of fluorine can be detected within the PRA area, from strata either above or below the Leduc Formation.

Lead and zinc sulphides are commonly found in rocks of igneous origin, and their presence in some carbonate host rocks is generally attributed to remobilization of the sulphide phases and mineralization via hydrothermal fluids. The most well-known example of sulphide mineralization in a carbonate host rock in the WCSB is the Pine Point mineral deposit, located in the Northwest Territories just north of the Alberta border. Thus, the appearance of late-stage sulphide minerals suggests that basinal fluids may have mixed with a late-stage extra-basinal fluid component.

5.3 Implications for Tectonically-Expelled "Squeegee" Flow in the Peace River Arch Area

The data presented in this study attempt to constrain the number of fluid events and possible sources for the fluids that affected the Leduc Formation in the PRA area. It has been argued that there have been at least five separate fluid events, three of which involved the transport of highly radiogenic, possibly extra-basinal radiogenic strontium to the Devonian carbonates.

The tectonic expulsion of fluids from mountain belts into foreland basins has been postulated in several models (Oliver, 1986; Bradbury and Woodwell, 1987; Ge and Garven, 1989, 1992, 1994; Deming *et al.*, 1990; Bachu, 1995). However, none of these studies provided mineralogical or geochemical evidence to support the remobilization of fluids from the Rocky Mountains into the WCSB. The first study to document that diagenetic products formed under the influence of tectonic-expulsion of fluids into the basin was that of Machel *et al.* (1996). In this study, late forming carbonate cements with highly radiogenic $^{87}\text{Sr}/^{86}\text{Sr}$ ratios in the Obed sour gas field were attributed to fluids sourced in the Rocky Mountains. Since then, additional studies (*i.e.* Machel and Cavell, 1999; Buschkuehle, in prep.; Skilliter, in prep.) have been conducted at the University of Alberta in an attempt to document late-stage, highly radiogenic Sr-bearing cements in Devonian sediments within, and near to, the disturbed belt in Alberta. Recent field studies in the Rocky Mountains have added outcrop data and field observations to the data set.

White, coarsely crystalline calcite spar has been observed in veins that cross-cut the Proterozoic and Cambrian sections of the Rocky Mountain Main and Front Ranges (Machel and Cavell, 1999). These coarse crystalline calcites are petrographically similar to the late milky calcites observed in the subsurface, and in exposed Devonian sections in the Rocky Mountains at Nigel Peak (Figure 5.2). Furthermore, Laramide-aged calcite in veins in the Miette Group in the Rocky Mountains has similarly high radiogenic strontium values as those documented in this study.

Additional geochemical studies by Nesbitt and Muehlenbachs (1994, 1995, 1997) on quartz and carbonate veins in the southwestern Rocky Mountains have led to the suggestion that a pre-Laramide, SW-NE fluid flow occurred in the Middle Cambrian aquifer. This remobilization of brines precipitated saddle dolomite, magnesite, talc, and

lead-zinc sulphides along a flow distance of 40-80 km in what is now the Rocky Mountain Main and Front Ranges. Furthermore, these researchers also asserted that syn- to post-Laramide fluid flow involving the convection of meteoric fluids was responsible for the precipitation of calcite and quartz veins in the Rocky Mountain Front Ranges.

5.3.1 Migration pathways of tectonically-expelled fluids

If the fluids that carried radiogenic strontium into the foreland basin were derived from the Proterozoic Miette Group, they would have had to reach the Devonian strata through a continuous aquifer. Cross-sections taken from the Rocky Mountain Main Ranges through to the disturbed belt (Figure 5.3) demonstrate the juxtaposition of Proterozoic and Palaeozoic strata by thrust faulting as a result of orogenesis. Many of these rocks are impermeable. However, where porosity and permeability within the thrust sheets were not conducive to fluid flow, the development of near-horizontal, extensional, tectonic fracturing occurred as observed in outcrop in the Proterozoic and Cambrian strata (Machel and Cavell, 1999). Finally, the tectonic expulsion of fluids would have occurred contemporaneously with orogenesis. Thus, the thrust faults themselves would have acted as conduits for fluid movement (*i.e.* Bradbury and Woodwell, 1987; Ge and Garven, 1994).

Recent stratigraphic correlations of the Devonian “shale” aquitards indicate that these aquitards pinch out and are absent next to the disturbed belt in the subsurface (Figure 5.4) (Skilliter *et al.*, 1998; Wendte *et al.*, 1998; Skilliter, in prep.). Thus, the Devonian section forms a continuous aquifer from the Elk Point Group, or D4, to the Wabamun Formation, or D1, at the edge of the disturbed belt. If fluids were expelled into the Devonian at the edge of the disturbed belt, both horizontal migration, within the Devonian, and vertical migration to other strata, could have taken place. The analogy of an “ill-fitting garden hose” has been presented by Machel and Cavell (1999) to describe the multi-directional flow that may have occurred as fluids were squeezed out of the thrust sheets and into the foreland basin. Bachu (1995) has also suggested that the deep Devonian strata close to the disturbed belt acted as a regional aquifer for the lateral, up-dip migration of northeasterly moving brines that may be tectonic in origin.

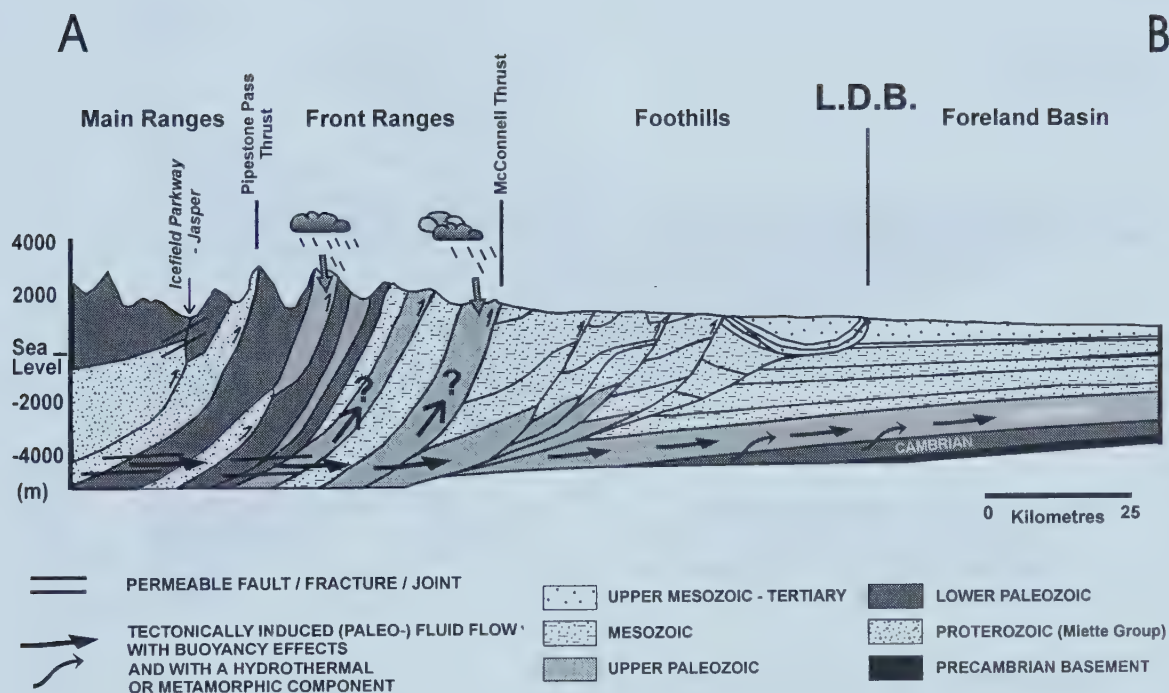


Figure 5.3 – Cross-section A-B from the Main Ranges to the deep foreland basin (see Figure 5.2 for location). Inferred tectonically-induced fluid flow is shown by the black arrows. Extensional fractures augmented fluid flow where matrix permeability was too low to facilitate significant squeegee flow. The townsite of Jasper is located a few km NW from this section in the valley marked by the Icefield Parkway. From Machel and Cavell (1999).

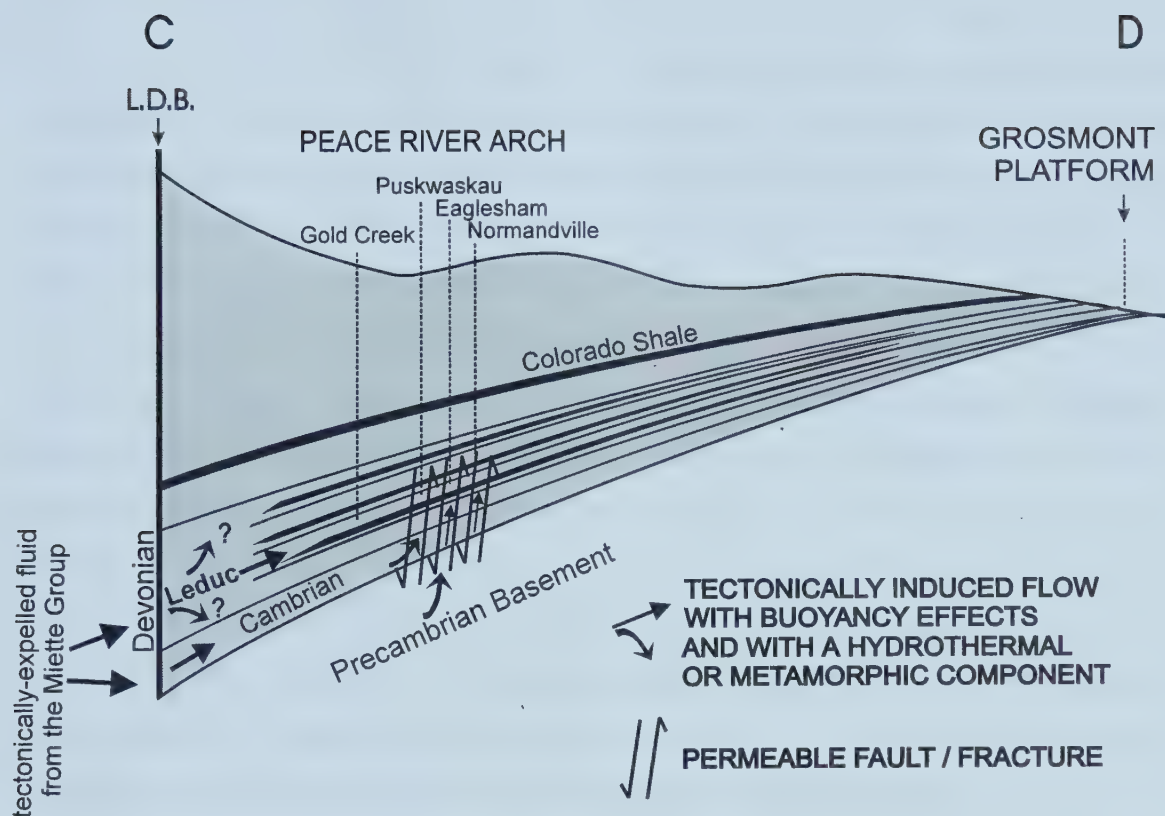


Figure 5.4 – Cross-section C-D. Mid Cretaceous to Devonian paleo-hydrostratigraphic flow systems in the southwestern PRA area (refer to Figure 5.2 for location). Included are the major aquitards, faults, and the inferred directions of tectonically-induced fluid flow. The Devonian aquifers are laterally extensive throughout most of the basin, but disappear near to the limit of the disturbed belt (L.D.B.) where the carbonates are stacked to form a continuous D4-D1 “mega-aquifer”. At the L.D.B., because of the missing aquitards, much of the tectonically-induced flow did not get funnelled into discrete Devonian aquifers. Instead fluids escaped upwards, sideways, and downwards. Tectonically-induced fluid flow may have also taken place through the Cambrian sandstones, from where it may have ascended at various locations through sub-vertical faults. Modified after Machel and Cavell (1999).

In the case of the PRA, vertical faulting created a secondary conduit to transport tectonically-expelled fluids upward from the Precambrian basement and/or Cambrian clastics to the overlying Devonian strata. If fluids had migrated laterally at a deeper level they could have been channelled upwards into the Devonian and overlying strata via fault conduits. This process of fluid migration has been argued as an explanation for the emplacement of late-stage fault-related mineralization in 1) the Wabamun Formation in the PRA area (Packard *et al.*, 1990); 2) the Swan Hills Formation at Simonette (Duggan, 1997; Duggan and Mountjoy, 1998); 3) the Swan Hills Formation at Kaybob South (Green and Mountjoy, 1997; Green, 1999); and 4) the Leduc and Wabamun Formations at Pine Creek field (Green and Mountjoy, 1997; Green, 1999). This may well be the preferred fluid conduit system present in parts of the PRA where basement faulting is documented (*i.e.* at Normandville, Eaglesham, Puskwaskau and Sturgeon Lake fields in Figures 1.2 and 2.11). However, there are also areas around the arch where highly radiogenic cements have been detected, and where no basement faulting is present. An example of this may be found in the Gold Creek area (wells 12-22-66-06W6 and 11-30-66-07W6). Thus, radiogenic strontium may have reached the Leduc Formation by another method of transport in at least part of the PRA. The tectonic-expulsion and subsequent lateral migration of fluids cannot be ruled out at this location.

Finally, flow may have been different for the different “arms” of the PRA. Variations between Dix’s (1993) paragenetic sequence and that which has been documented in this study suggest that there may have been different processes affecting the north and south “arms of the Leduc fringing reef. The PRA structure may have acted as a barrier separating the two “arms” into two distinct diagenetic and hydrodynamic realms.

5.3.2 Fluid flux and the lateral extent of fluid movement

The fluid fluxes associated with the tectonic-expulsion of fluids during orogenesis may be estimated from the amount and extent of the late-stage cement phases from the disturbed belt. Mathematical and hydrogeological modelling by Ge and Garven (1989, 1992, 1994) and Deming *et al.* (1990) suggest that the fluid volume involved in such a process is quite small. This is consistent with the relatively small volume percent of

cements with radiogenic strontium signatures that have been documented both in this study and in the others described herein. Late-stage pore filling cements do not volumetrically make up a large portion of the total rock (up to ~ 5% over a 10 m core interval). Additionally, the rate of flow for tectonically-expelled fluids has been estimated to be in the order of a few centimetres per year, and lasting only a short time between 1000 to 10,000 years (Ge and Garven, 1989, 1992, 1994; Deming *et al.*, 1990). This observation suggests that fluids may have been expelled from the Rocky Mountains in a series of short-lived, discontinuous pulses during mountain building. If tectonically-expelled fluids from the Rockies were episodically released into the basin during orogenesis, one would expect to see distinct cement phases, all exhibiting similar radiogenic strontium signatures. Diagenetic cement phases in the PRA area, including saddle dolomite, milky and limpid calcites, and fluorite, were formed as petrographically distinct phases, even though many of them share the same highly radiogenic strontium signature.

The extent of the effect of tectonically-expelled fluids in the Obed area has been suggested to be within about 100 km of the disturbed belt (Machel *et al.*, 1996). It has also been noted that the high $^{87}\text{Sr}/^{86}\text{Sr}$ signature of cements derived from tectonically-expelled fluids decreases laterally outward from the disturbed belt into the basin. Therefore, the decreasing $^{87}\text{Sr}/^{86}\text{Sr}$ signature of cements may be used to trace the extent of influence that tectonically-expelled fluids have in the foreland basin. In the PRA area, diagenetic cements with highly strontium signatures can be found as far east as range 26 west of the 5th Meridian. This is equal to a distance of approximately 200 km from the limit of the disturbed belt.

5.4 Comparison with Dix's (1993) Study

Dix's (1993) paragenetic sequence of the northeast portion of the PRA Leduc shares some, but not all components of the sequence developed during this study. For example, Dix has noted 5 periods of fracturing, 4 of which were seen in this study. Moreover, Dix identified ferroan and green luminescent dolomite cement, neither of which was seen by this author. However, the darker zones in rhombohedral dolomite

cements, identified with CL microscopy, are indicative of Fe-enrichment in the crystal lattice (Marshall, 1988). As well, minor silicate cements were noted by Dix along the northern margin of the Leduc fringing reef (Dix, 1994). Very little geochemistry was performed on the diagenetic phases in Dix's study.

Some features that were not described in detail in Dix's study include both calcite cements and multiple anhydrite phases, which comprise the greatest volume of cements in this study. Also, Dix did not observe late-fluorite cement in the northeast PRA. This contrast between the two studies suggests that the NE and SW portions of the arch may have undergone different diagenetic histories. The main difference seems to be the types and volumes of cements found in the Leduc Formation along the two "arms" of the PRA. Since the SW portion of the arch investigated in this study lies closer to the disturbed belt, it may have been more readily affected by the Laramide Orogeny than the more distal NW portion interpreted by Dix. Tectonically-expelled fluids would have migrated a shorter distance to reach the Leduc in the SW than in the NE. Perhaps this observation is an indication of the limit that these fluids could have travelled.

CHAPTER 6

SUMMARY

The Peace River Arch Leduc Formation has undergone a complex and distinct diagenetic history that was largely influenced by the unique tectonic regime existing throughout the evolution of the Peace River Arch structure. The paragenetic sequence for the Leduc Formation involves at least 21 separate diagenetic phases, and a minimum of five fluid events have been interpreted. The major diagenetic mineral phases include matrix dolomite, rhombohedral and saddle dolomite cements, milky and limpid calcite cements, three types of anhydrite cement, fluorite cement, and disseminated lead-zinc sulphide minerals.

Carbon, oxygen, and strontium geochemical analyses of the diagenetic phases indicate that matrix dolomitization, rhombohedral dolomite cementation, and A1 and A2 anhydrite cementation occurred at relatively shallow to intermediate burial depths prior to the injection of radiogenic strontium in the system, whereas saddle dolomite, milky calcite, A3 anhydrite, and limpid calcite all formed in the intermediate to deep burial regime at elevated temperatures. These cements have high strontium isotope ratios that are not characteristic of “normal” basinal brines indicating that a ^{87}Sr -bearing fluid was injected into the fluid system as these cements precipitated. The latest stage fluorite cement also displays a high strontium ratio, but it is lower than the limpid calcite phase that precipitated from an earlier fluid event. Fluorite cementation marks the abatement of ^{87}Sr -bearing fluid injection in the Leduc Formation.

Possible sources for radiogenic strontium in the Peace River Arch area include: 1) the Granite Wash Formation, 2) the Precambrian basement rocks, and 3) the Miette Group metasediments in the Rocky Mountains. There are numerous fluid pathways in the Peace River Arch area as a result of repeated basement faulting along the flanks of the arch. Hot, circulating basement-derived brines could have been channelled upward via fault conduits into the Devonian strata. Additionally, tectonically-expelled fluids from the Rocky Mountains could have been injected into the Devonian or Cambrian aquifer system at the edge of the disturbed belt, subsequently migrating laterally and vertically in

the Devonian. Tectonically-expelled fluid flow would be of limited volume and extent, thus, mineral phases precipitated from these fluids would also be volumetrically little. The small volumes of late-stage cements in the Leduc that have highly radiogenic strontium signatures also suggest that they precipitated, in part, from fluids expelled from the Rocky Mountains during the Laramide Orogeny. The lateral extent of influence of the tectonically-expelled fluids in the PRA area cannot be definitively determined because ^{87}Sr may have been derived from both local (the Granite Wash Formation) and distal (the Rocky Mountains) sources.

Furthermore, late-stage cement precipitation temporally coincides with deep burial of the Leduc and the Laramide Orogeny suggesting that tectonically-expelled fluids affected Leduc diagenesis in the Peace River Arch area. However, the complexity of the fluid pathways and tectonism during the Arch's evolution also suggest that additional hydrodynamic processes than those interpreted here could have affected the Leduc Formation in this area.

REFERENCES

- Allan, J.R. and Wiggins, W.D., 1993, Dolomite Reservoirs - Geochemical Techniques for Evaluating Origin and Distribution. AAPG Continuing Education Course Note Series No. 36, 129 pp.
- Amthor, J.E., Mountjoy, E.W., and Machel, H.G., 1993, Subsurface dolomites in Upper Devonian Leduc Formation buildups, central part of Rimby-Meadowlark reef trend, Alberta, Canada. *Bulletin of Canadian Petroleum Geology*, v. 41, p. 164-185.
- Aulstead, K.L. and Spencer, R.J., 1985, Diagenesis of the Keg River Formation, northwestern Alberta: Fluid inclusion evidence. *Bulletin of Canadian Petroleum Geology*, v. 33, No. 2, p. 167-183.
- Aulstead, K.L., Spencer, R.J., and Krouse, H.R., 1987, Fluid inclusion and isotopic evidence on dolomitization, Devonian of Western Canada. *Geochimica et Cosmochimica Acta*. v. 52, p. 1027-1035.
- Bachu, S., 1995, Synthesis and model of formation-water flow, Alberta Basin, Canada. *American Association of Petroleum Geologists Bulletin*, v. 79, p. 1159-1178.
- Bachu, S. and Cao, S., 1992, Present and past geothermal regimes and sources rock maturation, Peace River Arch area, Canada. *American Association of Petroleum Geologists Bulletin*, v. 76, No. 10, p. 1533-1549.
- Bachu, S. and Underschultz, J.R., 1992, Regional-scale porosity and permeability variations, Peace River Arch Area, Alberta, Canada. *American Association of Petroleum Geologists Bulletin*, v. 76, No. 4, p. 547-562.
- Banner, J.L., 1995, Application of the trace element and isotope geochemistry of strontium to studies of carbonate diagenesis. *Sedimentology*, v. 42, p. 805-824.
- Barclay, J.E., Krause, F.F., Campbell, R.I., and Utting, J., 1990, Dynamic casting and growth faulting: Dawson Creek Graben Complex, Carboniferous-Permian Peace River Arch Embayment, western Canada. *In*: O'Connell, S.C. and Bell, J.S., (eds.), *Geology of the Peace River Arch*. *Bulletin of Canadian Petroleum Geology*, v 38A, p.146-148.
- Barfoot, G.L., and Rodgers, R.J., 1984, Leduc, a new life at 38. *Journal of Canadian Petroleum Technology*, May-June, p. 41-46.
- Bethke, C.M. and Marshak, S., 1990, Brine migrations across North America - the plate tectonics of groundwater. *Annual Reviews in Earth Planetary Sciences*, v. 18, p. 287-315.
- Bond, G.C. and Kominz, M.A., 1984, Construction of tectonic subsidence curves for the early

Paleozoic miogeocline, southern Canadian Rocky Mountains: implications for subsidence mechanisms, age of breakup, and crustal thinning. *Geological Society of America Bulletin*, v. 95, p. 155-173.

Bradbury, H.J. and Woodwell, G.R., 1987, Ancient fluid flow within foreland terrains. *In*: Goff, J.C. and Williams, B.P.J., (eds.), *Fluid flow in sedimentary basins and aquifers*. Geological Society Special Publication, No. 34, p. 87-102

Burke, W.H., Denison, R.E., Hetherington, E.A., Koepnick, R.B., Nelson, H.F., and Otto, J.B., 1982. Variations of seawater $^{87}\text{Sr}/^{86}\text{Sr}$ throughout Phanerozoic time. *Geology*, v. 10, p. 516-519.

Burwash, R.A., and Krupicka, J., 1970. Cratonic reactivation in the Precambrian basement of Western Canada. II. Metasomatism and isostasy. *Canadian Journal of Earth Sciences*, v. 7, 1275-1294.

Buschkuehle, B.E., Machel, H.G., and Cavell, P.A., 1998, Paleofluid flow within the Middle and Upper Devonian Southesk-Cairn carbonate complex, Rocky Mountain foreland basin, as determined from carbonate cements. CSPG/CSEG/CWLS Joint Annual Convention, Geo-Triad '98, Abstracts, p. 121-122.

Buschkuehle, B.E., Ph.D. thesis, University of Alberta, Edmonton, Alberta, in preparation.

Cant, D.J., 1988, Regional structure and development of the Peace River Arch, Alberta: A Paleozoic failed-rift system?. *Bulletin of Canadian Petroleum Geology*, v. 36, No. 3, p. 284-295

Carpenter, S.J. and Lohmann, K.C., 1989, $\delta^{18}\text{O}$ and $\delta^{13}\text{C}$ variations in Late Devonian marine cements from the Golden Spike and Nevis reefs, Alberta, Canada. *Journal of Sedimentary Petrology*, v. 59, p. 792.

Cavell, P.A. and Machel, H.G., 1996, Tectonic expulsion of fluids into Devonian paleoaquifers in the Alberta Basin. *In*: Ross, G.M. ed., *Alberta Basement Transects Workshop*, LITHOPROBE Report #51, LITHOPROBE Secretariat, University of British Columbia, p. 225-233

Cavell, P.A. and Machel, H.G., 1997, Concretions and isotopic compositions of strontium leached from Upper Devonian shales of the Alberta Basin - implications for regional paleofluid flow. CSPG-SEPM Joint Convention, June 1-6, Program with Abstracts, p. 57.

Connolly, C.A., 1990, Geochemical and isotopic tracing of water/rock interactions in the Western Canada Sedimentary Basin. Unpublished Ph.D thesis, University of Alberta, Edmonton, Alberta, 330 pp.

- Connolly, C.A., Walter, I.M., Baadsgaard, H., and Longstaffe, F., 1990a, Origin and evolution of formation waters, Alberta Basin, Western Canada Sedimentary Basin - I. Applied Geochemistry, v. 5, p. 375-395.
- Connolly, C.A., Walter, I.M., Baadsgaard, H., and Longstaffe, F., 1990b, Origin and evolution of formation waters, Alberta Basin, Western Canada Sedimentary Basin – II. Applied Geochemistry, v. 5, p. 397-413.
- Crawford, M.L., 1981, Phase equilibria in aqueous fluid inclusions. *In*: Hollister, L.S. and Crawford, M.L., (eds.), Mineralogical Association of Canada Short Course In Fluid Inclusions: Applications to Petrology, v. 6, p. 75-100.
- Creaney, S. and Allen, J., 1990, Hydrocarbon generation and migration in the Western Canada Sedimentary Basin. *In*: Brooks, J., (ed.), Classic Petroleum Provinces, Geological Society Special Publication No. 50, p. 189-202.
- Dec, T., Hein, F.J., and Trotter, J., 1996, Granite wash alluvial fans, fan-deltas and tidal environments, northwestern Alberta: implications for controls on distribution of Devonian clastic wedges associated with the Peace River Arch. Bulletin of Canadian Petroleum Geology, v. 44, No. 3, p. 541-565.
- deMille, G., 1958, Pre-Mississippian history of the Peace River Arch. Symposium on the Peace River Arch.
- Deming, D., Nunn, J.A., and Evans, D.G., 1990, Thermal effects of compaction-driven groundwater flow from overthrust belts. Journal of Geophysical Research, v. 95, No. B5, p. 6669-6683.
- Deming, D. and Nunn, J.A., 1991, Numerical simulations of brine migration by topography-driven recharge. Journal of Geophysical Research, v. 96, No. B2, p. 2485-2499.
- Dix, G.R., 1990, Stages of platform development in the Upper Devonian (Frasnian) Leduc Formation, Peace River Arch, Alberta, Bulletin of Canadian Petroleum Geology, v. 38A, p. 66-92.
- Dix, G.R., 1993, Patterns of burial- and tectonically controlled dolomitization in an Upper Devonian fringing-reef complex: Leduc Formation, Peace River Arch area, Alberta, Canada. Journal of Sedimentary Petrology, v. 63, p.628-640.
- Dix, G.R., 1994, Deep-burial replacement of detrital silicates in a Leduc carbonate platform, Peace River Arch. Alberta. Bulletin of Canadian Petroleum Geology, v. 42, No. 1, p. 74-82.
- Drivet, E. and Mountjoy, E.W., 1997, Dolomitization of the Leduc Formation (Upper Devonian), southern Rimby-Meadowlark Reef Trend, Alberta. Journal of Sedimentary Research, V. 67, p. 411-423.

- Duggan, J.P., 1997, Sedimentology and diagenesis of Swan Hills Simonette oil field, west-central Alberta. Unpublished M.Sc. thesis, McGill University, Montreal, Quebec, 177 pp.
- Duggan, J.P. and Mountjoy, E.W., 1998, Fault-controlled dolomitization at Swan Hills Simonette Oil Field (Devonian), deep basin west-central Alberta, Canada. Submission to Sedimentology, September 1998.
- Dunham, J.B., 1962, Classification of carbonate rocks according to depositional texture. *In*: Ham, W.E. (ed.), Classification of Carbonate Rocks. American Association of Petroleum Geologists Memoirs, v. 1, p. 108-121.
- Dunham, J.B., Crawford, G.A., and Panasiuk, W., 1983, Sedimentology of the Slave Point Formation (Devonian) at Slave Field, Lubicon Lake, Alberta. *In*: Harris, P.M., ed., Carbonate Build-ups - A Core Workshop, SEPM Core Workshop #4, Dallas, April 16-17, p. 73-111.
- Epstein, S., Graf, D.L., and Degens, E.T., 1964, Oxygen isotope studies on the origin of dolomites. *In*: Craig, H., Miller, S.L., and Wasserburg, G.J., (eds.), Isotopic and Cosmic Chemistry. North-Holland Publishing Co., Amsterdam, p. 169-180.
- Friedman, I., and O'Neil, J.R., 1977, Compilation of stable isotope fractionation factors of geochemical interest. USGS Professional Paper 440KK, 12pp.
- Fritz, P., and Smith, D.G.W., 1970, The isotopic composition of secondary dolomites. *Geochimica et Cosmochimica Acta*, v. 34, p. 1161-1173.
- Ge, S. and Garven, G., 1989, Tectonically induced transient groundwater flow in foreland basin. *In*: Price, R.A., (ed.), Origin and Evolution of Sedimentary Basins and their Energy and Mineral Resources. AGU Geophysical Monograph, No. 48, p. 145-157.
- Ge, S. and Garven, G., 1992, Hydrothermal modeling of tectonically driven groundwater flow with application to the Arkoma foreland basin. *Journal of Geophysical Research*, v. 97, No. B6, p. 9119-9144.
- Ge, S. and Garven, G., 1994, A theoretical model for thrust-induced deep groundwater expulsion with application to the Canadian Rocky Mountains. *Journal of Geophysical Research*, v. 99, No. B7, p. 13,851-13,868.
- Green, D.G., 1999, Dolomitization and deep burial diagenesis of the Devonian of west-central Alberta deep basin: Kaybob South and Fox Creek (Swan Hills Formation) and Pine Creek fields (Leduc and Wabamun Formations). Unpublished Ph.D. thesis, McGill University, Montreal, Quebec, 267 pp.
- Green, D.G. and Mountjoy, E.W., 1997, Possible fault-fracture controlled dolomitization of the west-central Alberta deep basin: Pine Creek (Leduc Fm., Wabamun Fm.) and Kaybob South (Swan Hills Fm.). CSPG-SEPM Joint Convention, June 1-6, Calgary, Alberta, Program with Abstracts, p. 114.

- Gregory, R.T., 1991, Oxygen isotope history of seawater revisited: timescales for boundary event changes in the oxygen isotope composition of seawater. *In*: Taylor, H.P. Jr., O'Neill, J.R., and Kaplan, I.R. (eds.), *Stable Isotope Geochemistry: a tribute to Samuel Epstein*: Geochemical Society Special Publication No. 3, p. 65-76.
- Halbertsma, H.L. and Meijer-Drees, N.C., 1987, Wabamun limestone sequences in north-central Alberta. *In*: Krause, F.F. and Burrowes, O.G., *Devonian Lithofacies and Reservoir Styles in Alberta* Second International Symposium on the Devonian System, Calgary, p. 21-37.
- Hearn, M., 1996, Stratigraphic and diagenetic controls on aquitard integrity and hydrocarbon entrapment, Bashaw Reef Complex, Alberta, Canada. Unpublished M.Sc. thesis, University of Alberta, Edmonton, Alberta, 135pp.
- Hedinger *et al.*, 1994, The Devonian Woodbend and Winterburn Groups. *In*: Geological Atlas of the Western Canada Sedimentary Basin: Mossop, G., and Shetsen, I. (Compilers). Calgary, Canadian Society of Petroleum Geologists & Alberta Research Council.
- Hitchon B., Bachu, S., and Underschultz, J.R., 1990, Regional subsurface hydrogeology, Peace River Arch area, Alberta and British Columbia. *Bulletin of Canadian Petroleum Geology*, v. 38A, p. 196-217.
- Holmden C., and Muehlenbachs, K., 1993, The origin of oxygen isotope variations in Paleozoic carbonates: GAC-MAC Programs with abstracts, v. 18, p. A45.
- Holmden C., Creaser, R.A., and Muehlenbachs, K., 1997, Paleosalinities in ancient brackish water systems determined by $^{87}\text{Sr}/^{86}\text{Sr}$ ratios in carbonate fossils: a case study in the Western Canada Sedimentary Basin. *Geochimica et Cosmochimica Acta*, v. 61, no. 10, p. 2105-2118.
- Hunt, J.M., 1996, *Petroleum Geochemistry and Geology*, Second Edition. W.H. Freeman and Company, 743 pp.
- Hurley, N.F., and Lohmann, K.C., 1989, Diagenesis of Devonian reefal carbonates in the Oscar Range, Canning Basin, western Australia. *Journal of Sedimentary Petrology*, v. 59, p. 127-145.
- James, N.P. and Choquette, P.W., 1990, Limestones - The sea-floor diagenetic environment. *In*: McIlreath, I.A. and Morrow, D.W., (eds.), *Diagenesis*. Geological Association of Canada - Geoscience Series, v. 10, No. 4, p. 13-34.
- Kaufman, J., Hanson, G.N., and Meyers, W.J., 1991, Dolomitization of the Swan Hills Formation, Rosevear field, Alberta, Canada. *Sedimentology*, v. 38, p. 41-66.
- Klovan, J.E., 1964, Facies analysis of the Redwater reef complex, Alberta, Canada. *Bulletin of Canadian Petroleum Geology*, v. 12, p. 1-100.

- Koffyberg, A., 1994, Strontium isotopic constraints on the geochemistry and origins of regional vein-forming fluids in the southern Canadian Cordillera. Unpublished M.Sc thesis, University of Alberta, Edmonton, Alberta, 102 pp.
- Laflamme, A.K., 1990, Replacement dolomitization in the Upper Devonian Leduc and Swan Hills Formations, Caroline area, Alberta, Canada. Unpublished M.Sc. thesis, McGill University, Montreal, Quebec, 138 pp.
- Land, L.S., 1983, The application of stable isotopes to studies of the origin of dolomite and to problems of diagenesis of clastic sediments. *In: Stable Isotopes in Sedimentary Geology: SEPM Short Course No. 10*, p. 4-1 to 4-22.
- Land, L.S., 1985, The origin of massive dolomite. *Journal of Geological Education*, v. 33, p. 112-125.
- Land, L.S., Salem, R.I., and Morrow, D.W., 1975, Paleohydrology of ancient dolomites: Geochemical Evidence. *American Association of Petroleum Geologists*, v. 59, No. 9, p. 1602-1625.
- Lind, I.L., 1993, Stylolites in chalk from Leg 130, Ontong Java Plateau. *In: Berger, W.H., Kroenke, J.W., and Mayer, L.A. (eds.), Proceedings of the Ocean Drilling Program, Scientific Results*, v. 130, p. 445-451.
- Linke, W.F., 1958, Solubilities of inorganic and metal-organic compounds (4th Edition), 1. Van Nostrand, Princeton, N.J., 1407 pp.
- Linke, W.F., 1965, Solubilities of inorganic and metal-organic compounds (4th Edition), 2. American Chemistry Society, 1914 pp.
- Machel, H.G., 1990, Burial diagenesis, porosity and permeability development in carbonates. *In: Bloy, G.R. and Hadley, M.G., (eds.), The Development of Porosity in Carbonate Reservoirs. Canadian Society of Petroleum Geologists Short Course Notes*, p. 2-1 - 2-18.
- Machel, H.G., 1998, Comment on "The effects of thermochemical sulfate reduction upon formation water salinity and oxygen isotopes in carbonate reservoirs" by W.H. Worden, P.C. Smalley, and N.H. Oxtoby. *Geochimica et Cosmochimica Acta*, v. 62, No. 2, p.337-341.
- Machel, H.G., 1999, Effects of groundwater flow on mineral diagenesis, with emphasis on carbonate aquifers. *Hydrogeology Journal*, v. 7, p. 94-107.
- Machel, H.G. and Hunter, I.G., 1994, Facies models for Middle to Late Devonian shallow-marine carbonates, with comparisons to modern reefs - a guide for facies analysis. *Facies*, v. 30, p. 155-176.
- Machel, H.G., Krouse, R.H., Riciputi, L.R., and Cole, D.R., 1995a, Devonian Nisku sour gas play,

- Canada: A unique natural laboratory for study of thermochemical sulfate reduction. *In*: Vairavamurthy, M.A. and Schoonens, M.A.A., (eds.), American Chemical Society Symposium Series No. 612, p. 439-454
- Machel, H.G., Krouse, H.R., and Sassen, R., 1995b, Products and distinguishing criteria of bacterial and thermochemical sulfate reduction. *Applied Geochemistry*, v. 10, p. 373-389.
- Machel, H.G., Cavell, P.A., and Patey, K.S., 1996, Isotopic evidence for carbonate cementation and recrystallization, and for tectonic expulsion of fluids into the Western Canada Sedimentary Basin. *Geological Society of America Bulletin*, v. 108, p. 1108-1119.
- Machel, H.G. and Cavell, P.A., 1999, Low-flux, tectonically induced squeegee fluid flow ("hot flash") into the Rocky Mountain Foreland Basin, *Bulletin of Canadian Petroleum Geology*, in press.
- Machel, H.G. and Mountjoy, E.W., 1987, General constraints on extensive pervasive dolomitization - and their application to the Devonian carbonates of Western Canada. *Bulletin Canadian Petroleum Geology*, v. 35, p. 143-158.
- Marshall, D.J., 1988, Cathodoluminescence of Geological Materials. Unwin Hyman Ltd. 146 pp.
- Mattes, B.W. and Mountjoy, E.W., 1980, Burial dolomitization of the Upper Devonian Miette Buildup, Jasper National Park, Alberta. *In*: Zenger, D.H., Dunham, J.B., and Ethington, R.L., (eds.), Concepts and Models of Dolomitization. SEPM Special Publication, No. 28, p. 259-297
- McCrea, J.M., 1950, On the isotopic chemistry of carbonates and a paleothermometer scale. *Journal of Chemical Physics*, v. 18, p. 849-857.
- McCrossan, R.G., 1957, Colour variations in the Ireton shale. *Journal of the Alberta Society of Petroleum Geologists*, v. 5, p. 48-51.
- McGillivray, J.G. and Mountjoy, E.W., 1975, Facies and related reservoir characteristics, Golden Spike Reef Complex, Alberta. *Bulletin of Canadian Petroleum Geology*, v. 23, No. 4, p.753-809.
- McMechan, M.E., 1990, Upper Proterozoic to Middle Cambrian history of the Peace River Arch: evidence from the Rocky Mountains. *Bulletin of Canadian Petroleum Geology*, v. 38A, p.36-44.
- Mountjoy, E.W. and Amthor, J.E., 1994, Has burial dolomitization come of age? Some answers from the Western Canada Sedimentary Basin. *International Association of Sedimentology Special Publication*, v. 21, p. 203-229

- Mountjoy, E.W. and Halim-Dihardja, K., 1991, Multiple-phase fracture and fault-controlled burial dolomitization, Upper Devonian Wabamun Group, Alberta. *Journal of Sedimentary Petrology*, v. 61, p. 590-612.
- Mountjoy, E.W., Quing, H., and McNutt R.H., 1992, Strontium isotopic composition of Devonian dolomites, Western Canada Sedimentary Basin: significance of sources of dolomitizing fluids. *Applied Geochemistry*, v. 7, p. 59-75.
- Mountjoy, E.W., Whittaker, S., Williams-Jones, A., Quing, H., Drivet, E., and Marquez, X., 1997, Basin-wide diagenetic patterns: integrated petrologic, geochemical, and hydrologic considerations. SEPM Society for Sedimentary Geology Special Publication No. 57, p. 119-137.
- Moller, P., Schulz, S., and Jacob, K.H., 1980, Formation of fluorite in sedimentary basins. *Chemical Geology*, v. 30, p. 97-117.
- Nesbitt, B.E. and Muehlenbachs, K., 1994, Paleohydrogeology of the Canadian Rockies and origins of brines, Pb-Zn deposits and dolomitization in the Western Canada Sedimentary Basin. *Geology*, v. 22, p. 243-246.
- Nesbitt, B.E. and Muehlenbachs, K., 1995, Importance of plaeo-flow systems in the southern Canadian Rockies in the genesis of mineral deposits in the Rockies and Western Canada Sedimentary Basin. *In*: Ross, G.M., (ed.), 1995 Alberta Basement Transects Workshop, LITHOPROBE Report #47, p. 250-253.
- Nesbitt, B.E. and Muehlenbachs, K., 1997, Paleo-hydrogeology of Late Proterozoic units of southeastern Canadian Cordillera. *American Journal of Science*, v. 297, p. 359-392.
- O'Connell, S.C., 1994, Geologic history of the Peace River Arch. *In*: Geological Atlas of the Western Canada Sedimentary Basin: Mossop, G., and Shetsen, I. (Compilers). Calgary, Canadian Society of Petroleum Geologists & Alberta Research Council.
- O'Connell, S.C. Dix, G.R., and Barclay, J.E., 1990, The origin, history, and regional development of the Peace River Arch, Western Canada. *Bulletin of Canadian Petroleum Geology*, v. 38A, p. 4-24.
- Oliver, J., 1986, Fluids expelled tectonically from the orogenic belts: their role in hydrocarbon migration and other geologic phenomena. *Geology*, v. 14, p. 99-102.
- Orr, W.L., 1977, Geologic and geochemical controls on the distribution of hydrogen sulphide in natural gas. *In*: Campos, R., and Goni, I. (eds.), *Advances in Organic Geochemistry*, p. 571-597.
- Packard, J.J., Pellegrin, G.J., Al-Aasm, I.S., Samson, I., and Gagnon, J., 1990, Diagenesis and

- dolomitization associated with hydrothermal karst in Fammennian Upper Wabamun ramp sediments, northwestern Alberta. *In*: Bloy, G.R. and Hadley, M.G., (eds.), The Development of Porosity in Carbonate Reservoirs. Canadian Society of Petroleum Geologists Short Course Notes, p. 9-1 - 9-27.
- Patey, K.S., 1995, Upper Devonian carbonates in the Obed area. Unpublished M.Sc thesis, University of Alberta, Edmonton, Alberta, 147 pp.
- Popp, B.N., Anderson, T.F., and Sandberg, P.A., 1986, Brachiopods as indicators of original isotopic compositions in some Paleozoic limestones. *GSA Bulletin*, v. 97, p. 1262-1269.
- Roedder, E., 1981, Origin of fluid inclusions and changes that occur after trapping. *In*: Hollister, L.S. and Crawford, M.L. (eds.), Mineralogical Association of Canada Short Course In Fluid Inclusions: Applications to Petrology, v. 6, p. 101-137
- Ross, R.M., 1990, Deep crust and basement structure of the Peace River Arch region: constraints on mechanisms and formation. *In*: O'Connell, S.C. and Bell, J.S., (eds.), Geology of the Peace River Arch. *Bulletin of Canadian Petroleum Geology*, v. 38A, p. 25-35.
- Rostron, B.J., 1995, Cross-formational flow in Upper Devonian to Lower Cretaceous strata, west-central Alberta. Unpublished Ph.D. thesis, University of Alberta, Edmonton, Alberta, 201 pp.
- Quing, H. and Mountjoy, E.W., 1994, Formation of coarsely crystalline, hydrothermal dolomite reservoirs in the Presqu'île Barrier, Western Canada Sedimentary Basin. *AAPG Bulletin*, v. 78, No. 1, p. 55-77.
- Saller, A.H., and Yaremko, K., 1994, Dolomitization and porosity development in the middle and upper Wabamun Group, southeast Peace River Arch, Alberta, Canada. *AAPG Bulletin*, v.78, no. 9, p. 1406-1430.
- Sibley, D.F. and Gregg, J.M., 1987, Classification of dolomite rock textures. *Journal of Sedimentary Petrology*, v. 57, No. 6, p. 967-975.
- Simpson, G., Yang, C., and Hutcheon, I., 1996, Thermochemical sulphate reduction: a local process that does not generate thermal anomalies. *In*: 1995 Alberta Basement Transects Workshop, Lithoprobe Report #51, Lithoprobe Secretariat, University of British Columbia, G.M. Ross, comp. 241-245.
- Skilliter, C.C., Machel, H.G., and Cavell, P.A, 1998, A stratigraphic and geochemical investigation of Middle to Upper Devonian "aquitards" in west-central Alberta, Canada - preliminary results. *GSA Abstracts with Programs*, p. A-234.
- Skilliter, C.C., M.Sc. thesis, University of Alberta, Edmonton, Alberta, in preparation.

- Smalley, P.C., Higgins, A.C., Howarth, R.J., Nicholson, H., Jones, C.E., Swinburne, N.M.H., and Bessa, J., 1994, Seawater isotope variations through time: a procedure for constructing a reference curve to date and correlate marine sedimentary rocks. *Geology*, v. 22, p. 431-434.
- Stoakes F.A., 1980, Nature and control of shale basin fill and its effect on reef growth and termination: Upper Devonian Duvernay and Ireton Formations of Alberta, Canada. *Bulletin of Canadian Petroleum Geology*, v. 28, No. 3, p. 345-410.
- Stoakes, F.A., 1987, Fault-controlled dolomitization of the Wabamun Group, Tanjant Field, Peace River Arch, Alberta, In: Krause, F.F. and Burrowes, O.G., eds., *Devonian Lithofacies and Reservoir Styles in Alberta. Second International Symposium on the Devonian System*, Calgary, Alberta, p. 73-86.
- Toth, J., 1978, Gravity-induced cross-formational flow of formation fluids, Red Earth region, Alberta, Canada: analysis, patterns, evolution. *Water Resources Research*, v.14, no. 5, p. 805-843.
- van Wagoner, J.C., Posamentier, H.W., Mitchum Jr., R.M., Vail, P.R., Sarg., J.F., Loutit, T.S., and Hardenbol, J., 1988, An overview of the fundamentals of sequence stratigraphy and key definitions. In: Wilgus, C.K., Hastings, B.S., Kendall, C.G.St.C., Posamentier, H.W., Ross, C.A., and van Wagoner, J.C., (eds.), *Society of Economic Paleontologists and Mineralogists, Special Publication No. 42*, p. 39-46.

APPENDIX A

Geochemical Database

Southwest Peace River Arch Leduc Data

Well Location	Sample (Well-ID)	Diagenetic Phase	$\delta^{13}\text{C}$	$\delta^{18}\text{O}$	$\text{Sr}^{87}/\text{Sr}^{86}$
11-03-70-11-W6	MCM96-10	Limpid Calcite	-0.834	-13.691	0.71622
14-35-74-01W6	MCM96-35	Limpid Calcite	0.444	-13.431	0.73355
04-34-74-01W6	MCM96-43	Limpid Calcite	-0.443	-16.400	0.72920
04-34-74-01W6	MCM96-44a	Limpid Calcite	-0.568	-15.397	0.72940
12-18-74-02W6	MCM96-49	Limpid Calcite	0.119	-16.409	0.73187
02-08-76-26W5	MCM96-56a	Limpid Calcite	-0.346	-13.105	0.72679
11-30-66-07W6	MCM96-01	Milky Calcite	-7.559	-11.998	0.72775
11-30-66-07W6	MCM96-02	Milky Calcite	-8.672	-9.920	0.72102
11-30-66-07W6	MCM96-05	Milky Calcite	-9.827	-10.118	0.71934
11-30-66-07W6	MCM96-06	Milky Calcite	-7.577	-11.272	0.72943
11-30-66-07W6	MCM96-09	Milky Calcite	-8.472	-10.651	0.71775
12-22-66-06W6	MCM97-02	Milky Calcite	-7.368	-9.794	0.72189
12-22-66-06W6	MCM97-03	Milky Calcite	-7.711	-11.031	0.72663
11-30-66-07W6	MCM97-04	Milky Calcite	Not Run	Not Run	0.73160
12-22-66-06W6	MCM97-06a	Milky Calcite	-9.041	-4.726	0.73218
11-30-66-07W6	MCM97-07	Milky Calcite	-6.787	-11.562	0.73131
11-30-66-07W6	MCM97-09	Milky Calcite	Not Run	Not Run	0.73354
11-30-66-07W6	MCM97-11	Milky Calcite	-6.025	-11.119	0.72620
11-30-66-07W6	MCM97-12	Milky Calcite	-7.479	-7.599	0.72267
11-30-66-07W6	MCM97-13	Milky Calcite	-6.742	-10.915	0.72659
11-30-66-07W6	MCM97-15	Milky Calcite	-6.631	-10.735	0.72488
11-30-66-07W6	MCM97-16a	Milky Calcite	0.284	-5.415	0.72948
11-30-66-07W6	MCM96-03	Rhombohedral Dolomite	1.021	-5.148	0.71151
09-31-71-23W5	MCM96-14b	Rhombohedral Dolomite	2.223	-5.756	0.70948
12-22-66-06W6	MCM97-06b	Rhombohedral Dolomite	1.003	-4.726	0.70996

Well Location	Sample (Well-ID)	Diagenetic Phase	$\delta^{13}\text{C}$	$\delta^{18}\text{O}$	$\text{Sr}^{87}/\text{Sr}^{86}$
11-03-70-11W6	MCM96-12	Saddle Dolomite	-0.931	-10.753	0.72704
02-05-72-23-W5	MCM96-24	Saddle Dolomite	3.07	-5.397	0.70938
10-20-73-01W6	MCM96-32	Saddle Dolomite	2.452	-10.529	0.71374
14-23-74-01W6	MCM96-38	Saddle Dolomite	1.855	-6.186	0.71275
01-26-74-01W6	MCM96-41	Saddle Dolomite	1.686	-9.406	0.72281
01-26-74-01W6	MCM96-42	Saddle Dolomite	Not Run	Not Run	0.71933
12-18-74-02W6	MCM96-48a	Saddle Dolomite	Not Run	Not Run	0.73367
02-08-76-26W5	MCM96-60	Saddle Dolomite	0.956	-9.763	0.72280
06-04-74-01W6	MCM96-84a	Saddle Dolomite	0.676	-11.100	0.72688
11-30-66-06W6	MCM97-16b	Saddle Dolomite	Not Run	Not Run	0.71404
04-34-67-04W6	MCM97-22	Saddle Dolomite	0.814	-6.658	0.71740
09-31-71-23W5	MCM96-14a	Matrix Dolomite	2.248	-4.747	0.70867
04-34-74-01W6	MCM96-44b	Matrix Dolomite	0.327	-6.149	0.70969
04-34-74-01W6	MCM96-48b	Matrix Dolomite	1.728	-9.333	0.70897
02-08-76-26W5	MCM96-54	Matrix Dolomite	-0.036	-7.033	0.70866
09-06-77-25W5	MCM96-74	Matrix Dolomite	0.794	-5.006	0.71002
11-06-67-26W5	MCM97-17	Primary Anhydrite	Not Run	Not Run	0.70819
11-06-67-26W5	MCM97-18	Primary Anhydrite	Not Run	Not Run	0.70818
06-04-74-01W6	MCM96-84b	A2 Anhydrite	Not Run	Not Run	0.70920
04-34-67-04W6	MCM97-21	A2 Anhydrite	Not Run	Not Run	0.70981
02-05-72-23W6	MCM96-21	A3 Anhydrite	Not Run	Not Run	0.71246
04-34-74-01W6	MCM96-47	A3 Anhydrite	Not Run	Not Run	0.72338
12-22-66-06W6	MCM97-04	A3 Anhydrite	Not Run	Not Run	0.73160
11-30-66-06W6	MCM96-01	Fluorite	Not Run	Not Run	0.71891
11-30-66-06W6	MCM97-07a	Fluorite	Not Run	Not Run	0.71925
11-30-66-06W6	MCM97-07b	Fluorite	Not Run	Not Run	0.71917
11-30-66-06W6	MCM97-10	Fluorite	Not Run	Not Run	0.71748

George Dix's Data (1993)

Well Location	Diagenetic Phase	$\delta^{13}\text{C}$	$\delta^{18}\text{O}$	$\text{Sr}^{87}/\text{Sr}^{86}$
	Matrix Dolomites			

Well Location	Diagenetic Phase	$\delta^{13}\text{C}$	$\delta^{18}\text{O}$	$^{87}\text{Sr}/^{86}\text{Sr}$
11-03-70-11 W6	RL	1.66	-5.59	Not Run
01-16-79-22 W5	RL	0.09	-5.45	Not Run
10-23-87-09 W6	RL	0.20	-5.26	Not Run
02-11-87-13 W6	RL	0.17	-7.25	Not Run
02-08-76-26 W5	M	0.13	-5.81	Not Run
04-15-79-22 W5	M	-0.56	-5.93	Not Run
08-16-79-22 W5	M	0.10	-5.13	Not Run
16-13-83-24 W5	M	-0.86	-5.77	0.7092
10-23-84-18 W5	M	0.56	-5.25	Not Run
11-19-87-04 W6	M	0.70	-5.30	0.7098
11-09-79-22 W5	M	0.80	-5.82	0.7084
16-13-83-24 W5	M	-1.53	-4.93	Not Run
13-18-80-23 W5	M	4.53	-5.26	Not Run
Well Location	Diagenetic Phase	$\delta^{13}\text{C}$	$\delta^{18}\text{O}$	$^{87}\text{Sr}/^{86}\text{Sr}$
02-05-72-23 W5	Xa	3.22	-9.69	0.7144
	Fracture-Related Dolomites			
10-23-87-10 W6	M	0.74	-6.84	Not Run
02-14-77-25 W5	M	0.68	-6.64	Not Run
02-08-76-26 W5	M	0.48	-6.32	Not Run
10-23-87-10 W6	M	0.57	-6.77	Not Run
10-23-87-10 W6	M	0.32	-6.20	Not Run
06-26-74-12 W6	Xa	0.83	-7.01	Not Run
06-26-74-12 W6	Xa	0.26	-6.80	Not Run
10-23-87-09 W6	Xb	0.45	-7.02	Not Run
10-23-87-09 W6	Xb	0.72	-6.96	Not Run
11-19-87-04 W6	Xb	1.10	-6.41	Not Run
	Fracture-Fill Dolomites			
10-23-87-09 W6	F3	0.40	-8.18	0.7108
10-23-87-09 W6	F3	0.23	-7.96	Not Run
02-08-76-26 W5	F4	-0.62	-15.05	Not Run

Fluid Inclusion Data

Well	Sample	Cement	Th	Tf	Te	Tm _{ice}
11-30-66-07W6	MCM96-07	Milky Calcite	143.5			
			142.7			
			142.8			
			143.5			
			143.8			
			136.4	-50.1	-49.2	-10.0
			138.8			
			151.1			
			137.4			
			138.9			
			139.3	-57.0	-47.0	-11.0
			138.5	-54.5	-46.0	-9.9
			141.0	-53.2	-46.0	-16.1
			136.2	-57.8	-46.0	-10.0
			134.4	-58.0	-46.0	-13.0
			148.5	-52.3	-47.0	-11.4
			143.9	-62.4	-46.0	-9.9
			134.0			
11-03-70-11W6	MCM96-10	Limpid Calcite	141.1			
			135.4			
			125.0			
			115.0			
			129.2			
12-22-66-06W6	MCM97-05	Milky Calcite	154.7			
			154.1			
			155.3			

Well	Sample	Cement	Th	Tf	Te	Tm _{ice}
			140.7			
			146.6			
			136.1			
			127.1			
			155.4			
			145.0			
			141.7			
				-62.2	-48.0	-13.8
				-61.6	-48.0	-14.2
			147.0	-54.2	-46.0	-11.4
				-61.6	-48.0	-14.3
				-60.0	-48.7	-18.1
				-51.7	-48.7	-13.5
			124.0	-51.3	-45.0	-10.2
				-60.5	-45.0	-12.1
				-58.0	-45.0	-18.0
				-58.5	-45.3	-19.8
11-30-66-07W6	MCM97-16	Milky Calcite	136.5			
			109.0			
			115.9			
			118.1			
			130.4			
			137.3			
			134.2			
			124.9			
			106.3			
			125.4			
			134.3			
			131.6			
				-57.9	-54.7	-22.9
				-73.5	-53.8	-23.4
				-59.0	-53.0	-23.3

Well	Sample	Cement	Th	Tf	Te	Tm _{ice}
				-59.2	-53.5	-23.4
				-75.3	-53.4	-22.7
				-65.2	-54.1	-21.2
				-78.4	-53.5	-23.1
				-76.4	-54.7	-22.8
				-59.8	-53.6	-23.2
				-76.4	-54.0	-23.1
				-77.1	-54.0	-23.4
12-18-74-02W6	MCM96-49	Limpid Calcite	150.7			
			158.5			
			142.6			
			150.2			
			141.0			
			153.3			
			168.0 +			
			149.5			
			150.1			
				-74.4	-62.6	-19.9
				-75.5	-58.4	-21.4
				-72.8	-58.4	-20.4
				-71.3	-59.0	-21.3
				-75.4	-58.2	-20.5
				-74.9	-57.4	-20.4
				-58.6	-46.4	-20.4
				-73.9	-58.3	-21.4
				-74.0	-45.8	-20.5
				-67.1	-50.0	-23.7
				-70.7	-48.2	-20.1

APPENDIX B

Geochemical Methods

Strontium extraction

I. Sample dissolution of carbonates

1. Weigh 25-30 mg of powdered calcite/dolomite into a 15 ml polypropylene centrifuge tube.
2. Add 3 ml of 0.75N HCl dropwise with a disposable pipette.
3. Cap samples and leave at room temperature overnight to ensure complete dissolution.

II. Sample dissolution of anhydrite

1. Weigh 50 mg of powdered anhydrite into a teflon dissolution vessel.
2. Add 3 ml of 0.75N HCl.
3. Cap samples and leave on hotplate overnight at ~60°C to ensure complete dissolution.

III. Sample dissolution of fluorite

1. Weigh 100-125 mg of powdered fluorite into a teflon dissolution vessel.
2. Add 5 ml of 6N HCl + 2 ml concentrated HNO₃ (16N).
3. Cap teflon dissolution vessel, place in jacket on hotplate (~60°C), and leave overnight to ensure complete dissolution.
4. Uncap samples **in fumehood** and leave on hotplate overnight at ~60°C to evaporate completely.
5. Add 5 ml 6N HCl to sample, cap teflon dissolution vessel, place in jacket on hotplate (~60°C), and leave overnight to ensure complete dissolution.
6. Uncap samples **in fumehood** and leave on hotplate overnight at ~60°C to evaporate completely.

7. Repeat steps 5 and 6 **two times**, or until sample residue dissolves readily upon addition of HCl.
8. Add 3 ml 0.75 HCl, cap teflon dissolution vessel, and dissolve on hotplate overnight at ~60°C.

IV. Chromatography

Unspiked Sr separation from cation columns

Columns: glass/polypropylene Bio-Rad Econo-Columns; 15 x 0.7 cm containing 4.4 ml of wet cation resin. Columns 1-12.

Resin: Bio-Rad AG50W-X8 cation resin, 200 - 400 mesh, H⁺ form.

Loading Solution: 3 ml 0.75N HCl

1. Centrifuge dissolved samples at 5000 rpm for 10 minutes.
2. Filter samples with a 0.2 µm, PTFE filter disc fitted to a 5 ml syringe prior to column loading.
3. Load supernate on to each column using a clean disposable pipette. Add dropwise so as not to disturb the resin keeping pipette tip close to resin and without touching column walls.
4. Carefully rinse the glass walls of the columns close to the top of the resin with 3 x 1 ml 0.75N HCl using a clean, disposable pipette for each column.
5. Rinse the glass walls and reservoirs of the columns with 3 x 1 ml of 2.5N HCl using clean, disposable pipettes.
6. Using an attachable large plastic 40 ml reservoir, wash the columns with 20 ml of 2.5N HCl. Collect waste fluid from the columns and discard.
7. Add 7 ml of 2.5N HCl to the columns to remove the separated strontium from the resin. Collect the fluid in small, labeled, teflon dissolution vessels and place uncapped on the hotplate overnight at ~60°C.

Sr cleanup columns

Columns: Heat-shrink TFE 4:1 (Zeus #164553, 7/8") containing 1.7 ml wet cation resin. Columns 1-8.

Resin: Bio-Rad AG50W-X8 cation resin, 200 - 400 mesh, H⁺ form.

Loading solution: 0.25 ml of a 1:1 mixture of 0.25N oxalic acid and 1N HCl

Elution solution: 2.5N HCl.

1. Clean column with 5 ml 6N HCl, then equilibrate resin with 1.5N HCl.
2. Dissolve sample in 0.25 ml loading solution, and centrifuge at 10000 rpm for 5 minutes in disposable 1.5 ml polypropylene centrifuge tube.
3. Load supernate on to each column using clean disposable pipette. Add dropwise so as not to disturb the resin keeping pipette tip close to resin and without touching column walls.
4. Rinse stem walls with 3 x 0.25 ml new loading solution using clean, disposable pipette.
5. Rinse stem walls with 2 x 0.5 ml new elution solution using clean, disposable pipette.
6. Wash columns with 7 ml of new elution solution. Dispose of all waste fluid.
7. Add a final 5 ml of new elution solution to remove the separated strontium from the resin. Collect the fluid in small, labeled, teflon dissolution vessels and place uncapped on the hotplate overnight at $\sim 60^{\circ}\text{C}$.

Holmden *et al.* (1997) and Koffyberg (1994) provide descriptions and theory of analytical procedures on the TIMS.

University of Alberta Library



0 1620 1084 2662

B45739